Excitation Energies and Response Properties of Molecules using Internally Contracted Multireference Coupled Cluster Methods

Von der Fakultät Chemie der Universität Stuttgart
zur Erlangung der Würde eines Doktors der
Naturwissenschaften (Dr. rer. nat.) genehmigte Abhandlung

Vorgelegt von
Pradipta Kumar Samanta
aus West Bengal, Indien

Hauptberichter: Prof. Dr. A. Köhn, Universität Stuttgart
Mitberichter: Prof. Dr. J. Gauss, Universität Mainz
Prüfungsvorsitzender: Prof. Dr. J. van Slageren, Universität Stuttgart
Tag der mündlichen Prüfung: 27.10.2017

Institut für Theoretische Chemie
der Universität Stuttgart

2017

To my Parents...

Abstract

English

Calculation of molecular properties is one of the most important aspects of quantum chemistry. The response theory, which is a general framework applied to different electronic structure methods, is widely used to calculate several static and frequency dependent molecular properties. In response theory, properties are obtained as the response of an electronic state to the external perturbations like electromagnetic field. Several electrical properties, like dipole moment and frequency-dependent polarizability, along with different magnetic properties like magnetizability and electronic g-tensor can be evaluated following this formalism. Response theories have been developed for single reference methods, such as the coupled cluster method and they are routinely used for calculating molecular properties for closed shell molecules. However, there is no well established method to calculate these molecular properties for multireference systems where more than one determinant is used as the zeroth order reference. This thesis aims to develop a response formalism for internally contracted multireference coupled cluster (ic-MRCC) method in order to calculate highly accurate properties for multireference systems. ic-MRCC has been developed and used successfully, in recent years, to calculate energies with very high accuracy for different kinds of multireference systems such as open shell molecules, dissociating bonds and transition metal compounds.

As the first step of the response formalism, a time-dependent Lagrangian is formulated for the ic-MRCC theory. Formulation of this Lagrangian introduces Lagrange multipliers as a new set of parameters. The first derivative of the Lagrangian with respect to the perturbation produces the expression for the first order properties as an expectation value. Equations to obtain the zeroth order Lagrange multipliers, which are required to calculate the first order properties, are also formulated. A second derivative of the Lagrangian gives the linear response function as a function of the frequency of the external perturbation. The response equations are formulated and solved to get the first order wave function parameters which are used in evaluating this linear response function. Frequency dependent second order properties are obtained as the values of this linear response function for different frequencies. Poles of the linear response function represent the excitation energies of molecules. The excitation energies are thus obtained for ic-MRCC by finding these poles of the response function. But, the linear response function, as obtained from the formulation of response theory for ic-MRCC, gives unphysical second order poles. Appearance of these second order poles are avoided through approximations while obtaining both the second order properties and the excitation energies. Results obtained from these approximated versions of the ic-MRCC response formulation do not show any other spurious poles, like some other MRCC methods, as ic-MRCC deals with a linearly independent excited space.

This response formulation is applied to calculate several molecular properties and corresponding results are presented. Electrical properties such as dipole moments, quadrupole moments and electric field gradients, along with the spin-dependent properties, such as hyperfine coupling constants, are calculated as the expectation values. On the other hand, the second order properties, such as the frequency dependent electrical polarizabilities, are calculated from the expression of the linear response function. Excitation energies are also calculated for several molecules and compared with the results obtained from other quantum chemical methods. All these results show that ic-MRCC provides very accurate properties and excitation energies for different multireference systems.

Deutsch

Die Berechnung molekularer Eigenschaften ist einer der bedeutendsten Aspekte der Quantenchemie. Die Theorie der Antwortfunktion (engl. response theory) — eine allgemeine Vorgehensweise die auf verschiedene Elektronenstrukturmethoden angewendet werden kann — wird häufig verwendet, um mehrere statische und frequenzabhängige molekulare Eigenschaften zu berechnen. In der response theory werden Eigenschaften als Antwort eines elektronischen Zustands auf periodische, externe Störungen, wie ein elekromagnetisches Feld, erhalten. Mehrere elektronische Eigenschaften wie das Dipolmoment und die frequenzabhängige Polarisierbarkeit, sowie verschiedene magnetische Eigenschaften wie die Magnetisierbarkeit und der elektrische g-Tensor befinden sich unter den Eigenschaften, welche mit dem Formalismus der response theory berechnet werden können. Response theories wurden für Single-Referenz Methoden wie die coupled cluster Methode entwickelt und routinemäig verwendet, um molekulare Eigenschaften geschlossenschaliger Moleküle zu berechnen. Allerdings gibt es keine etablierte Methode, um diese molekularen Eigenschaften in Multi-Referenz Systemen zu berechnen, für welche mehr als eine Determinante als Referenz nullter Ordnung verwendet wird. Ziel dieser Arbeit ist die response theory für die intern kontrahierte multi reference coupled cluster Methode (ic-MRCC) zu entwickeln, um Eigenschaften für molekulare Systeme mit starkem Multi-Referenz Charakter hochgenau berechnen zu können. In den vergangenen Jahren wurde ic-MRCC entwickelt und erfolgreich eingesetzt, um Energien mit hoher Genauigkeit für unterschiedliche Multi-Referenz Systeme wie offenschalige Moleküle, Bindungsdissoziationen und übergangsmetallverbindungen zu berechnen. Im ersten Schritt der Formulierung der response theory für ic-MRCC wird die zeitabhängige Lagrange-Funktion gebildet. Dabei werden die Lagrange-Multiplikatoren als neue Parameter eingeführt. Die erste Ableitung der Lagrange-Funktion bezüglich der Störung ermöglicht die Berechnung der Eigenschaften erster Ordnung als Erwartungswert. Dabei werden auch Gleichungen zur Bestimmung der Lagrange-Multiplikatoren nullter Ordnung formuliert, wobei diese Multiplikatoren benötigt werden um die Eigenschaften erster Ordnung zu berechnen. Die zweite Ableitung der Lagrange-Funktion ergibt die lineare Antwortfunktion als Funktion der Frequenz der externen Störung. Die Gleichungen der Antwortfunktionen werden formuliert und gelöst, um die Parameter der Wellenfunktion erster Ordnung zu erhalten, welche dazu genutzt werden die lineare Antwortfunktion zu lösen. Frequenzabhängige Eigenschaften zweiter Ordnung werden als Werte der linearen

Antwortfunktion bei verschiedenen Frequenzen erhalten. Polstellen der linearen Antwortfunktion stellen die Anregungsenergien des betrachteten Moleküls dar. Die Anregungsenergien werden also für ic-MRCC erhalten, indem die Polstellen der linearen Antwortfunktion gefunden werden. Allerdings enthält die lineare Antwortfunktion, welche aus der Formulierung der response theory für ic-MRCC erhalten wurde, unphysikalische Polstellen zweiter Ordnung. Das Auftreten dieser Polstellen zweiter Ordnung wird durch Näherungen verhindert, während dennoch die Eigenschaften zweiter Ordnung und die Anregungsenergien erhalten werden können. Die Ergebnisse dieser Formulierung für die ic-MRCC response theory mit den erwähnten Näherungen zeigen keine störenden Polstellen wie manche andere MRCC Methoden, da ic-MRCC einen linear unabhängigen Anregungsraum behandelt. Diese Formulierung der response theory wird zur Berechnung mehrerer molekularer Eigenschaften angewendet und die Ergebnisse dieser Rechnungen werden vorgestellt. Elektrische Eigenschaften wie das Dipolmoment, Quadrupolmoment und der elektrische Feldgradient, sowie Spin-abhängige Eigenschaften wie Hyperfeinkopplungskonstanten, werden als Erwartungswerte berechnet. Die Eigenschaften zweiter Ordnung, wie die frequenzabhängige elektrische Polarisierbarkeit, werden aus dem Ausdruck für die linearen Antwortfunktion berechnet. Außerdem werden die Anregungsenergien mehrerer Moleküle berechnet und mit den Ergebnissen anderer quantenchemischer Methoden verglichen. Zusammengefasst zeigen die Ergebnisse dieser Arbeit, dass ic-MRCC sehr genaue Eigenschaften und Anregungsenergien für verschiedene Multi-Referenz Systeme liefert.

Acknowledgements

I would like to express my earnest appreciation and thanks to everyone who supported, advised and encouraged me in the course of my doctoral research. I convey my sincere thanks to my advisor Prof. Andreas Köhn for his guidance at every stage of this Ph.D. program. His perspective always helped me see things in a new light. It is a true privilege to have the opportunity to work with him.

Part of this work is done in collaboration with Prof. Debashis Mukherjee of Indian Association for the Cultivation of Science at Kolkata, India. I convey my gratitude to him. His unique scientific approach has always served as a guidance in the course of my research. My sincere thanks to Matthias Hanauer and Yuri Aoto for always indulging my scientific queries and for all the academic and non-academic discussions we had. I convey my gratitude to Dr. George Booth for a stimulating and fruitful collaboration.

I want to thank all my colleagues and friends at the institute Wenlan Liu, David Coughtrie, Shuangying Ma, Arne Bargholz, Florian Bauer, Jan Schnabel, Sebastian Miranda, Christoph Köpple, Thanja Lambert, Sonia Alvarez, Laura Comprido, Andreas Löhle for their association, help and advice.

It has been a very nice experience to work at the institute for theoretical chemistry. It has an environment conducive to lively academic discussions and collaborations. I am also very fortunate to be a part of the Simtech graduate school here at the University of Stuttgart. Different academic and non-academic programs in the graduate school have helped me in developing my outlook about different facets of scientific research. Thanks are also due to them for their financial support, especially funding my extended academic visit to the King's college, London in 2016.

During my stay at IACS, Kolkata, I was very fortunate to have friends like Rahul Maitra, Shubhrodeep Pathak, Avijit Sen, Debalina Sinha, Sangita Sen and Avijit Shee. Academic as well as non-academic conversations with them have always been a source of inspiration and enjoyment.

Since my school days I have acquainted myself with some excellent teachers. They instilled in me an interest in scientific knowledge and rational thinking. I would like to thank Angshuman Moitra, Debasis Jana, Naba Kumar Bera, Chandan Saha, Madhav Ranganathan, K. Srihari, Sadasivam Manogaran, Deb Shankar Roy and Shankar Prasad Bhattacharyya for their guidance and inspiration.

My thanks to Saswati for her amazing friendship and unwavering support. My sincere thanks to my Ma(Archana Samanta), Baba(Dilip Samanta) and Didi(Tanusree Samanta) for giving a meaning to all my endeavors and accomplishments. Thanks to my entire family for their resolute unconditional support.

Pradipta Samanta
Stuttgart, August 2017

Contents

1 | Introduction

Molecular properties provide insights to understand the nature of a chemical system. These molecular properties are experimentally obtained by studying the response of a chemical system in presence of electromagnetic fields as perturbations. Over the past few decades several quantum chemical methods have been developed to determine these molecular properties theoretically to have a better understanding of the complicated nature of the experimental results. The work in this thesis aims to develop methods for calculating highly accurate molecular properties, along with excitation energies, of chemical systems with complicated electronic structures. The complexity of electronic structure, which will be addressed in this thesis, arises due to the requirement of two or more quasi-degenerate configurations to properly describe a system. Such molecular systems, known also as the multireference systems, include di-radicals, dissociative bonds, states with avoided curve crossings and transition metal complexes, among others. This thesis focuses on the molecular properties like the different electrical properties, such as dipole moments, quadrupole moment, and electrical polarizabilities, along with the first order spin-dependent properties, such as hyperfine coupling constants, which are important to understand EPR spectra.

Molecular properties are derived from the changes in the energy of a system due to the presence of external perturbations. As a first step of calculating molecular properties, the energy and the wave function of the unperturbed system are obtained. The main challenge of getting this zeroth order description of the system is to include the effect of the electronic correlations properly. For simple quantum chemical systems like closed-shell molecules, a single determinant obtained from the Hartree-Fock (HF) theory [1] is used as the reference to develop methods that include this correlation effect. These methods, known as the single-reference methods, incorporate several configurations into the wave function by applying ansatz of excitation operators on top of the HF determinant. Among many single-reference methods [2], such as coupled cluster (CC), configuration interaction (CI) and perturbation theory (PT), the CC theory [3, 4] with its single and double excitations, and a perturbative inclusion of triple excitations is the most popular and routinely used for the energy and property calculations of molecular systems [2, 5].

However, for the multireference systems, a multideterminantal representation of the reference function is needed. The multiconfigurational self-consistent field (MCSCF) theory [6] provides this multideterminantal reference for further development of different suite of multireference methods [7–9]. Several formulations of multireference theories in the coupled cluster framework have been attempted in recent years as it is not possible to formulate an unique ansatz for the multireference CC (MRCC) theory [10, 11], unlike its single-reference counterpart. The main difference between all of these different formulations of MRCC is the way by which the space of excited configurations is chosen for each of the cases. The MRCC theories can be broadly classified into Fock-space MRCC (FSMRCC) [12, 13] , state-universal MRCC (SUMRCC) of Jeziorski and Monkhorst [14], contracted [15–18] and decontracted [16, 19, 20] variants of state-specific MRCC (SSMRCC) methods. It is important for any MRCC formulation to fulfill the following requirements of: a) proper scaling with the size of the system (size-extensivity), b) invariance with respect to the rotation of the orbitals (orbital invariance) and c) use of a linearly independent sets of excited configurations (non-redundancy). Where most of the MRCC formulations fail to meet one or more of these requirements, a variant of the internally contracted MRCC (ic-MRCC), implemented recently by Hanauer and Köhn [18], manages to fulfill all of these criteria. This variant of ic-MRCC has been developed following the first introduction of the theory using an wave operator that includes only limited classes of excitation operator, by Banerjee and Simons [15, 21, 22]. Another implementation of the ic-MRCC theory has been done separately by Evangelista and Gauss [17] with the main difference with Ref. [18] being the way of selecting the linearly independent excitation operators. A general formulation of the theory using a normal ordered exponential ansatz [23] was also proposed [16, 24] but this is yet to be implemented. The variant of the ic-MRCC method, implemented in Ref. [18], has been further extended to include the contributions from perturbative triples [25] and explicit correlations [26]. While ic-MRCC has emerged as a very promising MRCC method, it has been applied mainly for the calculation of energy related quantities. The work in this thesis intends to extend the applicability of ic-MRCC for calculating molecular properties and excitation energies.

For the determination of the molecular properties, the external fields, such as electromagnetic radiation, are added as small perturbations to the electronic Hamiltonian. There are several methods designed for calculating the molecular properties with the oldest among them being the use of the numerical derivatives of energy with respect to the external fields. This method, known as the finite perturbation theory (FPT) [27] or the finite field method, has been used to calculate properties for different quantum chemical methods [28–30]. FPT has the advantage of not requiring any further implementation of a quantum chemical theory once the energy has been evaluated using it. But it has

a few disadvantages. It requires several calculations of energies, corresponding to different field strengths, with higher accuracy making it computationally expensive. It is also not possible to calculate dynamic properties using FPT. A better way of calculating molecular properties is to use expressions which are obtained by differentiating the molecular energy analytically. Following the first analytical formulation of the energy derivatives, obtained for Hartree-Fock method by Pulay [31], Monkhorst [32] came up with a similar formulation for the SRCC theory which was later extended to calculate dynamic properties [33]. According to this formulation for CC theory, first derivatives of the cluster amplitudes with respect to the perturbations are essential to calculate the first order properties. Bartlett *et al.* [34, 35] proposed an improved version of the method in Ref. [32] by replacing the perturbation dependent first order amplitudes with perturbation independent parameters for the calculation of first order properties. This technique is better known as analytic gradient method and is used for calculations of static properties and optimization of molecular structures. Apart from its application to different level of CC methods [36–40], the analytic gradient method was also applied for different single-reference methods, like Møller-Plesset perturbation [41–45], configuration interaction (CI) [46, 47] and quadratic CI [48, 49]. An alternative way of getting molecular properties as derivatives of Lagrangian was formulated [50, 51] for coupled cluster methods. This method is better known as response theory. The response formalism was also extended to calculate dynamic properties [52] and was applied to other single-reference methods [53]. In the static limit, both analytic gradient and response theories are equivalent with the extra parameters defined in the Analytic Gradient appearing to be the Lagrange multipliers used in the Linear response formalism. Another important aspect of both of these analytic methods is that they allow the orbitals, involved in the calculation, to relax in presence of the perturbation. However, attempts were made to calculate properties without relaxing the orbitals and thus making the process computationally less expensive. This unrelaxed approach simplifies the expression of the properties, for example: the expression for calculating the first order properties is now an expectation value of the perturbation operator within this approach. This expectation value approach was applied mainly to calculate first order properties for CC [54–57] and CI [58] methods and was compared with the 'relaxed' properties.

These existing methods of calculating molecular properties have been extended for different MRCC methods. While, Szalay [59] has evaluated the first order properties for both SUMRCC and FSMRCC invoking the generalized Hellmann-Feynman theorem, Pittner *et al.* [60] has developed an analytic gradient method for the state-specific Brillouin-Wigner MRCC (BWMRCC) and SUMRCC for optimizing molecular geometries. An analytic gradient formulation of the state-specific Mukherjee's multireference coupled-cluster (Mk-MRCC) has been implemented [61, 62] to optimize molecular structure. Molecular properties have also been calculated from Mk-MRCC using FPT [63] and

later by following a linear response formalism [64, 65]. However, the dynamic properties obtained from Mk-MRCC show several spurious poles which originate due the overcompleteness of the excitation operators involved in the theory. Though several of these formulations exist, none of these MRCC methods are routinely used to calculate static and dynamic properties till date.

Excitation energies are measured in spectroscopy by applying electromagnetic radiations to excite electrons from one state to another. In quantum chemistry, the excitation energy can be obtained in two different ways. In the first approach, excitation energies are obtained by calculating the absolute energies of the excited states. Multireference methods are generally capable of getting the energies of the excited states when they can be spanned by the determinants within the active space. Multireference configuration interaction (MRCI) and multireference perturbation theory have been used to calculate the energies of the excited states [7, 9]. As a second and better alternative, the excitation energies are calculated directly as the difference in energies between the excited states and the ground state. This direct way of calculating excitation energies is more useful as it cancels out the part of the correlation energy which is common to both the states. The methods of obtaining direct excitation energies can be formulated in two different ways. The excitation energies can be obtained as the poles of the linear response function within the linear response (LR) formalism. This is possible as the linear response function diverges whenever the frequency of the external field matches any of the excitation energies of the system. The second alternative uses an ansatz for the excited state on top of the ground state. Use of this additional ansatz produces the main contribution to the energy difference between the ground and the excited states. In the framework of the SRCC theory, these two approaches lead to the coupled cluster linear response (CC-LR) [32, 52, 53, 66, 67] and equation-of-motion coupled cluster (EOM-CC) [68–70] methods, respectively. It is important to mention that, within the single-reference framework, these two alternate methods produce the same excitation energies. With the singles-doubles approximation, EOM-CC is not very accurate for doubly excited states. Thus several methods were developed which include the further corrections coming from the triples, such as, the EOM-CCSDt [71, 72] method and completely renormalized EOMCC with single, doubles and non-iterative triples [CR-EOMCCSD(2,3)] [73]. However, these methods, as they are based on a single-reference framework, can not produce the excitation energies of similar accuracy for systems with strong multireference character.

Thus, for systems with multireference character, it is important to extend the linear response formalism to the MRCC methods. This has been achieved for the Mk-MRCC theory (Mk-MRCC-LR) in the work by Chattopadhyay *et al.* [74] and also recently by Jagau *et al.* [65]. However, these studies have revealed the problem of overcompleteness in the excitation manifold for Mk-MRCC-LR formalism, also mentioned in the context of

the linear response function earlier in this chapter. Due to this problem, Mk-MRCC-LR predicts unphysical spurious roots whenever it targets the excited state which lie outside the space spanned by the reference determinants.

The aim of this work is to extend the linear response approach in the framework of the ic-MRCC theory in order to calculate accurate molecular properties and excitation energies for molecular systems with prominent multireference character. Though the response approach can be extended to calculate properties of any general order, this work focuses mainly on deriving expressions to calculate first and second order properties by keeping the effect of the external field only linear on the response properties. The thesis is organised as follows. In Chapter 2, the relevant theoretical foundations are reviewed. This is divided into two parts, each of them being dedicated to the discussions of the methods for getting the wave functions and the properties, respectively. In Chapter 3, details of the ic-MRCC theory, which is the main framework of developing the response theory, are laid out. The formulation of the response theory for ic-MRCC, which is the main theoretical development done in this thesis, is presented in Chapter 4. The development of the linear response theory includes formulations of expressions of the first order property and the linear response function along with the eigenvalue equation to solve the excitation energies of molecules. The results for the first order properties of both electrical and spin-dependent natures are presented in the Chapter 5, while the results for the static and frequency-dependent second order properties are analysed in the Chapter 6. Chapter 7 deals with the study of the excitation energies. This chapter is divided into three parts. The linear response formalism for ic-MRCC, as developed in Chap. 4, is applied in the first part of the chapter to calculate excitation energies for different systems and then results are analyzed. An EOM-fashioned formulation of the eigenvalue equation to solve the excitation energy is then carried out in the next part of this chapter. The last part of this chapter compare both the formalism for calculating excitation energies. Chapter 8 finally summarizes all the work done in this thesis with suggestions of possible future directions.

2 | Theoretical Foundations

2.1 Methods in Quantum Chemistry

2.1.1 The Main Problem in Electronic Structure Theory

In quantum chemistry, the main goal is to get a description for an interacting system of nuclei and electrons solving the time-independent Schrödinger equation in the non-relativistic limit:

$$\mathcal{H}|\psi\rangle = \mathcal{E}|\psi\rangle. \tag{2.1}$$

This eigenvalue equation provides the solution for the wave function of the system as the eigenvector corresponding to the energies obtained as the eigenvalues. Here, $\mathcal{H}$ is the Hamiltonian of the whole system consisting of nuclei and electrons, each described by corresponding position vectors $\mathbf{R}_A$ and $\mathbf{r}_i$, respectively. The total Hamiltonian which depends on the internuclear distances ($R_{AB} = |\mathbf{R}_A - \mathbf{R}_B|$), distances between two electrons ($r_{ij} = |\mathbf{r}_i - \mathbf{r}_j|$) and distances between electrons and nuclei ($r_{iA} = |\mathbf{r}_i - \mathbf{R}_A|$) has the form:

$$\begin{aligned}\mathcal{H} = \quad & \underbrace{-\sum_{i=1}^{n} \tfrac{1}{2}\nabla_i^2}_{\hat{T}_e} \quad \underbrace{-\sum_{A=1}^{N} \frac{1}{2M_A}\nabla_A^2}_{\hat{T}_n} \quad \underbrace{-\sum_{i=1}^{n}\sum_{A=1}^{N} \frac{Z_A}{r_{iA}}}_{\hat{V}_{ne}} \\ & \underbrace{+\sum_{i=1}^{n}\sum_{j>i}^{n} \frac{1}{r_{ij}}}_{V_{ee}} \quad \underbrace{+\sum_{A=1}^{N}\sum_{B>A}^{N} \frac{Z_A Z_B}{R_{AB}}}_{V_{nn}}.\end{aligned} \tag{2.2}$$

The form of the Hamiltonian is expressed here using the atomic units with n and N being the number electrons and nuclei, respectively. Here, Z_A denotes the charge of the nucleus A while M_A denotes corresponding atomic mass. The terms $\hat{T}_e$ and $\hat{T}_n$ in Eq. 2.2 represent the kinetic energy of the electrons and nuclei, respectively, with ∇_i^2 and ∇_A^2 being corresponding Laplacian operators. The Coulomb interaction of the particles, as

represented in the Eq. 2.2, are: the nucleus-electron attraction $\hat{V}_{ne}$, the electron-electron repulsion $\hat{V}_{ee}$ and the nucleus-nucleus repulsion $\hat{V}_{nn}$.

The Schrödinger equation can be further simplified by following the Born-Oppenheimer approximation, which uses the fact that nuclei are much heavier than the electrons and thus move much slower. This approximation decouples the respective motions of electrons and nuclei considering the electronic movements to be carried out in the field of fixed nuclei. The separated electronic Hamiltonian ($\hat{H}$) can then be employed to solve the electronic part of the Schrödinger equation which gives the description and energy (E) of the electronic states for a fixed geometry $\mathbf{R}$ of a system of nuclei:

$$\hat{H}|\Psi\rangle = \big(\hat{T}_e + \hat{V}_{ne} + \hat{V}_{ee}\big)|\Psi\rangle = \sum_{i=1}^{n} \Bigg[\underbrace{\big(-\tfrac{1}{2}\nabla_i^2 - \sum_{A=1}^{N} \frac{Z_A}{r_{iA}}\big)}_{\hat{h}_i} + \sum_{j>i}^{n} \frac{1}{r_{ij}} \Bigg] |\Psi\rangle = E|\Psi\rangle. \quad (2.3)$$

Here, the Hamiltonian, the wave function and the energy are function of $\mathbf{R}$. Thus a multidimensional potential energy surface can be obtained by solving the energy for different $\mathbf{R}$ from this electronic Schrödinger equation which can then further be used to solve the nuclear Schrödinger equation to calculate the vibrational and rotational energy levels.

However, the solution of the electronic Schrödinger equation, in Eq. 2.3, is the central point of the electronic structure theory. The exact solution of this equation is only possible for an one-electron system, such as hydrogen atom, where only the one-body term $\hat{h}$ is involved. For any system with more than one electron, the exact solution of Eq. 2.3 is hindered due to the presence of the two body $\hat{V}_{ee}$ term which couples the motion of electrons and thus approximated methods are needed to solve this equation. The traditional way in electronic structure theory is to use one-electron basis to expand the Hamiltonian operators and then to express the Schrödinger equation as matrix eigenvalue equation. Another important aspect of the solution of Eq. 2.3 is that it has to be antisymmetric with respect to exchange of electrons, as the Pauli principle demands,

$$\Psi(\mathbf{x}_1, \ldots, \mathbf{x}_i, \ldots, \mathbf{x}_j, \ldots, \mathbf{x}_n) = -\Psi(\mathbf{x}_1, \ldots, \mathbf{x}_j, \ldots, \mathbf{x}_i, \ldots, \mathbf{x}_n). \quad (2.4)$$

Here $\mathbf{x}_i$ represents the collection of the spatial ($\mathbf{r}_i$) and the spin (σ_i) components of the i-th electron. A simple n-electron function which obeys the Pauli principle is a Slater

determinant which has the form:

$$\Phi_{12\ldots n}(\mathbf{x}_1, \mathbf{x}_2, \ldots, \mathbf{x}_n) = \frac{1}{\sqrt{n!}} \begin{vmatrix} \varphi_1(\mathbf{x}_1) & \varphi_2(\mathbf{x}_1) & \cdots & \varphi_n(\mathbf{x}_1) \\ \varphi_1(\mathbf{x}_2) & \varphi_2(\mathbf{x}_2) & \cdots & \varphi_n(\mathbf{x}_2) \\ \vdots & \vdots & \ddots & \vdots \\ \varphi_1(\mathbf{x}_n) & \varphi_2(\mathbf{x}_n) & \cdots & \varphi_n(\mathbf{x}_n) \end{vmatrix}. \tag{2.5}$$

This Slater determinant is comprised of one-electron functions $\varphi(\mathbf{x})$, known as spin orbitals. Each $\varphi(\mathbf{X})$ can be written as a product of its spatial and spin components, $\phi(\mathbf{r})$ and $s(\sigma)$, respectively. In the infinite limit, where these spin orbitals form a complete one-particle basis and thus the set of all possible n-electron Slater determinants span the complete space for the electronic system, an exact representation of the electronic wave function can be obtained.

However, theoretical calculations are possible only the one-electron and n-electron basis functions of finite size. So approximations are done to work with these finite basis functions so that minimum error is introduced in the description of the electronic state. For the one-electron basis functions, the dimension of the space is reduced to a finite one in a way that it can still emulate the appropriate form and functions of the infinite basis for the different regions of the space. For the n-electron basis functions, on the other hand, several quantum chemical methods have been developed for the purpose of choosing a proper truncated space that includes most of the important configuration determinants so that all the physical effects of the electronic interactions can be described. Some of these methods for getting the electronic wave function will be presented in the following sections.

2.1.2 Mean Field Approach: The Hartree-Fock Theory

In the Hartree-Fock (HF) theory, the electronic state is represented by a single Slater determinant $|\Phi\rangle$ where the constituent spin-orbitals are variationally optimized to produce the lowest energy for the state. The energy for a Slater determinant is obtained as:

$$E = \langle\Phi|\hat{H}|\Phi\rangle = \sum_{i=1}^{n} h_{ii} + \sum_{i,j=1}^{n} \Big(\langle ij|ij\rangle - \langle ij|ji\rangle \Big). \tag{2.6}$$

Here h_{ij} is the general one body integral of the form:

$$h_{ij} = \langle\varphi_i|\hat{h}|\varphi_i\rangle = \int d\mathbf{x}_1 \varphi_i^*(\mathbf{x}_1)\hat{h}\varphi_j(\mathbf{x}_1), \tag{2.7}$$

with $\hat{h}$ being the one-body part of the electronic Hamiltonian defined in Eq. 2.3. There are two different two-electron integrals with the generic form:

$$\langle pq|rs\rangle = \int d\mathbf{x}_1 \int d\mathbf{x}_2 \varphi_p^*(\mathbf{x}_1)\varphi_q^*(\mathbf{x}_2)\frac{1}{r_{12}}\varphi_r(\mathbf{x}_1)\varphi_s(\mathbf{x}_2). \tag{2.8}$$

The first of the two-electron integrals, $\langle ij|ij\rangle$, is termed as the Coulomb integral as it simply presents the electrostatic interaction between two electronic charge distribution. The second integral, known as the exchange integral, appears due to the antisymmetry of the electronic wave function and acts to stabilize the state as oppose to the Coulomb repulsion term. The energy expression presented in the Eq. 2.6 is minimized by varying the underlying orbitals within the constraint of them being orthonormal, $\langle \varphi_i|\varphi_j\rangle = \delta_{ij}$. This constraint introduces the Lagrange multipliers ε by forming the Lagrangian to apply the variational principle.

The Hartree-Fock theory finally solves for the spin-orbitals from the set of equations:

$$\hat{F}|\varphi_i\rangle = \sum_{j=1}^{n} |\varphi_j\rangle\varepsilon_{ji}, \forall i = 1, n \tag{2.9}$$

The operator $\hat{F}$ is called Fock operator:

$$\hat{F} = \hat{h} + \sum_{j=1}^{n} \left(\hat{J}_j - \hat{K}_j\right). \tag{2.10}$$

The first operator contributing to the Fock operator, $\hat{h}$, includes the kinetic energy of the electron and its interaction with nuclei. The rest of the operator is an effective potential which describes the interaction of the electron with an average field created as combined effect of the other electrons. This effective potential is comprised of the Coulomb operator ($\hat{J}_j$) and the exchange operator ($\hat{K}_j$). These two operators are defined by their action on a given spin orbital φ_i as:

$$\hat{J}_j\varphi_i(\mathbf{x}_i) = \int d\mathbf{x}_j \varphi_j^*(\mathbf{x}_j)\frac{1}{r_{12}}\phi_j(\mathbf{x}_j)\varphi_i(\mathbf{x}_i), \tag{2.11}$$

$$\hat{K}_j\varphi_i(\mathbf{x}_i) = \int d\mathbf{x}_j \varphi_j^*(\mathbf{x}_j)\frac{1}{r_{12}}\phi_i(\mathbf{x}_j)\varphi_j(\mathbf{x}_i). \tag{2.12}$$

Both of the Coulomb and exchange operators are related to the Coulomb and exchange integrals as these integrals are obtained by projecting Eqs. 2.11 and 2.12 onto $\langle\phi_i|$ respectively.

For molecular systems, the spatial part of the molecular orbitals are considered to be a linear combination of the atomic orbitals:

$$\phi_i(\mathbf{r}) = \sum_{\mu} \chi_\mu(\mathbf{r}) c_{\mu i}, \tag{2.13}$$

with $c_{\mu i}$ being the combining coefficients. Insertion of the ansatz of the molecular orbitals into the Hartree-Fock equation gives the Roothaan-Hall equations:

$$\mathbf{FC} = \mathbf{SC}\boldsymbol{\varepsilon}, \tag{2.14}$$

where,

$$F_{ij} = \int \chi_i^*(\mathbf{x}) \hat{F}(\mathbf{x}) \chi_j(\mathbf{x}) d\mathbf{x}, \tag{2.15}$$

$$S_{ij} = \int \chi_i^*(\mathbf{x}) \chi_j(\mathbf{x}) d\mathbf{x}, \tag{2.16}$$

$\mathbf{C}$ is the coefficient matrix and $\boldsymbol{\varepsilon}$ is the diagonal matrix containing the orbital energies.

Approximations within the Hartree-Fock theory can be made in the way the spatial orbitals are solved. Use of same spatial part for solving the orbitals corresponding to the α and β pairs of electrons leads to the *restricted* Hartree-Fock (RHF) theory. Use of different spatial parts, in this regard, is more relevant for the open-shell molecules and the corresponding theory is known as *unrestricted* Hartree-Fock (UHF) theory.

2.1.3 Correlation Energy

The Hartree-Fock theory gives the lowest energy for the electronic states presented by a single determinant. According to this theory each electron feels only the average positions of all the other electrons exerting an average field to disturb its motion. That is why this wave functional form does not allow any correlation between electrons except the Fermi correlation which comes from the antisymmetric nature of the determinant. However, the main contribution of the electronic correlation comes as the electrons avoid each other due to the Coulombic repulsion.

The correlation energy (E_{corr}) for an electronic system is measured as the difference between the exact energy (E_{exact}) obtained solving the electronic Schrödinger equation (Eq. 2.3) and the Hartree-Fock energy:

$$E_{corr} = E_{exact} - E_{HF}. \tag{2.17}$$

Even though this correlation energy is very small compared to the total energy of the system, it is very important to describe several electronic phenomenon, such as homolytic bond-breaking and transition-state, properly.

The correlation energy can be separated in to two components: *dynamic* and *static* correlations. Dynamic correlation treats the instantaneous effect of Coulomb repulsion between the electrons and thus it is a very short-range phenomenon. This kind of correlation has the main contribution to the total correlation energy for the closed shell molecules and can be recovered by expanding the wave function Ψ as a linear combinations of Slater determinants obtained through excitations of electrons from a reference like the HF determinant. Static correlation, on the other hand, is present when two or more orbitals have nearly equal energies and thus a single determinant can not represent the whole state alone. To include the static correlation, the electronic wave function should be presented at least as a combination of two or more quasi-degenerate n-electron determinants.

The exact energy of an electronic state, and therefore total electronic correlation, can be obtained for an atomic orbital basis of finite size by using a complete n-particle basis set $\{\Phi_q\}$. This complete basis set can be obtained by distributing the electrons in all the Hartree-Fock orbitals. With this expansion, Ψ leads to the full configuration interaction (FCI) wave function:

$$|\Psi_{FCI}\rangle = \sum_q c_q |\Phi_q\rangle. \tag{2.18}$$

Here c_qs are the combining coefficients which are obtained following the variational principle. However, FCI is computationally very expensive as the size of the determinant space $\{\Phi_q\}$ increases exponentially with the increasing number of electrons. So, a truncation of that space is needed in a way that it retrieves most part of the correlation energy but with a much lower computational cost.

2.1.4 The Multiconfigurational Self-Consistent Field Theory

Multiconfigurational self-consistent field (MCSCF) theory is an extension of the Hartree-Fock theory to a space of more than one determinant. The MCSCF theory is used to treat the static correlation by combining quasi-degenerate determinants, which is otherwise not possible within the HF framework. The MCSCF wave function is written as:

$$|\Psi_{MCSCF}\rangle = \sum_\mu c_\mu |\Phi_\mu\rangle. \tag{2.19}$$

Here c_μ and the orbitals in $|\Phi_\mu\rangle$ are determined variationally. MCSCF is more relevant for systems with two or more quasi-degenerate orbitals; so a common way to get the set of the determinants is by alternatively placing electrons on these quasi-degenerate orbitals. These orbitals are known as active orbitals, where all the other orbitals which are either occupied or empty in all these determinants are called inactive. This new space of determinants is known as the active space. If this active space contains all the determinants formed by distributing m active electrons over n active orbitals, it is called the *complete active space* or CAS(m,n). This special type MCSCF is called the complete active space self-consistent field (CASSCF) theory.

The CI coefficients c_μ are optimized variationally and this leads following eigenvalue equation:

$$\sum_\nu \langle \Phi_\mu | \hat{H} | \Phi_\nu \rangle c_\nu = E_{MCSCF} \ c_\mu, \tag{2.20}$$

which is similar to the working equation for the configuration interaction method. Thus MCSCF can be viewed as an CI method applied within an active space, but includes further improvement though optimization of the orbitals.

2.1.5 The Single-Reference Coupled Cluster Theory

For the molecular systems dominated by the dynamic correlation, it is important to add more configurations of the n-electron Hilbert space to define the wave function. As FCI is computationally very expensive and therefore restricted to smaller systems, a truncated version of it can be used as an alternative way of representing the wave function. Truncated configuration interaction uses a reduced space of determinants obtained through lower rank excitations from the HF reference. Though, this is computationally favorable, truncated CI is also not used much in practice as it is not size extensive. Size extensivity of a theory, along with the allied condition of size consistency, ensure that the method scales properly with the increasing size of an electronic system and thus they are very important requirements for a good quantum chemical method.

Use of an exponential ansatz to describe the wave function circumvent the problem of proper scaling for methods using HF as the reference. This method, known as the coupled cluster (CC) theory, uses an exponential form of the excitation operators acting on the HF determinant $|0\rangle$ as the reference:

$$|\Psi_{SRCC}\rangle = e^{\hat{T}} |0\rangle. \tag{2.21}$$

Here the excitation operator $\hat{T}$, also known as the cluster operator, has the expanded form:

$$\hat{T} = \underbrace{\sum_{ia} t_a^i \hat{a}_i^a}_{\hat{T}_1} + \underbrace{\frac{1}{4}\sum_{ijab} t_{ab}^{ij} \hat{a}_{ij}^{ab}}_{\hat{T}_2} + \cdots + \underbrace{\frac{1}{n!^2}\sum_{i\cdots a\cdots} t_{a_1\cdots a_n}^{i_1\cdots i_n} \hat{a}_{i_1\cdots i_n}^{a_1\cdots a_n}}_{\hat{T}_n} = \sum_{\rho} \hat{\tau}_\rho t_\rho, \tag{2.22}$$

where t_ρ is the cluster amplitude associated with the cluster operator $\hat{\tau}_p$. The highest rank possible for the cluster operators is the number of electrons correlated in the calculations.

The cluster amplitudes and corresponding energy for the CC theory are not obtained variationally, but by following the projection technique. Inclusion of the CC ansatz into the time-independent Schrödinger equation and pre-multiplications of both sides of equation by $e^{-\hat{T}}$ lead to the equation

$$\underbrace{e^{-\hat{T}}\hat{H}e^{\hat{T}}}_{\bar{H}}|0\rangle = E_{SRCC}|0\rangle. \tag{2.23}$$

The energy for the method can be obtained by projecting the Eq. 2.23 on to $\langle 0|$:

$$E_{SRCC} = \langle 0|\bar{H}|0\rangle, \tag{2.24}$$

whereas, projecting the same equation to the excitation determinant $\langle \Phi_\rho| = \langle 0|\hat{\tau}_\rho^\dagger$ leads to the amplitude equation for solving the cluster amplitudes:

$$0 = \langle 0|\tau_\rho^\dagger \bar{H}|0\rangle, \quad \forall\rho. \tag{2.25}$$

The amplitude equation 2.25 is a set of non-linear equations which is obvious from the expansion of the $\bar{H}$ following the Baker-Campbell-Hausdorff formula:

$$\bar{H} = e^{-\hat{T}}\hat{H}e^{\hat{T}} = \hat{H} + [\hat{H},\hat{T}] + \tfrac{1}{2}\big[[\hat{H},\hat{T}],\hat{T}\big] + \cdots . \tag{2.26}$$

Inclusion of the excitations up to the rank 'n' in $\hat{T}$ would give the exact FCI results as it spans the complete basis functions. However, in practice, the use of a truncated $\hat{T}$ such as the singles and doubles for CCSD or singles, doubles and triples for CCSDT produce very accurate energy and description of electronic systems. The CCSD and CCSDT have the polynomial scaling of $\mathcal{O}(\mathcal{N}^6)$ and $\mathcal{O}(\mathcal{N}^8)$ with $\mathcal{N}$ being the measure of the molecular size. Due to the large computational scaling of the CCSDT methods, an intermediate method, known as CCSD(T), is used alternatively which includes the corrections for the triples perturbatively on top of the CCSD results and thus reducing the scaling to be $\mathcal{O}(\mathcal{N}^7)$. CCSD(T) is used extensively for the accuracy of the results that it provides at a

computational cost which makes it possible to be used for medium-sized molecules. That is why this method is often referred as the 'gold standard' in quantum chemistry.

2.1.6 Multireference Coupled Cluster: Overview

Multireference (MR) methods are very important in quantum chemistry, especially for systems with quasidegenerate states, as they give a balanced description of both the static and dynamical correlations of the system. These two different forms of correlations can be achieved individually through CASSCF and SRCC methods, respectively. Both CASSCF and SRCC results can be hierarchically improved, with respective increases in the size of the active space and in the rank of the cluster operator, to finally converge them to the FCI results. However, this comes at a cost of a rapid increase in the computational scaling. Multireference coupled cluster (MRCC) methods [75], can be used as a 'shortcut' towards FCI as they use the exponential ansatz of the coupled cluster theory acting on top of a multideterminantal reference of CASSCF. Thus MRCC theories treat both of the static and dynamic part of the correlation energy together.

The related multireference configuration interaction (MRCI) is a generalization of the single-reference CI method by applying the same ansatz on the top of a CASSCF reference [76]. However, like its single-reference counterpart, the truncated MRCI methods are not size-extensive even though several attempts have been made [77, 78] to correct this deficiency though approximations.

A direct use of an exponential ansatz on multideterminantal reference function would lead to a MRCC formalism which, similarly to its single-reference counterpart, will give size-extensive energies. But, unlike SRCC, there is no unique way to formulate the MRCC method as the excitation manifold which is generated through excitations from the determinants residing in the active space are not completely separated unique configurations.

There are two different ways to build up MRCC wave function on top of a multideterminantal reference. The first one, as proposed initially by Jeziorski and Monkhorst [14], uses a separate exponential form of cluster operators for each of the reference determinants before combining them together:

$$|\Psi_{\mathrm{JM}}\rangle = \sum_{\mu} e^{\hat{T}_\mu} |\Phi_\mu\rangle c_\mu. \tag{2.27}$$

This ansatz, known as the Jeziorski-Monkhorst (JM) ansatz, was first used in developing a state-universal formulation of MRCC (SUMRCC) where all states which can be spanned within the CAS are solved simultaneously [14, 79, 80]. The SUMRCC theory leads to the

intruder state problem whenever there is an overlap in energies between configurations inside and outside of the CAS. There are several approaches which use an alternative way by targeting one single state while using the same ansatz, known generally as state-specific multireference coupled cluster theory (SS-MRCC). The Brillouin-Wigner multireference coupled cluster theory (BW-MRCC) theory [81, 82] and the Mukherjee multireference coupled cluster (Mk-MRCC) theory [16, 19, 83–85] are well-known examples of such methods. As these methods solve for a particular state, they suffer from the problem of not having enough equations to match the number of parameters used within the JM ansatz. By introducing further restriction, known as *sufficiency conditions*, these methods produce more amplitude equations to solve this problem. However, this also introduces an over-complete space of the excited state configurations for these methods. There is another way out of this problem, explored in the MRexpT method [20, 86], where the number of amplitudes are rather reduced to match the number of equations.

Among the SSMRCC methods, Mk-MRCC obeys the important property of size-extensivity which makes it most popular among the allied methods. Mk-MRCC has also been extended for further developments of optimizing geometries through analytic gradient technique and calculating molecular properties along with excitation energies through a linear response formalism [64, 65]. However, there are shortcomings of the Mk-MRCC theory as it produces energies which are not invariant under rotation of the active orbitals and thus they depend heavily on the choice of the orbitals used for the calculations. Applications of Mk-MRCC for calculating the excitation energies and dynamic polarizabilities introduce further of its shortcomings by indicating spurious poles coming due to the over-complete space of excited configurations.

A completely different ansatz, as the alternative way of using MCSCF function as reference, can be designed where a single exponential form of cluster operator is applied on the entire multi-determinantal reference,

$$|\Psi_{\rm ic}\rangle = e^{\hat{T}} \sum_{\mu} |\Phi_\mu\rangle c_\mu. \tag{2.28}$$

which is a fully internally contracted ansatz. This ansatz leads to different variants of the internally contracted MRCC (ic-MRCC) theory. The ic-MRCC theory was first introduced by Banerjee and Simons [15, 21] in the context of a state-specific theory. The variant of ic-MRCC, as introduced in these references, involved limited classes of excitation operators. A full use of all the excitation classes for the same formulation have recently been done separately by Evangelista *et al.* [17] and Hanauer *et al.* [18]. Where all of these variants use the HF determinant to define the normal ordering of all the operators involved in the second quantization technique, a variant of ic-MRCC have also been proposed by Mukherjee *et al.* [16, 24] which uses the CASSCF reference to define

the normal ordering of the excitation operators following the *generalized normal ordering* framework [23, 87, 88].

The variant of ic-MRCC as implemented by Hanauer *et al.* has further been extended to include the perturbative correction due to triples [25] and the effect of explicit correlation through the F12 formalism [26]. In this work, formulation of a linear response (LR) theory based on this variant of ic-MRCC has been done and latter applied to calculate molecular properties along with excitation energies of molecules. Before staring the development of the LR formulation for the ic-MRCC theory, a brief description of this ic-MRCC variant is given in Chap. 3, whereas a description of LR theory is given in the next section.

2.2 Methods to Obtain Molecular Properties

2.2.1 Molecular Properties as Energy Derivatives

Molecular properties can be obtained as the derivatives of the energy with respect to the external perturbations [89, 90]. With the Hamiltonian being represented in presence of perturbations as:

$$\hat{H} = \hat{H}_0 + \sum_X \varepsilon_X \hat{X}, \tag{2.29}$$

the energy can be expanded following the Taylor expansion:

$$E(\boldsymbol{\varepsilon}) = E(\mathbf{0}) + \sum_X \varepsilon_X \frac{dE}{d\varepsilon_X}|_{\varepsilon_X=0} + \sum_{X,Y} \frac{1}{2}\varepsilon_X\varepsilon_Y \frac{d^2E}{d\varepsilon_X d\varepsilon_Y}|_{\varepsilon_X=\varepsilon_Y=0} + ... \tag{2.30}$$

Here, $\hat{H}_0$ represents the unperturbed electronic Hamiltonian and $\hat{X}$ is the perturbation operator with corresponding field-strength parameter ε_X. The energy derivatives of different order are identified as the molecular properties and they help describing the response of a molecular system in presence of the external perturbations [90]. For example, in presence of an electrical field, which is the case for most of the properties calculated in this thesis, the first and second derivatives of the energy represent the dipole moment (μ) and the polarizability (α) of the system, respectively:

$$\mu_X = -\frac{dE}{d\varepsilon_X}|_{\varepsilon_X=0}, \tag{2.31}$$

$$\alpha_{XY} = -\frac{d^2E}{d\varepsilon_X d\varepsilon_Y}|_{\varepsilon_X=\varepsilon_Y=0}. \tag{2.32}$$

These energy derivatives can be calculated by differentiating the energies numerically. Energies of the molecular system for different field-strength parameters are calculated and used to get the properties as the finite differences of these energies [27]. Use of the numerical differentiation technique is disadvantageous as it requires to calculate energies for several field-strength depending on the perturbative order of the properties. A better way of getting these energy derivatives is by differentiating the energy expression analytically which then involves derivatives of the different components of the energy such as the wave function parameters. Assuming the energy to be dependent of the field-strength parameters ($\boldsymbol{\varepsilon}$) and the wave function parameters ($\mathbf{c}$) as:

$$E = E(\boldsymbol{\varepsilon}, \mathbf{c}), \tag{2.33}$$

a simple first derivative will look like:

$$\frac{dE}{d\boldsymbol{\varepsilon}} = \frac{\partial E}{\partial \boldsymbol{\varepsilon}} + \frac{\partial E}{\partial \mathbf{c}} \frac{\partial \mathbf{c}}{\partial \boldsymbol{\varepsilon}}. \tag{2.34}$$

This shows the requirement of the first derivative of the wave function parameters with respect to $\boldsymbol{\varepsilon}$ for calculating the first order properties. However, this requirement can be avoided for the variational methods in quantum chemistry which ensures that the energy is optimized with respect to the wave function parameters, *i.e.* $\frac{\partial E}{\partial \mathbf{c}} = 0$. This requirement is extended for properties of any order through formulation of the (2n+1) rule [53] which says that the wave function parameters of order 'n' is sufficient for calculating properties of the order '2n+1'. However, for non-variational methods in quantum chemistry, such as the coupled cluster theory, the condition $\frac{\partial E}{\partial \mathbf{c}} = 0$ is not satisfied. Thus, a Lagrangian is formulated which is then variationally optimized with respect to all of its constituent parameters. The wave function parameters then follow the same (2n+1) rule, where the Lagrange multipliers, introduced while defining the Lagrangian, follow a new (2n+2) rule [52, 53].

The analytic expressions of molecular properties of different orders can be obtained through two different techniques. Where the analytic gradient method [34, 35] is used mostly for the time-independent perturbations, the response method [50, 51] is formulated considering the presence of the time-dependent perturbations. As the work in the thesis is based on formulating the response approach on top of a ic-MRCC wave function, the basics of this approach is given in the next section.

2.2.2 Response Theory

Response theory [32, 53, 66, 67, 91] is a formalism used for the calculation of the frequency-dependent molecular properties as it considers the presence of the time-dependent perturbations. Within this approach, a molecular system, with the electronic Hamiltonian H_0 and a time-dependent periodic perturbation $\hat{V}(\mathsf{t})$ applying on it, is described by an wave function determined from the time-dependent Schrödinger equation:

$$\hat{H}|\bar{0}\rangle = i\frac{\partial}{\partial \mathsf{t}}|\bar{0}\rangle, \tag{2.35}$$

where, $\hat{H} = \hat{H}_0 + \hat{V}(\mathsf{t})$. The explicit time-dependence of the wave function $|\bar{0}\rangle$ is suppressed here. The time-dependent periodic perturbation can be described as sum of different fields:

$$\begin{aligned} \hat{V}(\mathsf{t}) &= \sum_{k=-N}^{N} e^{-i\omega_k \mathsf{t}} \hat{V}(\omega_k) \\ &= \sum_{k=-N}^{N} e^{-i\omega_k \mathsf{t}} \sum_{X} \varepsilon_X(\omega_k)\hat{X}. \end{aligned} \tag{2.36}$$

Here, the total perturbation contains several monochromatic oscillating fields $\hat{V}(\omega_k)$ which could be expressed as a sum of perturbation operators X with corresponding strength parameters $\varepsilon_x(\omega_k)$. Here $\omega_k = k\omega$ where $\omega = (2\pi)/T$ is the fundamental frequency, T being the time period of the perturbation $\hat{V}(\mathsf{t})$. The perturbation operator is Hermitian:

$$\hat{V}(\mathsf{t}) = \hat{V}(\mathsf{t})^{\dagger}, \tag{2.37}$$

which ensures the following relations:

$$\hat{X}^{\dagger} = \hat{X}, \tag{2.38}$$

and

$$\varepsilon_X^*(\omega_k) = \varepsilon_X(\omega_{-k}). \tag{2.39}$$

The solution of the eq. 2.35, $|\bar{0}\rangle$, can be written as the phase isolated form of:

$$|\bar{0}\rangle = e^{-iF(\mathsf{t})}|\tilde{0}\rangle. \tag{2.40}$$

$|\tilde{0}\rangle$ is still time-dependent and it reduces to the time-independent wave function $|0\rangle$ in the unperturbed limit that follows,

$$\hat{H}_0|0\rangle = E_0|0\rangle. \tag{2.41}$$

Insertion of the ansatz in presented in Eq. 2.40 into the time-dependent Schrödinger equation gives,

$$e^{-iF(\mathsf{t})}\left(\hat{H} - i\frac{\partial}{\partial \mathsf{t}} - \dot{F}(\mathsf{t})\right)|\tilde{0}\rangle = 0. \tag{2.42}$$

The equation has the phase isolated form:

$$\left(\hat{H} - i\frac{\partial}{\partial \mathsf{t}} - \dot{F}(\mathsf{t})\right)|\tilde{0}\rangle = 0, \tag{2.43}$$

which after projecting onto $\langle\tilde{0}|$ gives $\dot{F}(\mathsf{t})$ as:

$$\dot{F}(\mathsf{t}) = \langle\tilde{0}|\left(\hat{H} - i\frac{\partial}{\partial \mathsf{t}}\right)|\tilde{0}\rangle = Q(\mathsf{t}). \tag{2.44}$$

In the unperturbed limit of eq. 2.44, $\dot{F}(\mathsf{t})$ reduces to the time-independent energy E_0. Thus the term $\dot{F}(\mathsf{t})$ is denoted as the quasienergy or $Q(\mathsf{t})$.

In Response theory, the strengths of the perturbations are assumed to be small in order to solve the time-dependent Schrödinger equation perturbatively. The quasienergy and wave function can be expanded, therefore, in orders of perturbation. Likewise, the time-dependent average value of a particular perturbation X can also be expanded in order of perturbation and the corresponding expansion coefficients give the response functions of different orders, as:

$$\begin{aligned}
\langle X\rangle(\mathsf{t}) &= \langle\bar{0}|\hat{X}|\bar{0}\rangle = \langle\tilde{0}|\hat{X}|\tilde{0}\rangle \\
&= \langle X\rangle_0 + \sum_Y \varepsilon_Y \langle\langle X;Y\rangle\rangle_{\omega_Y} e^{-i\omega_Y \mathsf{t}} \\
&+ \frac{1}{2}\sum_{Y,Z} \varepsilon_Y \varepsilon_Z \langle\langle X;Y,Z\rangle\rangle_{\omega_Y,\omega_Z} e^{-i(\omega_Y+\omega_Z)\mathsf{t}} + \cdots
\end{aligned} \tag{2.45}$$

For simplicity of the expressions, the frequencies now have the indices of the corresponding perturbation operators. Here $\langle\langle X;Y\rangle\rangle_{\omega_Y}$ is the linear response function of X under the influence of another perturbation Y with frequency ω_Y. Frequency dependent second order properties are obtained from the linear response function. For example, dynamic dipole polarizability is obtained from the linear response function as:

$$\alpha_{XY}(\omega_X,\omega_Y) = -\langle\langle\mu_X;\mu_Y\rangle\rangle_{\omega_Y}, \qquad \omega_Y = -\omega_X, \tag{2.46}$$

where μ_X and μ_Y are the components of the dipole operator. Here, the corresponding static polarizability is obtained in the zero frequency limit. The nonlinear response function, $\langle\langle X;Y,Z\rangle\rangle_{\omega_Y,\omega_Z}$, is used similarly to calculate the third order properties. Considering X to be a Hermitian operator, the expectation value $\langle X\rangle(\mathsf{t})$ is real. By comparing the expression of $\langle X\rangle(\mathsf{t})$ and its complex conjugate it can be shown that the response functions follow the symmetry properties:

$$\langle X\rangle_0 = \langle X\rangle_0^*, \tag{2.47}$$

$$\langle\langle X;Y\rangle\rangle_{\omega_Y} = \langle\langle X;Y\rangle\rangle_{-\omega_Y}^*, \tag{2.48}$$

and,

$$\langle\langle X;Y,Z\rangle\rangle_{\omega_Y,\omega_Z} = \langle\langle X;Y,Z\rangle\rangle_{-\omega_Y,-\omega_Z}^*. \tag{2.49}$$

For a variationally optimized wave function, the response functions are obtained directly from the time averaged quasienergy $\{Q(\mathsf{t})\}_T$ where time-averaging is done over the time-period of the perturbation. For a non-variationally optimized wave function, use of a time averaged Lagrangian $\{L(\mathsf{t})\}_T$ is necessary following the same argument as discussed in the previous section. The time-dependent Lagrangian $L(\mathsf{t})$ for a non-variational method is obtained by summing up the quasienergy and the equations to solve the wave function parameters multiplied by corresponding Lagrange multipliers. The time-averaged Lagrangian is obtained from this Lagrangian after expanding all the operators into its Fourier components and then integrating it over a time period as:

$$\{L(\mathsf{t})\}_T = \frac{1}{T}\int_{\mathsf{t}_0}^{\mathsf{t}_0+T} L(\mathsf{t})dt \tag{2.50}$$

The response functions are expressed as the derivatives of this time-averaged Lagrangian as follows:

$$\langle X\rangle_0 = \frac{d\{L(\mathsf{t})\}_T}{d\varepsilon_X(0)}, \tag{2.51}$$

$$\langle\langle X;Y\rangle\rangle_{\omega_Y} = \frac{d^2\{L(\mathsf{t})\}_T}{d\varepsilon_X(\omega_X)\varepsilon_Y(\omega_Y)}; \qquad \omega_X = -\omega_Y, \tag{2.52}$$

and

$$\langle\langle X;Y,Z\rangle\rangle_{\omega_Y,\omega_Z} = \frac{d^3\{L(\mathsf{t})\}_T}{d\varepsilon_X(\omega_X)\varepsilon_Y(\omega_Y)\varepsilon_Z(\omega_Z)}; \qquad \omega_X = -(\omega_Y+\omega_Z). \tag{2.53}$$

To further simplify the expressions of the response functions, the time-averaged Lagrangian can be expanded into components of different perturbative orders. The explicit

dependence of those components on the field-strength can be shown as:

$$\{L(\mathsf{t})\}_T^{(0)} = L^{(0)}, \tag{2.54}$$

$$\{L(\mathsf{t})\}_T^{(1)} = \sum_X \varepsilon_X(0) L^X(0) \tag{2.55}$$

$$\{L(\mathsf{t})\}_T^{(2)} = \frac{1}{2} \sum_{X,Y} \varepsilon_X(\omega_X)\varepsilon_Y(\omega_Y) L^{XY}(\omega_X, \omega_Y); \quad \omega_X = -\omega_Y \tag{2.56}$$

$$\{L(\mathsf{t})\}_T^{(3)} = \frac{1}{6} \sum_{X,Y,Z} \varepsilon_X(\omega_X)\varepsilon_Y(\omega_Y)\varepsilon_Z(\omega_Z) L^{XYZ}(\omega_X, \omega_Y, \omega_Z); \quad \omega_X = -(\omega_Y + \omega_Z) \tag{2.57}$$

Here the components of the Lagrangian — $L^X(0)$, $L^{XY}(\omega_X, \omega_Y)$ and others with higher order — are independent of the field-strength parameters. While these components are dependent of the frequencies of the external fields, the sum of these frequencies are zero due to the time averaging.

The expression of the time-averaged Lagrangian consists of different parameters, such as wave function parameters and the Lagrange multipliers, which are now frequency-dependent. Thus it is important to understand the Fourier decomposition of these frequency-dependent parameters of different orders. The Fourier decompositions of all the initial time-parameters are done after expanding the these parameters, denoted here generally as $\mathrm{p}(\mathsf{t})$, to their perturbative orders as:

$$p(\mathsf{t}) = p^{(0)} + p^{(1)}(\mathsf{t}) + p^{(2)}(\mathsf{t}) + \cdots . \tag{2.58}$$

Here, the zeroth order parameters can be obtained in absence of the perturbation and thus they are time-independent. The higher-order parameters can then be expanded as sums of their Fourier components which now depend on the frequencies of the periodic perturbations [53]:

$$p^{(1)}(\mathsf{t}) = \sum_X e^{-i\omega_X \mathsf{t}} \varepsilon_X(\omega_X) p^X(\omega_X), \tag{2.59}$$

and

$$p^{(2)}(\mathsf{t}) = \sum_{X,Y} e^{-i(\omega_X+\omega_Y)\mathsf{t}} \varepsilon_Y(\omega_X)\varepsilon_Y(\omega_Y) p^{XY}(\omega_X, \omega_Y). \tag{2.60}$$

Here the Fourier components of the parameters , p^X and p^{XY}, are independent of the field-strength parameters and they are used to calculate the response functions of the electronic system. Understanding of these Fourier components will be useful while developing the

linear response formalism for the ic-MRCC theory in Chap. 4.

Excitation energies can be found from the linear response function as its poles. The linear response function, which is generally obtained from the Lagrangian following Eq. 2.52, can also be written following the sum-over-state representation [52, 53] as:
.

$$\langle\langle X;Y\rangle\rangle_{\omega_Y} = \sum_{i\neq 0}\left[\frac{\langle\Psi_0|\hat{X}|\Psi_i\rangle\langle\Psi_i|\hat{Y}|\Psi_0\rangle}{\omega_Y-\omega_i} - \frac{\langle\Psi_0|\hat{Y}|\Psi_i\rangle\langle\Psi_i|\hat{X}|\Psi_0\rangle}{\omega_Y+\omega_i}\right] \tag{2.61}$$

Here, $|\Psi_0\rangle$ and $|\Psi_i\rangle$ are the ground and excited states respectively and ω_i is the corresponding excitation energy. The linear response function diverges to infinity when ω_Y approaches the excitation energies giving a pole here at ω_i. Excitation energies, thus, can be calculated by finding these poles of the linear response function.

3 | Fundamentals of ic-MRCC

Before developing the response formulation based on the ic-MRCC theory, the basics of the ic-MRCC theory are described here briefly following refs [18, 92]. Apart from formulating the equations for solving the wave function parameters and getting the energy, some other aspects of the theory, such as the procedures to get the linearly independent excitations and the formal truncation of the commutator approximation involved in ic-MRCC, are also discussed in this chapter.

3.1 Ansatz and Equations of ic-MRCC

The ic-MRCC ansatz is defined by a single exponential wave operator that acts on a reference function $|\Psi_0\rangle$ giving rise to the ic-MRCC wave function $|\Psi\rangle$:

$$|\Psi\rangle = e^{\hat{T}}|\Psi_0\rangle. \tag{3.1}$$

The reference used here is a CASSCF wave function which is a linear combination of the determinants coming from the complete active space (CAS):

$$|\Psi_0\rangle = \sum_{\mu} |\Phi_\mu\rangle c_\mu, \tag{3.2}$$

with c_μ being the corresponding coefficients. The cluster operator, $\hat{T}$

$$\hat{T} = \sum_{IA} t_A^I \hat{a}_I^A + \tfrac{1}{4} \sum_{IJAB} t_{AB}^{IJ} \hat{a}_{IJ}^{AB} + \ldots = \sum_{\rho} \hat{\tau}_\rho t_\rho, \tag{3.3}$$

includes all the possible excitation from the combined set of occupied and active orbitals (indexed by $I, J, \ldots$) to the combined set of active and unoccupied orbitals (indexed by $A, B, \ldots$). As the ansatz for ic-MRCC looks more like that of the single-reference coupled cluster theory, the subsequent equations for solving the cluster amplitudes and getting energy are also obtained similarly. Putting the ic-MRCC wave function into the

Schrödinger equations and then pre-multiplying it with $e^{-\hat{T}}$, an equation is obtained involving a similarity transformed Hamiltonian $\bar{H}$:

$$\bar{H}|\Psi_0\rangle = E|\Psi_0\rangle, \tag{3.4}$$

where $\bar{H} = e^{-\hat{T}}\hat{H}e^{\hat{T}}$. The energy for ic-MRCC can be obtained by projecting Eq. 3.4 onto the reference function $|\Psi_0\rangle$:

$$E = \langle\Psi_0|\bar{H}|\Psi_0\rangle, \tag{3.5}$$

where equations to solve the cluster amplitudes emerge from projecting the same equation onto the excited functions $\hat{\tau}_\rho|\Psi_0\rangle$:

$$\langle\Psi_0|\hat{\tau}_\rho^\dagger\bar{H}|\Psi_0\rangle = 0. \tag{3.6}$$

The right-hand side of Eq. 3.6 is zero as the internal excitations, involving only the active-active transition, are excluded from the set of cluster operators in contrary to its general definition in Eq. 3.3. However the contributions of these configurations to the final wave function are rather obtained by relaxing the reference coefficients c_μ. These coefficients are obtained by solving the eigenvalue equation which is produced through the projection of Eq. 3.4 onto the reference determinants $|\Phi_\mu\rangle$:

$$\sum_\nu \langle\Phi_\mu|\bar{H}|\Phi_\nu\rangle c_\nu = Ec_\mu. \tag{3.7}$$

The energy for ic-MRCC can also be obtained as an eigenvalue of this equation.

There are redundancies in Eq. 3.6 due to linear dependencies between the excited functions $\hat{\tau}_\rho|\Psi_0\rangle$. These redundancies are avoided by finding a set of linearly independent excited functions $\hat{\tau}'_\rho|\Psi_0\rangle$, where the new set of excitation operators $\hat{\boldsymbol{\tau}}'$ are obtained through a transformation of the primitive excitation operators following:

$$\hat{\tau}'_\rho = \sum_\sigma \hat{\tau}_\sigma X_\rho^\sigma, \tag{3.8}$$

with the $\mathbf{X}$ being the transformation matrix. The cluster operator can now be written in terms of the new excitation operators and corresponding cluster amplitudes t' as:

$$\hat{T} = \sum_\rho \hat{\tau}'_\rho t'_\rho. \tag{3.9}$$

After this transformation the new cluster amplitudes are solved from a modified form of the Eq. 3.6:

$$\langle \Psi_0 | \hat{\tau}_\rho'^\dagger \bar{H} | \Psi_0 \rangle = 0. \tag{3.10}$$

The ic-MRCC wave function and its energy are then obtained by simultaneously solving the eigenvalue equation and the amplitude equation presented in the Eqs. 3.7 and 3.10, respectively.

The ic-MRCC wave function and energy depend on the way the redundancy in the excitation manifold is removed. Details about how the linearly independent excitation manifold are obtained in different ways are discussed in Sec. 3.3.

3.2 Approximation in the Commutator Expansion

After applying the BCH expansion, the similarity transformed Hamiltonian, $\bar{H}$, can be written in a similar way of the SRCC theory as:

$$\bar{H} = e^{-\hat{T}} \hat{H} e^{\hat{T}} = \hat{H} + [\hat{H}, \hat{T}] + \tfrac{1}{2}\big[[\hat{H}, \hat{T}], \hat{T}\big] + \cdots . \tag{3.11}$$

With this expansion, both of the amplitude equation and the eigenvalue equation for solving reference coefficients, Eqs. 3.6 and 3.7 respectively, can now be visualized as series of terms with increasing polynomials of the cluster operators which comes from the commutation presented in Eq. 3.11. One of the important aspect for ic-MRCC is, therefore, to study the formal truncation of these terms in both of these equations. The facts that the Hamiltonian includes excitations till rank two and that the cluster operators commute with each other, the expansion of $\bar{H}$ truncates in the quartic power for SRCC. For ic-MRCC, however, the cluster operators do not commute with each other due the simultaneous creation and annihilation of the active orbitals and thus the expansion does not truncate formally at ranks as low as quartic. Inclusion of terms higher in polynomial order of $\hat{T}$ increases the computational cost of the calculations.

The operators in ic-MRCC are divided in several classes, each having a specific number of inactive hole (n_h) and particle (n_p) indices. Within the same class, operators can be of different ranks which are solely determined by the number of electrons getting excited by the operator. All the different classes of excitation operators used in the ic-MRCC theory with singles and doubles (ic-MRCCSD) are depicted in the Ref. [18]. By definition, this excitation operators have at least one inactive line. The highest number of $\hat{T}$ operators which can be present trough the commutator expansion will then be governed by how many of their inactive lines can be absorbed by the two-body Hamiltonian.

Therefore, for eigenvalue equation (Eq. 3.7) $\bar{H}$ truncates at quartic power irrespective of the rank of $\hat{T}$. For the amplitude equation, on the other hand, this truncation is bounded by the maximum excitation rank of $\hat{T}$ according to

$$N_{\text{com}} \leq 4 + 2N_{\text{rank}}, \tag{3.12}$$

where N_{com} denotes the order of the commutator used in $\bar{H}$ which also determines the polynomial order of the $\hat{T}$. For ic-MRCCSD, the full amplitude equation will involve up to eight fold commutators. However, inclusion of all these terms will cost the computational efficiency of the method. Thus, for an efficient implementation of ic-MRCCSD, the commutator expansion of $\bar{H}$ should be truncated at a lower order as an approximation. Truncating the commutator expansion at the quadratic level has been proved very useful in this regards, as presented in the Ref. [92]. This approximation procures most of the correlation energy of the full method but with much less computational effort. Use of the reference functions to produce the static part of the correlation energy facilitate the accuracy of this approximation. The ic-MRCC calculations done in this thesis are mostly done using the quadratic truncation of the $\bar{H}$ for both the amplitude equation and the eigenvalue equation, unless it is mentioned otherwise.

3.3 Redundancy Problem in ic-MRCC

The redundancy problem in ic-MRCC arises as the excited functions $\{\hat{\tau}_\rho|\Phi_0\rangle\}$ are not linearly independent. This leads to a non-diagonal overlap (metric) matrix $\mathbf{S}$ for ic-MRCC with the matrix elements being:

$$S^\sigma_\rho = \langle\Psi_0|\hat{\tau}^\dagger_\sigma\hat{\tau}_\rho|\Psi_0\rangle. \tag{3.13}$$

The metric matrix $\mathbf{S}$ can be further written as direct sum of metric matrices corresponding to individual excitation classes of the operators. Here, for ic-MRCC, the different excitation classes are defined depending on the specific number of inactive holes (n_h) and inactive particles (n_p) that the operators have. For each classes $\mathbf{S}$ can again be decomposed into a product of a tensor $\mathbf{S}^{n_h,n_p}_{act}$ with active indices and an unit tensor with inactive indices. Thus, $\mathbf{S}$ has the form:

$$\mathbf{S} = \bigoplus_{n_h,n_p}\left(\mathbf{S}^{n_h,n_p}_{act} \otimes \mathbf{1}^{n_h,n_p}_{inact}\right). \tag{3.14}$$

This shows that the linear dependencies arise because of the mixing of operators within the same operator class and with the same inactive orbital index.

There are two main reasons behind the occurrence of these linear dependence in the set of excited functions. Use of a combination of determinants as a reference function is the first reason. Different operators with the same inactive lines but different active lines can produce the same configuration when acted on the reference. As an example, the operators $\hat{a}^{ab}_{uv}$ and $\hat{a}^{ab}_{wx}$ lead to same excited function when they are acted on a multi-determinantal reference of $|\Psi_0\rangle = \hat{a}^{uv}|0\rangle c_{uv} + \hat{a}^{wx}|0\rangle c_{wx}$. A second type of linear dependencies arises due to the presence of the excitation operators which excite electron from one active orbital to the same one. This kind of excitations, known as the *spectator* excitations, are inherent to the multireference theories. This kind of linear dependencies occur simply because of the inclusion of the higher rank excitations within a class of operators.

Removal of these redundancies for an internally contracted ansatz has been achieved in various ways [16, 93–98]. The common technique used in all of these methods is the singular value decomposition (SVD) of the metric matrix. SVD is done by first diagonalizing the metric matrix $\mathbf{S}$ as:

$$\mathbf{s} = \mathbf{U}^{\dagger}\mathbf{S}\mathbf{U}, \tag{3.15}$$

where $\mathbf{s}$ is a diagonal matrix containing the eigenvalues of the metric matrix $\mathbf{S}$. Now, as there are linear dependencies in the excited functions which construct $\mathbf{S}$, some of the corresponding eigenvalues will be very small. The linearly independent set of excitations is, therefore, obtained after discarding the eigenvectors corresponding to the eigenvalues below a certain threshold η. The choice of this threshold η is more important for active spaces greater that CAS(2e,2o), as different choices of η change the ic-MRCC results significantly for the larger CAS. The transformation matrix $\mathbf{X}$, as defined in the Eq. 3.8 in the context of obtaining the set of linearly independent excitations, is obtained through the Löwdin orthogonalization [17, 98, 99]:

$$\mathbf{X} = \mathbf{U}\mathbf{s}_{\eta}^{-\frac{1}{2}}. \tag{3.16}$$

Here $\mathbf{s}_{\eta}$ is the same as $\mathbf{s}$ but has all the eigenvalues which are below the threshold η replaced by zero. Use of this transformation matrix $\mathbf{X}$ ensures that the resulting excited functions $\{\hat{\tau}'_{\rho}|\Phi_0\rangle\}$ are mutually orthogonal with the corresponding metric matrix being a truncated unit matrix:

$$\mathbf{S}' = \mathbf{X}^{\dagger}\mathbf{S}\mathbf{X} = \mathbf{1}_{\eta}. \tag{3.17}$$

Within this common set up of the singular value decomposition technique, various approaches of choosing the set of non-redundant operators differ in the way operators of different ranks are mixed. As it is mentioned earlier in this section, the linear dependencies occur within the same class of operators and hence operators of different ranks can

mix through $\mathbf{X}$ while defining the new set of excited functions through SVD. This can be easily exemplified by the full orthogonalization of $\mathbf{S}$ which has non-zero off-diagonal elements as they are the overlaps between operators of different ranks. Hence, operators of different ranks get mixed through the diagonalization. ic-MRCC methods as developed by Evangelista *et al.* [17] used this formulation for the extraction of the linearly independent excitations. However, mixing of operators with different rank is not a desirable feature for a internally contracted method, as i) it would not be possible to assign different perturbation orders to operators of different ranks which is necessary in the realm of perturbative approximations of the theory and ii) it will no longer be a size-extensive theory [17].

Use of the sequential orthogonalization procedure in the internally contracted formulations [18, 98] has been proven to be very useful in this regard. In this approach, orthogonalization procedures are done separately for operators of different ranks with the aim of a minimal mixing between them. Where a projective approach has been used for the sequential orthogonalization technique in the Ref. [18], there exists an alternative approach implemented in a unpublished work of Köhn *et al.* where a Gram-Schmidt like scheme has been used getting inspired by the work of Mukherjee and co-workers [100]. A brief descriptions about how the operators of different ranks are mixed for the different orthogonalization techniques is shown in Tab. 3.1 by writing out the structure of respective transformation matrices.

TABLE 3.1: Structure of the transformation matrix ($\mathbf{X}$) for different orthogonalization technique while using singular value decomposition (SVD) method [101]. Different forms of $\mathbf{X}$ show how operators of different rank combine to form the linearly independent set of orbitals. $\mathbf{Q}_2$ is a projector that projects into the space of operators of rank 2.

	full orthogonalization	Sequential orthogonalization	
		Projective	Gram-Schmidt-based
transformation matrix ($\mathbf{X}$)	$\begin{pmatrix} \tilde{\mathbf{X}}_{11} & \tilde{\mathbf{X}}_{12} \\ \tilde{\mathbf{X}}_{21} & \tilde{\mathbf{X}}_{22} \end{pmatrix}$	$\begin{pmatrix} \mathbf{X}_1 & 0 \\ 0 & \mathbf{Q}_2\mathbf{X}_2 \end{pmatrix}$	$\begin{pmatrix} \mathbf{X}_1 & -\mathbf{X}_1\mathbf{X}_1^\dagger\mathbf{S}_{12}\mathbf{X}_2 \\ 0 & \mathbf{X}_2 \end{pmatrix}$
size-extensivity	no	core-extensive	yes

3.4 The ic-MRCC Lagrangian

The Lagrangian for the ic-MRCC theory has been formulated in the Refs. [18, 92]. The form of this Lagrangian has been used to include the correction due to triples perturbatively in ic-MRCCSD(T) [25]. This Lagrangian can also be used to calculate time-independent properties and gradients for ic-MRCC by adding the perturbations to the electronic Hamiltonian. The Lagrangian for ic-MRCC has been formulated by adding the amplitude equation (Eq. 3.6) and the eigenvalue equation (Eq. 3.7), each multiplied by two new Lagrange multipliers, to the ic-MRCC energy E. After some rearrangement, the Lagrangian gets the final form:

$$\mathcal{L} = \langle\overline{\Psi}_0|\bar{H}|\Psi_0\rangle + \langle\Psi_0|\hat{\Lambda}\bar{H}|\Psi_0\rangle - E\big(\langle\overline{\Psi}_0|\Psi_0\rangle - 1\big). \tag{3.18}$$

The Lagrangian is expressed by defining two new operators made using the Lagrange multipliers. The left-hand reference function absorbs the Lagrange multiplier $\bar{c}_\mu$:

$$\langle\overline{\Psi}_0| = \sum_\mu \bar{c}_\mu\langle\Phi_\mu|, \tag{3.19}$$

where the other multiplier λ'_ρ is absorbed in to the Lambda operator:

$$\hat{\Lambda} = \sum_\rho \lambda'_\rho \hat{\tau}'^{\dagger}_\rho. \tag{3.20}$$

If this Lagrangian is variationally optimized with respect to the Lagrange multipliers $\bar{c}_\mu$ and λ'_ρ, it leads to the equations for solving the wave function parameters c_μ and t'_ρ which are equivalent to the Eqs. 3.7 and 3.6, respectively. So, at its stationary point when the Lagrangian is optimized with respect to all of its parameters, it is reduced to the ground state energy. While formulating the response theory for the ic-MRCC theory, a time-dependent equivalent of this Lagrangian will be developed which will be a more general form of this Lagrangian and will consider any general form of Hamiltonian.

4 | Response Formalism for the ic-MRCC Theory

In this chapter, the response theory, details of which has been described in Sec. 2.2.2, is applied on top of the ic-MRCC wave function. As a first step of this response approach, a time-dependent Lagrangian is formulated for the ic-MRCC theory considering the presence of a periodic external field. The time-dependent Lagrangian is transformed into a time-averaged one where the averaging is done over its time-period. Properties of different orders are obtained as derivatives of this time-averaged Lagrangian. Even though response functions, and therefore properties, of any general order can be obtained from this response formalism, the work in thesis is restricted in deriving expressions for first and second order properties obtained within the realm of the linear response formalism. The lambda equations and the response equations, which need to be solved to obtain the wave function parameters and Lagrange multipliers, respectively, are also derived here. These new parameters are then used in the expression of the properties formulated here. The linear response function, as obtained from this formalism, gives the excitation energies as its poles. The eigenvalue equation which gives these poles, and therefore the excitation energies, is then derived at the end of this chapter.

4.1 Formulation of the Time-Dependent Lagrangian

In the presence of a periodic perturbation, the time-evolution of the ic-MRCC wave function can be found by solving the time-dependent Schrödinger equation:

$$(\hat{H} - i\frac{\partial}{\partial \mathtt{t}})|\Psi(\mathtt{t})\rangle = 0. \tag{4.1}$$

Here, $\hat{H} = \hat{H}(\mathtt{t}) = \hat{H}_0 + \hat{V}(\mathtt{t})$ with $\hat{H}_0$ and $\hat{V}(\mathtt{t})$ being the electronic Hamiltonian and the perturbation, respectively. The form of the perturbation, $\hat{V}(\mathtt{t})$, has been presented before in Eq. 2.36. Following Eq. 2.40, the time-dependent ic-MRCC ansatz in a phase

isolated form, $\Psi(\mathsf{t})$, can be written as

$$|\Psi(\mathsf{t})\rangle = e^{-iQ(\mathsf{t})\mathsf{t}} e^{\hat{T}(\mathsf{t})} |\Psi_0(\mathsf{t})\rangle, \tag{4.2}$$

where $Q(\mathsf{t})$ is the quasienergy. Here $e^{\hat{T}(\mathsf{t})}|\Psi_0(\mathsf{t})\rangle$ is a periodic Floquet state [102]. The cluster amplitudes and the reference coefficients are also periodic in time in the presence of this periodic perturbation. The explicit time dependencies of these parameters are omitted while writing further expressions. Insertion of the above ansatz into the time-dependent Schödinger Eq. 4.1 yields:

$$e^{-iQ\mathsf{t}}\hat{H}e^{\hat{T}}|\Psi_0\rangle - e^{-iQ\mathsf{t}}\left(Qe^{\hat{T}}|\Psi_0\rangle + i\frac{\partial e^{\hat{T}}}{\partial \mathsf{t}}|\Psi_0\rangle + ie^{\hat{T}}|\frac{\partial \Psi_0}{\partial \mathsf{t}}\rangle\right) = 0. \tag{4.3}$$

An expression for the quasienergy can be obtained following a projection onto $\langle\Psi_0|e^{-\hat{T}}e^{iQ\mathsf{t}}$:

$$\langle\Psi_0|e^{-\hat{T}}\hat{H}e^{\hat{T}}|\Psi_0\rangle - Q - i\langle\Psi_0|e^{-\hat{T}}\frac{\partial e^{\hat{T}}}{\partial \mathsf{t}}|\Psi_0\rangle - i\langle\Psi_0|\frac{\partial \Psi_0}{\partial \mathsf{t}}\rangle = 0. \tag{4.4}$$

The second term in Eq. 4.4 arises as $|\Psi_0\rangle$ is normalized to unity. The part $\partial e^{\hat{T}}/\partial \mathsf{t}$ in the third term of Eq. 4.4 always creates at least one hole or particle in the active orbital space when acting on $|\Psi_0\rangle$ yielding a function orthogonal to $|\Psi_0\rangle$. Therefore the whole term vanishes. Thus Q can now be written as:

$$Q = \langle\Psi_0|\bar{H}|\Psi_0\rangle - i\sum_{\mu} c_{\mu}^{*}\frac{\partial c_{\mu}}{\partial \mathsf{t}}, \tag{4.5}$$

after defining $\bar{H} = e^{-\hat{T}}\hat{H}e^{\hat{T}}$. The equation for the reference function can be obtained by projecting Eq. 4.3 onto $\langle\Phi_\mu|e^{-\hat{T}}e^{iQ\mathsf{t}}$,

$$\langle\Phi_\mu|\bar{H}|\Psi_0\rangle - Q\langle\Phi_\mu|\Psi_0\rangle - i\frac{\partial c_\mu}{\partial \mathsf{t}} = 0, \tag{4.6}$$

while the projection of Eq. 4.3 onto $\langle\Psi_0|\hat{\tau}_\rho'^{\dagger}e^{-\hat{T}}e^{iQt}$ gives the amplitude equation:

$$\langle\Psi_0|\hat{\tau}_\rho'^{\dagger}\bar{H}|\Psi_0\rangle - i\langle\Psi_0|\hat{\tau}_\rho'^{\dagger}e^{-\hat{T}}\frac{\partial e^{\hat{T}}}{\partial \mathsf{t}}|\Psi_0\rangle = 0. \tag{4.7}$$

The product $e^{-\hat{T}}\frac{\partial e^{\hat{T}}}{\partial \mathsf{t}}$ in the second term of Eq. 4.7 can be expanded [P1] as:

$$\begin{aligned} e^{-\hat{T}}\frac{\partial e^{\hat{T}}}{\partial \mathsf{t}} &= (1-\hat{T}+\tfrac{1}{2}\hat{T}\hat{T}-\ldots) \\ &\quad\times(\dot{T}+\tfrac{1}{2}\dot{T}\hat{T}+\tfrac{1}{2}\hat{T}\dot{T}+\tfrac{1}{6}\dot{T}\hat{T}\hat{T}+\tfrac{1}{6}\hat{T}\dot{T}\hat{T}+\tfrac{1}{6}\hat{T}\hat{T}\dot{T}+\ldots) \\ &= \dot{T}+\tfrac{1}{2}[\dot{T},\hat{T}]+\tfrac{1}{6}[[\dot{T},\hat{T}],\hat{T}]+\ldots, \end{aligned} \tag{4.8}$$

which is a commutator expansion using the cluster amplitudes and its first order time-derivative $\dot{T}$. Defining a new metric matrix $\mathbf{S}_t$ such that:

$$(\mathbf{S}_t)_{\rho\sigma} = \langle\Psi_0|\hat{\tau}'^{\dagger}_{\rho}\left(\hat{\tau}'_{\sigma}+\tfrac{1}{2}[\hat{\tau}'_{\sigma},\hat{T}]+\tfrac{1}{6}[[\hat{\tau}'_{\sigma},\hat{T}],\hat{T}]+\ldots\right)|\Psi_0\rangle, \tag{4.9}$$

Eq. 4.7 takes the form

$$\langle\Psi_0|\hat{\tau}'^{\dagger}_{\rho}\bar{H}|\Psi_0\rangle - i(\mathbf{S}_t)_{\rho\sigma}\frac{\partial t'_{\sigma}}{\partial \mathsf{t}} = 0. \tag{4.10}$$

Here, $\mathbf{S}_t$ is a non-unit matrix as the multi-commutator terms involving $\hat{\tau}'_{\sigma}$ and $\hat{T}$ in the expression of $(\mathbf{S}_t)_{\rho\sigma}$ are nonzero following the fact that the excitation operators in the ic-MRCC theory are not commutative.

Now, the time-dependent ic-MRCC Lagrangian $\mathcal{L}$ can be assembled by adding to the quasienergy Q the constraints (4.6) and (4.10), each multiplied by the corresponding time-dependent Lagrange multipliers. The final Lagrangian has the form:

$$\mathcal{L} = \langle\overline{\Psi}_0|\bar{H}|\Psi_0\rangle + \langle\Psi_0|\hat{\Lambda}\bar{H}|\Psi_0\rangle - Q\big(\langle\overline{\Psi}_0|\Psi_0\rangle-1\big) - i\begin{pmatrix}\bar{\mathbf{c}} & \boldsymbol{\lambda}'\end{pmatrix}\begin{pmatrix}\mathbf{1} & \mathbf{0}\\ \mathbf{0} & \mathbf{S}_t\end{pmatrix}\begin{pmatrix}\frac{\partial \mathbf{c}}{\partial \mathsf{t}}\\ \frac{\partial \mathbf{t}'}{\partial \mathsf{t}}\end{pmatrix}. \tag{4.11}$$

The new operators are defined as:

$$\langle\overline{\Psi}_0| = \sum_{\mu}\bar{c}_{\mu}\langle\Phi_{\mu}| = \bar{\mathbf{c}}\langle\boldsymbol{\Phi}| \tag{4.12}$$

and

$$\hat{\Lambda} = \sum_{\rho}\lambda'_{\rho}\hat{\tau}'^{\dagger}_{\rho} = \boldsymbol{\lambda}'\hat{\boldsymbol{\tau}}'^{\dagger}, \tag{4.13}$$

where, $\bar{c}_{\mu}$ and λ'_{ρ} are the Lagrange multipliers for Eqs. 4.6 and 4.10 respectively. $\mathbf{c}$ and $\mathbf{t}'$ are the row vectors comprising all the components of the reference coefficients and the cluster amplitudes respectively, where $\bar{\mathbf{c}}$ and $\boldsymbol{\lambda}'$ are the column vectors corresponding to the Lagrange multipliers. In the absence of any perturbation, the Lagrangian defined here reduces to the time-independent Lagrangian introduced for ic-MRCC theory earlier in Eq. 3.18. The Lagrangian defined in Eq. 4.11 is not strictly bi-orthogonal as the second term of the Lagrangian contains the adjoint of the reference function, i.e. $\langle\Psi_0|$, instead of

its bi-orthogonal component $\langle\overline{\Psi}_0|$. Lack of bi-orthogonality of the ic-MRCC Lagrangian introduces some important aspects in the linear response formulation of the ic-MRCC theory which will be discussed in the forthcoming sections.

4.2 Zeroth Order Lagrangian and Parameters

The zeroth order Lagrangian is obtained in the unperturbed limit and has the same form as the time-independent Lagrangian defined in Ref. [18].

$$\mathcal{L}^{(0)} = \langle\overline{\Psi}_0^{(0)}|\bar{H}_0|\Psi_0^{(0)}\rangle + \langle\Psi_0^{(0)}|\hat{\Lambda}^{(0)}\bar{H}_0|\Psi_0^{(0)}\rangle + E_0(\langle\overline{\Psi}_0^{(0)}|\Psi_0^{(0)}\rangle - 1). \tag{4.14}$$

This Lagrangian becomes the ic-MRCC energy when it is made stationary with respect to all the parameters. The stationary conditions with respect to the zeroth order Lagrange multipliers, $\bar{c}_\mu^0$ and $\lambda_\rho'^0$, give the equations to solve the zeroth order wave function parameters, c_μ^0 and $t_\rho'^0$, respectively:

$$\frac{\partial\mathcal{L}^{(0)}}{\partial\bar{c}_\mu^0} = \langle\phi_\mu|(\bar{H}_0 - E_0)|\Psi_0^{(0)}\rangle = 0, \tag{4.15}$$

$$\frac{\partial\mathcal{L}^{(0)}}{\partial\lambda_\rho'^0} = \langle\Psi_0^{(0)}|\hat{\tau}_\rho'^\dagger\bar{H}_0|\Psi_0^{(0)}\rangle = 0. \tag{4.16}$$

These equations are identical to Eqs. 3.7 and 3.6 respectively and thus ensure that the ic-MRCC energy is obtained in the zeroth order limit. The other stationary conditions, with respect to the wave function parameters c_μ^0 and $t_\rho'^0$, produce the equations to solve $\bar{c}_\mu^0$ and $\lambda_\rho'^0$ respectively:

$$\frac{\partial\mathcal{L}^{(0)}}{\partial c_\mu^0} = \langle\overline{\Psi}_0^{(0)}|(\bar{H}_0 - E_0)|\phi_\mu\rangle + \langle\phi_\mu|\hat{\Lambda}^{(0)}\bar{H}_0|\Psi_0^{(0)}\rangle + \langle\Psi_0^{(0)}|\hat{\Lambda}^{(0)}\bar{H}_0|\phi_\mu\rangle = 0, \tag{4.17}$$

$$\frac{\partial\mathcal{L}^{(0)}}{\partial t_\rho'^0} = \langle\overline{\Psi}_0^{(0)}|\frac{\partial\bar{H}_0}{\partial t_\rho'^0}|\Psi_0^{(0)}\rangle + \langle\Psi_0^{(0)}|\Lambda^{(0)}\frac{\partial\bar{H}_0}{\partial t_\rho'^0}|\Psi_0^{(0)}\rangle = 0. \tag{4.18}$$

The second term in the left hand side of Eq. 4.17 appears as the wave function parameter c_μ is real-valued.

The important aspect of Eqs. 4.17 and 4.18 is that these equations form a set of *homogeneuos* linear equations. This is inherent to the ic-MRCC theory and is a clear distinction from the single-reference coupled cluster theory. The non-trivial solution of this set of equations is obtained by casting them as an eigenvalue problem and then the solution is obtained as the eigenvector corresponding to the zero eigenvalue. This

eigenvalue equation has the form:

$$\begin{pmatrix} \bar{\mathbf{c}}^0 & \boldsymbol{\lambda}'^0 \end{pmatrix} \begin{pmatrix} \mathbf{A}_{\bar{c}c} & \mathbf{A}_{\bar{c}t} \\ \mathbf{A}_{\lambda c} + \mathbf{B}_{\lambda c} & \mathbf{A}_{\lambda t} \end{pmatrix} = \mathbf{0}. \tag{4.19}$$

All the matrix elements used here are elaborately defined in Tab. 4.1. This equation is equivalent to what is known as the lambda equation in the single-reference framework. An alternative equation is also formulated here to solve these Lagrange multipliers that includes the approximation of neglecting the term $\boldsymbol{B_{\lambda c}}$ altogether. The equation would then look like:

$$\begin{pmatrix} \bar{\mathbf{c}}^0 & \boldsymbol{\lambda}'^0 \end{pmatrix} \begin{pmatrix} \mathbf{A}_{\bar{c}c} & \mathbf{A}_{\bar{c}t} \\ \mathbf{A}_{\lambda c} & \mathbf{A}_{\lambda t} \end{pmatrix} = \mathbf{0}. \tag{4.20}$$

While this approximation is not necessary in the present context of first order properties, for neither computational nor formal reasons, the size of the introduced error is of interest. This is, because this approximation is inevitable in the case of dynamic properties and excitation energies [P1]. This issue will also be addressed in detail in the forthcoming Sec. 4.4. It is important to mention here that the term $B_{\lambda c}$ is appearing additionally in Eq. 4.19 as a consequence of the lack of bi-orthogonality in the form of the Lagrangian (see Sec. 4.1). Use of these two different equations to solve the Lagrange multipliers, Eqs. 4.19 and 4.20, leads to two variants of the current formulation of evaluating first order properties which are labeled as ic-MRCC(1) and ic-MRCC(2) respectively.

TABLE 4.1: Tensors appearing in this chapter.

Tensor	Expression	Tensor	Expression
$(\mathbf{A}_{\bar{c}c})_{\mu\nu}$	$\langle\Phi_\mu\vert(\bar{H}_0 - E_0)\vert\Phi_\nu\rangle$	$(\mathbf{A}_{\bar{c}t})_{\mu\rho}$	$\langle\Phi_\mu\vert\frac{\partial\bar{H}_0}{\partial t'^0_\rho}\vert\Psi_0^{(0)}\rangle$
$(\mathbf{A}_{\lambda c})_{\rho\mu}$	$\langle\Psi_0^{(0)}\vert\hat{\tau}'^\dagger_\rho\bar{H}_0\vert\Phi_\mu\rangle$	$(\mathbf{B}_{\lambda c})_{\rho\mu}$	$\langle\Phi_\mu\vert\hat{\tau}'^\dagger_\rho\bar{H}_0\vert\Psi_0^{(0)}\rangle$
$(\mathbf{A}_{\lambda t})_{\rho\sigma}$	$\langle\Psi_0^{(0)}\vert\hat{\tau}'^\dagger_\rho\frac{\partial\bar{H}_0}{\partial t'^0_\sigma}\vert\Psi_0^{(0)}\rangle$	$(\boldsymbol{\xi}^X_{\bar{c}})_\mu$	$\langle\Phi_\mu\vert\bar{X}\vert\Psi_0^{(0)}\rangle$
$(\boldsymbol{\xi}^X_{\lambda})_\rho$	$\langle\Psi_0^{(0)}\vert\hat{\tau}'^\dagger_\rho\bar{X}\vert\Psi_0^{(0)}\rangle$	$(\boldsymbol{\eta}^{\boldsymbol{X}}_{\boldsymbol{c}})_\mu$	$\langle\overline{\Psi}_0\vert\bar{X}\vert\phi_\mu\rangle + \langle\Psi_0\vert\Lambda\bar{X}\vert\phi_\mu\rangle$
$(\boldsymbol{\eta}^{\boldsymbol{X}}_{\boldsymbol{t}})_\rho$	$\langle\overline{\Psi}_0\vert\frac{\partial\bar{X}}{\partial t'^0}\vert\Psi_0\rangle + \langle\Psi_0\vert\Lambda\frac{\partial\bar{X}}{\partial t'^0}\vert\Psi_0\rangle$	$(\boldsymbol{\zeta}^{\boldsymbol{X}}_{\boldsymbol{c}})_\mu$	$\langle\phi_\mu\vert\Lambda\bar{X}\vert\Psi_0\rangle$
$(\boldsymbol{F_{ct}})_{\mu\rho}$	$\langle\overline{\Psi}_0\vert\frac{\partial\bar{H}_0}{\partial t'^0_\rho}\vert\phi_\mu\rangle + \langle\Psi_0\vert\Lambda\frac{\partial\bar{H}_0}{\partial t'^0_\rho}\vert\phi_\mu\rangle$	$(\boldsymbol{F_{tc}})_{\sigma\nu}$	$\langle\overline{\Psi}_0\vert\frac{\partial\bar{H}_0}{\partial t'^0_\sigma}\vert\phi_\nu\rangle + \langle\Psi_0\vert\Lambda\frac{\partial\bar{H}_0}{\partial t'^0_\sigma}\vert\phi_\nu\rangle$
$(\boldsymbol{F_{tt}})_{\sigma\rho}$	$\langle\overline{\Psi}_0\vert\frac{\partial^2\bar{H}_0}{\partial t'^0_\sigma t'^0_\rho}\vert\Psi_0\rangle + \langle\Psi_0\vert\Lambda\frac{\partial^2\bar{H}_0}{\partial t'^0_\sigma t'^0_\rho}\vert\Psi_0\rangle$	$(\tilde{\boldsymbol{F}}_{\boldsymbol{cc}})_{\mu\nu}$	$\langle\phi_\mu\vert\hat{\Lambda}\bar{H}_0\vert\phi_\nu\rangle$
$(\tilde{\boldsymbol{F}}_{\boldsymbol{ct}})_{\rho\sigma}$	$\langle\phi_\mu\vert\Lambda\frac{\partial\bar{H}_0}{\partial t'^0_\rho}\vert\Psi_0\rangle$	$(\boldsymbol{\Sigma}_{\lambda t})_{\rho\sigma}$	$\langle\Psi_0^{(0)}\vert\hat{\tau}'^\dagger_\rho e^{-\hat{T}^{(0)}}\frac{\partial e^{\hat{T}^{(0)}}}{\partial t'^{(0)}_\sigma}\vert\Psi_0^{(0)}\rangle$

4.3 First Order Properties

The expression for the first order property corresponding to the perturbation $\hat{X}$ is obtained by differentiating the first order time-averaged Lagrangian with respect to the strength parameter of the perturbation. Using the stationary conditions derived in Eqs. 4.15-4.18, the final expression of the first order property can be simplified as:

$$\langle X \rangle = \frac{d\{\mathcal{L}^{(1)}\}_T}{d\varepsilon_X} = \langle \overline{\Psi}_0^{(0)} | \bar{X} | \Psi_0^{(0)} \rangle + \langle \Psi_0^{(0)} | \hat{\Lambda}^{(0)} \bar{X} | \Psi_0^{(0)} \rangle. \tag{4.21}$$

The first order properties thus depend on the solution of all the zeroth order parameters which also complies with the (2n+1) and (2n+2) rule. The use of the generalized Hellmann-Feynman theorem [59, 103] starting from the time-independent ic-MRCC Lagrangian would also provide the same expression for the first order property. Alternatively, the expectation value may be expressed by introducing the one particle density matrix γ_q^p:

$$\langle X \rangle = \sum_{p,q} x_q^p \gamma_p^q, \tag{4.22}$$

where x_p^q is the scalar component of the perturbation for the spatial orbitals p and q. In order to arrive at spin-free quantities, the charge-density matrix is introduced here as:

$${}^1\Gamma_p^q = \langle \overline{\Psi}_0 | e^{-\hat{T}} \hat{E}_p^q e^{\hat{T}} | \Psi_0 \rangle + \langle \Psi_0 | \hat{\Lambda} e^{-\hat{T}} \hat{E}_p^q e^{\hat{T}} | \Psi_0 \rangle, \tag{4.23}$$

where

$$\hat{E}_p^q = \hat{a}_{p_\alpha}^{q_\alpha} + \hat{a}_{p_\beta}^{q_\beta}. \tag{4.24}$$

During the implementation, the appropriate projection (or M_S averaging) is carried out in case of non-singlet reference functions in order to arrive at a correctly singlet symmetric charge density.

For spin-dependent properties, the corresponding one-particle spin-density matrix can be defined as:

$${}^3\Gamma_p^q = \langle \overline{\Psi}_0 | e^{-\hat{T}} \hat{F}_p^q e^{\hat{T}} | \Psi_0 \rangle + \langle \Psi_0 | \hat{\Lambda} e^{-\hat{T}} \hat{F}_p^q e^{\hat{T}} | \Psi_0 \rangle, \tag{4.25}$$

with

$$\hat{F}_p^q = \hat{a}_{p_\alpha}^{q_\alpha} - \hat{a}_{p_\beta}^{q_\beta}. \tag{4.26}$$

The expectation values of the first order properties, as presented in Eq. 4.21, do not consider any direct effect of relaxation due to perturbation on molecular orbitals. The properties thus obtained are known as "unrelaxed" properties. The expectation values are therefore not identical to the results obtained from the finite difference approach, where the orbitals are recomputed in the presence of the perturbation ("relaxed" properties). The differences between these relaxed and unrelaxed properties were investigated for truncated single-reference methods, like CCSD [54, 55] and CISD [58]. Ref. [54] shows analytically that most of the orbital relaxation effect are introduced in the CCSD wave function, without explicitly using relaxed orbitals, through the presence of single excitation operators. Similar numerical comparisons are made in Sec. 5.1 for the ic-MRCC theory to show that the unrelaxed properties, as they are defined here, also take care of most of the effects of orbital relaxation.

In the single-reference framework, the effect of orbital relaxation can be incorporated analytically into the expectation value of the first order properties by solving the Coupled Perturbed HF (CPHF) equation [104–106]. A similar relaxation effect is introduced for multireference methods by solving a similar Coupled Perturbed MCSCF equation [107–110]. For the case of internally contracted multireference methods, such as ic-MRCI [95, 111, 112], CASPT2 [113, 114] and ic-MRCC, relaxation of the reference coefficients due to the perturbation also needs to be taken into account [115]. For ic-MRCC, this contribution is included through the inclusion of the Lagrange multipliers $\bar{c}_\mu$s.

However, an additional effect needs to be considered in order to match the corresponding relaxed properties for ic-MRCC. This is because, the ic-MRCC Lagrangian implicitly depends on the transformation matrix $\mathbf{X}$, as defined in Eq. 3.16, which is required to get the linearly independent set of operators. Now considering $\mathbf{C}$ and $\mathbf{t}$ to be the tensors containing the MO coefficients and the wave function parameters respectively, the ic-MRCC Lagrangian can be expressed as a function $\mathcal{L}(\varepsilon, \mathbf{t}, \mathbf{X}, \mathbf{C})$. A derivative of the Lagrangian with respect to the perturbation would then look like:

$$\frac{d\mathcal{L}}{d\varepsilon} = \frac{\partial \mathcal{L}}{\partial \varepsilon} + \frac{\partial \mathcal{L}}{\partial \mathbf{C}} \frac{\partial \mathbf{C}}{\partial \varepsilon} + \frac{\partial \mathcal{L}}{\partial \mathbf{X}} \frac{\partial \mathbf{X}}{\partial \varepsilon}, \tag{4.27}$$

considering the fact that the Lagrangian is variational with respect to $\mathbf{t}$. This relation shows the occurrence of an additional effect of relaxation which is coming from the change in $\mathbf{X}$ following the term $\frac{\partial \mathbf{X}}{\partial \epsilon}$. However, this particular relaxation effect is rather small as it is analyzed in forthcoming Sec. 5.1 and that gives the reason to ignore this additional orbital relaxation effect in the current formulation.

4.4 Response Equations to get First Order Parameters

Following the (2n+1) rule, the first order wave function parameters, $\mathbf{c}^{\mathbf{X}}(\omega_X)$ and $\mathbf{t}'^{\mathbf{X}}(\omega_X)$, are needed to calculate the linear response functions and therefore the second order properties. The response equations to obtain $\mathbf{c}^{\mathbf{X}}(\omega_X)$ and $\mathbf{t}'^{\mathbf{X}}(\omega_X)$ are produced by making the second order component of the Lagrangian, $\mathcal{L}^{XY}(\omega_X, \omega_Y)$, stationary with respect to the the Lagrange multipliers following the conditions:

$$\frac{\partial \mathcal{L}^{XY}(\omega_X, \omega_Y)}{\partial \bar{\mathbf{c}}^{\mathbf{Y}}(\omega_Y)} = \frac{\partial \mathcal{L}^{XY}(\omega_X, \omega_Y)}{\partial \boldsymbol{\lambda}'^{\boldsymbol{Y}}(\omega_Y)} = 0. \tag{4.28}$$

For simplicity, the frequencies corresponding to the operators X and Y are denoted as ω_X and ω_Y, respectively, from now on. Here, $\mathcal{L}^{XY}(\omega_X, \omega_Y)$ is the field-strength independent component of the second order time-averaged Lagrangian as it is defined in Eq. 2.56. For the ic-MRCC theory, $\mathcal{L}^{XY}(\omega_X, \omega_Y)$ has the form:

$$\begin{aligned}
\mathcal{L}^{XY}(\omega_X, \omega_Y) &= C^{\pm\omega} f(\omega) P^{XY} \Bigg[\begin{pmatrix} \boldsymbol{\eta}_{\boldsymbol{c}}^{\boldsymbol{Y}} \\ \boldsymbol{\eta}_{\boldsymbol{t}}^{\boldsymbol{Y}} \end{pmatrix}^T \begin{pmatrix} \mathbf{c}^{\mathbf{X}}(\omega_X) \\ \mathbf{t}'^{\mathbf{X}}(\omega_X) \end{pmatrix} + \begin{pmatrix} \bar{\mathbf{c}}^{\mathbf{Y}}(\omega_Y) \\ \boldsymbol{\lambda}'^{\boldsymbol{Y}}(\omega_Y) \end{pmatrix}^T \begin{pmatrix} \boldsymbol{\xi}_{\bar{\boldsymbol{c}}}^{\boldsymbol{X}} \\ \boldsymbol{\xi}_{\boldsymbol{\lambda}}^{\boldsymbol{X}} \end{pmatrix} \\
&+ \mathbf{c}^{\mathbf{Y}^*}(-\omega_Y) \boldsymbol{\zeta}_{\boldsymbol{c}}^{\boldsymbol{X}} + \begin{pmatrix} \bar{\mathbf{c}}^{\mathbf{Y}}(\omega_Y) \\ \boldsymbol{\lambda}'^{\boldsymbol{Y}}(\omega_Y) \end{pmatrix}^T \begin{pmatrix} \mathbf{A}_{\bar{c}c} & \mathbf{A}_{\bar{c}t} \\ \mathbf{A}_{\lambda c} & \mathbf{A}_{\lambda t} \end{pmatrix} \begin{pmatrix} \mathbf{c}^{\mathbf{X}}(\omega_X) \\ \mathbf{t}'^{\mathbf{X}}(\omega_X) \end{pmatrix} \\
&+ \begin{pmatrix} \mathbf{c}^{\mathbf{Y}}(\omega_Y) \\ \mathbf{t}'^{\mathbf{Y}}(\omega_Y) \end{pmatrix}^T \begin{pmatrix} \mathbf{0} & \mathbf{F}_{ct} \\ \mathbf{F}_{tc} & \mathbf{F}_{tt} \end{pmatrix} \begin{pmatrix} \mathbf{c}^{\mathbf{X}}(\omega_X) \\ \mathbf{t}'^{\mathbf{X}}(\omega_X) \end{pmatrix} \\
&- \omega_X \begin{pmatrix} \bar{\mathbf{c}}^{\mathbf{Y}}(\omega_Y) \\ \boldsymbol{\lambda}'^{\boldsymbol{Y}}(\omega_Y) \end{pmatrix}^T \begin{pmatrix} \mathbf{1} & \mathbf{0} \\ \mathbf{0} & \boldsymbol{\Sigma}_{\lambda t} \end{pmatrix} \begin{pmatrix} \mathbf{c}^{\mathbf{X}}(\omega_X) \\ \mathbf{t}'^{\mathbf{X}}(\omega_X) \end{pmatrix} \\
&+ \mathbf{c}^{\mathbf{X}^*}(-\omega_X) \boldsymbol{B}_{\boldsymbol{\lambda c}} \boldsymbol{\lambda}'^{\boldsymbol{Y}}(\omega_Y) + \mathbf{c}^{\mathbf{Y}^*}(-\omega_Y) \tilde{\boldsymbol{F}}_{\boldsymbol{cc}} \mathbf{c}^{\mathbf{X}}(\omega_X) \\
&+ \mathbf{c}^{\mathbf{Y}^*}(-\omega_Y) \tilde{\boldsymbol{F}}_{\boldsymbol{ct}} \mathbf{t}'^{\mathbf{X}}(\omega_X) \Bigg]
\end{aligned} \tag{4.29}$$

The expressions of all the different matrices used to formulate $\mathcal{L}^{XY}(\omega_X, \omega_Y)$ are presented in Tab. 4.1. It is important here to note the presence of the complex conjugate of the first order reference coefficients $\mathbf{c}^{\mathbf{X}}$ in this component of the second order Lagrangian. The use of the permutation operator P ensures the symmetry of any response property

with the exchange of its Cartesian labels:

$$P\left(f(x,y)\right) = f(x,y) + f(y,x). \tag{4.30}$$

The use of the symmetry operator $C^{\pm\omega}$, on the other hand, makes an average of the Lagrangian and its complex conjugates, following the operation:

$$C^{\pm\omega} f(\omega_X, \omega_Y) = \left[f(\omega_X, \omega_Y) + f(-\omega_X, -\omega_Y)^*\right]. \tag{4.31}$$

The use of $C^{\pm\omega}$ ensures that the response functions satisfy the symmetry relations described in Eqs. 2.47-2.49.

Following the stationary conditions as mentioned in Eq. 4.28, the response equations to calculate $\mathbf{c}^{\mathbf{X}}(\omega_X)$ and $\mathbf{t'}^{\mathbf{X}}(\omega_X)$ are derived to be:

$$\begin{aligned}\frac{\partial \mathcal{L}^{XY}(\omega_X,\omega_Y)}{\partial \bar{\mathbf{c}}^{\mathbf{Y}}(\omega_Y)} = \quad & \langle \mathbf{\Phi}|(\bar{H}_0 - E_0)|\mathbf{\Phi}\rangle \mathbf{c}^{\mathbf{X}}(\omega_X) \quad + \quad \langle \mathbf{\Phi}|\frac{\partial \bar{H}_0}{\partial \mathbf{t'^0}}|\Psi_0^{(0)}\rangle \mathbf{t'}^{\mathbf{X}}(\omega_X) \\ + \quad & \langle \mathbf{\Phi}|\bar{X}|\Psi_0^{(0)}\rangle \quad - \quad \langle X\rangle\langle \mathbf{\Phi}|\Psi_0^{(0)}\rangle \quad - \quad \omega_X \mathbf{c}^{\mathbf{X}}(\omega_X) \quad = \quad 0,\end{aligned} \tag{4.32}$$

and,

$$\begin{aligned}\frac{\partial \mathcal{L}^{XY}(\omega_X,\omega_Y)}{\partial \boldsymbol{\lambda'}^{\boldsymbol{Y}}(\omega_Y)} \quad = \quad & \mathbf{c}^{\mathbf{X}^*}(-\omega_X)\langle \mathbf{\Phi}|\hat{\boldsymbol{\tau}}'^{\dagger}\bar{H}_0|\Psi_0^{(0)}\rangle \quad + \quad \langle \Psi_0^{(0)}|\hat{\boldsymbol{\tau}}'^{\dagger}\bar{H}_0|\mathbf{\Phi}\rangle \mathbf{c}^{\mathbf{X}}(\omega_X) \\ + \quad & \langle \Psi_0^{(0)}|\hat{\boldsymbol{\tau}}'^{\dagger}\frac{\partial \bar{H}_0}{\partial \mathbf{t'^0}}|\Psi_0^{(0)}\rangle \mathbf{t'}^{\mathbf{X}}(\omega_X) \quad + \quad \langle \Psi_0^{(0)}|\hat{\boldsymbol{\tau}}'^{\dagger}\bar{X}|\Psi_0^{(0)}\rangle \\ - \quad & \omega_X \langle \Psi_0^{(0)}|\hat{\boldsymbol{\tau}}'^{\dagger}\tilde{\boldsymbol{\tau}}'|\Psi_0^{(0)}\rangle \mathbf{t'}^{\mathbf{X}}(\omega_X) \quad = \quad 0.\end{aligned} \tag{4.33}$$

Here Eq. 4.33 shows a coupling between $\mathbf{c}^{\mathbf{X}}(\omega_X)$ and $\mathbf{c}^{\mathbf{X}^*}(-\omega_X)$ following the presence of the latter in Eq. 4.29. So in this case these two equations have to be solved along with the equations for $\mathbf{c}^{\mathbf{X}^*}(-\omega_X)$ and $\mathbf{t'}^{\mathbf{X}^*}(-\omega_X)$. The coupled response equations can then be represented as:

$$\left[\begin{pmatrix}\mathbf{A} & \mathbf{B}\\ \mathbf{B}^* & \mathbf{A}^*\end{pmatrix} - \omega_X \begin{pmatrix}\mathbf{\Sigma} & \mathbf{0}\\ \mathbf{0} & -\mathbf{\Sigma}^*\end{pmatrix}\right]\begin{pmatrix}\mathcal{X}\\ \mathcal{Y}\end{pmatrix} = -\begin{pmatrix}\boldsymbol{\xi}^X\\ \boldsymbol{\xi}^{X*}\end{pmatrix}. \tag{4.34}$$

where,

$$\mathbf{A} = \begin{pmatrix}\mathbf{A}_{\bar{c}c} & \mathbf{A}_{\bar{c}t}\\ \mathbf{A}_{\lambda c} & \mathbf{A}_{\lambda t}\end{pmatrix}, \tag{4.35}$$

$$\mathbf{B} = \begin{pmatrix}\mathbf{0} & \mathbf{0}\\ \mathbf{B}_{\lambda c} & \mathbf{0}\end{pmatrix}, \tag{4.36}$$

$$\boldsymbol{\Sigma} = \begin{pmatrix} \mathbf{1} & \mathbf{0} \\ \mathbf{0} & \boldsymbol{\Sigma}_{\lambda t} \end{pmatrix}, \tag{4.37}$$

$$\mathcal{X} = \begin{pmatrix} \mathbf{c}^{\mathbf{X}}(\omega_X) \\ \mathbf{t}'^{\mathbf{X}}(\omega_X) \end{pmatrix}, \tag{4.38}$$

$$\mathcal{Y} = \begin{pmatrix} \mathbf{c}^{\mathbf{X}*}(-\omega_X) \\ \mathbf{t}'^{\mathbf{X}*}(-\omega_X) \end{pmatrix}, \tag{4.39}$$

$$\boldsymbol{\xi}^X = \begin{pmatrix} \boldsymbol{\xi}^X_{\bar{c}} - \langle X \rangle \mathbf{c_0} \\ \boldsymbol{\xi}^X_{\lambda} \end{pmatrix}. \tag{4.40}$$

This coupling between the wave function parameters for frequencies ω_X and $-\omega_X$, represented here as $\mathcal{X}$ and $\mathcal{Y}$ respectively, changes the pole structure of the resulting response function. At the poles of the response function the $\mathcal{X}$ attains the singularity. Now due to the appearance of the coupling term $\boldsymbol{B_{\lambda c}}$ (as only term inside $\mathbf{B}$), the solution of $\mathcal{Y}$ also becomes singular simultaneously. Terms in the linear response function that are quadratic in these parameters may then give rise to unphysical second order poles (cf. refs. [53, 116, 117]). Nature of these kind of second order poles, occurring due to the coupled response equations, will be discussed in Sec. 6.1.1.

The coupling term $\mathbf{B}_{\lambda c}$ arises due to the occurrence of the (time-dependent) reference function in the projection manifold. It contains projections of $\bar{H}_0|\Psi_0^{(0)}\rangle$ onto excited functions $\langle\Phi_\mu|\hat{\tau}'^{\dagger}_\rho$. Since projections onto functions from the projection manifold vanish due to fulfillment of the ic-MRCC equations for the reference state, the $\mathbf{B}_{\lambda c}$ term will only contain contributions from an *extended* ground state residual arising from projections onto functions excited by operators of higher rank [P1]:

$$(\mathbf{B}_{\lambda c})_{\rho\mu} = \sum_{\substack{\sigma \\ \mathrm{rank}(\sigma)>\mathrm{rank}(\rho)}} \langle\Phi_\mu|\hat{\tau}'^{\dagger}_\rho \hat{\tau}'_\sigma|\Psi_0^{(0)}\rangle\langle\Psi_0^{(0)}|\hat{\tau}'^{\dagger}_\sigma \bar{H}_0|\Psi_0^{(0)}\rangle. \tag{4.41}$$

The first factor in Eq. 4.41 naturally vanishes in the FCI limit, and it vanishes individually for each excitation class (number of inactive annihilation and creation operators in $\hat{\tau}'_\rho$), for which the maximum operator rank is large enough to cover the complete space of functions within this excitation class. Like the internally contracted MRCI method [95], the ic-MRCC method relies on the observation that one can truncate the excitations in each class at a global rank, i.e. rank 2 in ic-MRCCSD, without deteriorating the accuracy of the method. The residual terms in Eq. 4.41 are thus expected to be small in general. Though one can also replace the left-hand reference function in the Lagrangian by a bi-orthogonal complement of the reference function which would have eliminated the second order contributions to the poles. However, this would require a simultaneous solution of

the equations for wave function parameters and Lagrange multipliers [18] and thus it is not followed in the ic-MRCC formulation. Naturally, the $\mathbf{B}_{\lambda c}$ term is also not present when one chooses to fix the reference function and instead uses internal excitations in the cluster operator.

Although $\mathbf{B}_{\lambda c}$ is expected to be small, Eq. 4.34 can be simplified in the spirit of the Tamm-Dancoff approximation by neglecting term $\boldsymbol{B}_{\boldsymbol{\lambda c}}$ altogether while solving it. This removes the coupling between solutions for the parameters $\mathcal{X}$ and $\mathcal{Y}$. The final equation then has the form:

$$\big[\mathbf{A} - \omega_X \boldsymbol{\Sigma}\big]\mathcal{X} = -\boldsymbol{\xi}^X, \tag{4.42}$$

which, after expanding the matrices it contains, looks like:

$$\left[\begin{pmatrix} \mathbf{A}_{\bar{c}c} & \mathbf{A}_{\bar{c}t} \\ \mathbf{A}_{\lambda c} & \mathbf{A}_{\lambda t} \end{pmatrix} - \omega_X \begin{pmatrix} \mathbf{1} & \mathbf{0} \\ \mathbf{0} & \boldsymbol{\Sigma}_{\lambda t} \end{pmatrix}\right] \begin{pmatrix} \mathbf{c}^{\mathbf{X}}(\omega_X) \\ \mathbf{t}^{\mathbf{X}\prime}(\omega_X) \end{pmatrix} = \begin{pmatrix} \boldsymbol{\xi}^X_{\bar{c}} \\ \boldsymbol{\xi}^X_{\lambda} \end{pmatrix}. \tag{4.43}$$

However, in the static limit, the basis of this approximation is no longer valid as $\mathcal{X}$ and $\mathcal{Y}$ are then just the complex conjugates of each other without any frequency dependence. Therefore, it is justified to solve Eqs. 4.32 and 4.33, which gives the first order wave function parameters, without involving any further approximation. Now, for a real perturbation, which is the case for all the second order properties calculated in this thesis, these two equations can be written in the matrix form as:

$$\begin{pmatrix} \mathbf{A}_{\bar{c}c} & \mathbf{A}_{\bar{c}t} \\ \mathbf{A}_{\lambda c} + \mathbf{B}_{\lambda c} & \mathbf{A}_{\lambda t} \end{pmatrix} \begin{pmatrix} \mathbf{c}^{\mathbf{X}}(0) \\ \mathbf{t}^{\mathbf{X}\prime}(0) \end{pmatrix} = \begin{pmatrix} \boldsymbol{\xi}^X_{\bar{c}} \\ \boldsymbol{\xi}^X_{\lambda} \end{pmatrix}. \tag{4.44}$$

Both of the equations 4.43 and 4.44 have been used to calculated static properties in Chap. 6 and the effect of this approximation has been analyzed using different molecular systems.

The response equations involve further difficulties as the matrix $\mathbf{A}_{\bar{c}c}$, present in both of Eqs. 4.43 and 4.44, is singular as its lowest eigenvalue is zero. Thus, in the static limit, to get a non-singular solution the first order reference coefficients should be orthogonal to their zeroth order counterparts. Here the constraint:

$$\sum_{\mu} c^X_{\mu}(\omega_X) c^{(0)}_{\mu} = 0, \tag{4.45}$$

is used while solving the response equations to ensure that the first order wave function parameters only have contributions from the space orthogonal to $c^{(0)}_{\mu}$.

4.5 Linear Response Function

The linear response function is obtained from the second order time-averaged Lagrangian following Eq. 2.52 and has the expression:

$$
\begin{aligned}
\langle\langle X;Y\rangle\rangle_{\omega_Y} &= \frac{d^2\{L(t)\}_T}{d\varepsilon_X(\omega_X)d\varepsilon_Y(\omega_Y)} \\
&= \tfrac{1}{2}C^{\pm\omega}P(X,Y)\times\Bigg\{\underbrace{\begin{pmatrix}\boldsymbol{\eta}_{\boldsymbol{c}}^{\boldsymbol{X}}\\ \boldsymbol{\eta}_{\boldsymbol{t}}^{\boldsymbol{X}}\end{pmatrix}^T\begin{pmatrix}\mathbf{c}^{\mathbf{Y}}(\omega_Y)\\ \mathbf{t}'^{\mathbf{Y}}(\omega_{\mathbf{Y}})\end{pmatrix}}_{\text{I}} \\
&+ \underbrace{\frac{1}{2}\begin{pmatrix}\mathbf{c}^{\mathbf{X}}(\omega_X)\\ \mathbf{t}'^{\mathbf{X}}(\omega_{\mathbf{X}})\end{pmatrix}^T\begin{pmatrix}\mathbf{0} & \boldsymbol{F}_{\boldsymbol{ct}}\\ \boldsymbol{F}_{\boldsymbol{tc}} & \boldsymbol{F}_{\boldsymbol{tt}}\end{pmatrix}\begin{pmatrix}\mathbf{c}^{\mathbf{Y}}(\omega_{\mathbf{Y}})\\ \mathbf{t}'^{\mathbf{Y}}(\omega_{\mathbf{Y}})\end{pmatrix}}_{\text{II}} + \underbrace{\boldsymbol{c}^{\boldsymbol{Y}^*}(-\omega_Y)\boldsymbol{\zeta}_{\boldsymbol{c}}^{\boldsymbol{X}}}_{\text{III}} \\
&+ \underbrace{\boldsymbol{c}^{\boldsymbol{X}^*}(-\omega_X)\tilde{\boldsymbol{F}}_{\boldsymbol{cc}}\boldsymbol{c}^{\boldsymbol{Y}}(\omega_Y) + \boldsymbol{c}^{\boldsymbol{X}^*}(-\omega_X)\tilde{\boldsymbol{F}}_{\boldsymbol{ct}}\boldsymbol{t}'^{\boldsymbol{Y}}(\omega_Y)}_{\text{IV}}\Bigg\}.
\end{aligned}
\tag{4.46}
$$

Each of the matrix elements used in the above equation are presented in its expanded form in Tab. 4.1. Static and dynamic second order properties are directly related to the linear response function calculated for a certain frequency. For the electrical polarizability this relation is presented in Eq. 2.46.

Another important aspect of the linear response function is that it produces poles when ω_Y approaches excitation energies of any state of the molecular system under study. As the space of the excitation operators involved in the ic-MRCC theory is non-redundant, each of this poles coming from the linear response function correspond only to the physically possible excited states of the system [P1], unlike other multireference methods which are based on the JM ansatz, such as Mk-MRCC [64, 65]. Apart from this correspondence, the structure of each of these poles is also important to analyze here. Following the spectral representation of the linear response function, as given by Eq 2.2.2, the poles of this function should be of first order in nature. However, for ic-MRCC, a theoretical analysis of the linear response function shows that this function produces second order poles through the contributions of some of the terms it contains. Analysis of this second order nature of the poles is mainly relevant for the diagonal components of the linear response function (with $X = Y$ and $\omega_Y = -\omega_X$). Among the different terms of the linear response function, presented in Eq. 4.46, the terms in II and IV are the ones quadratic with respect to the first order wave function parameters and therefore they can lead to second order

poles. As it has already been discussed briefly in the last section, the coupling between the first order parameters of different frequencies in Eq. 4.42 leads to simultaneous divergence of both of these parameters near the poles. These two parameters then contribute simultaneously in the term II of the response function in Eq. 4.46 making the corresponding poles of second order in nature. Through the approximation made in the response equations 4.43, these two parameters are decoupled and thus corresponding second order contribution to the poles is avoided. The other contribution to the second order poles, the terms denoted by IV in Eq. 4.46, is quadratic in the first order wave function parameters corresponding to the same frequency (as $\omega_Y = -\omega_X$). This contribution can only be avoided through an approximation in the expression of the linear response function.

The terms in IV of Eq. 4.46, along with the allied term in III, appear due to the presence of $\langle\Psi_0|$ in the definition of the ic-MRCC Lagrangian. As that particular term in the Lagrangian also leads to the problematic $B_{\lambda c}$ term in the response equations, as presented in 4.34, an approximation similar to the one done for the response equations can be made also for the linear response function. By this approximation, all the terms involving the response of the reference function in the projection manifold, i.e. the terms in III and IV in Eq. 4.46, are excluded from the expression of the linear response function. This approximation reduces the expression of the linear response function to be:

$$\begin{aligned}\langle\langle X;Y\rangle\rangle_{\omega_Y} = \tfrac{1}{2}C^{\pm\omega}P(X,Y)\times\Bigg\{&\begin{pmatrix}\boldsymbol{\eta}_{\boldsymbol{c}}^{\boldsymbol{X}}\\ \boldsymbol{\eta}_{\boldsymbol{t}}^{\boldsymbol{X}}\end{pmatrix}^{T}\begin{pmatrix}\mathbf{c}^{\mathbf{Y}}(\omega_Y)\\ \mathbf{t}'^{\mathbf{Y}}(\omega_{\mathbf{Y}})\end{pmatrix}\\ &+\frac{1}{2}\begin{pmatrix}\mathbf{c}^{\mathbf{X}}(\omega_X)\\ \mathbf{t}'^{\mathbf{X}}(\omega_{\mathbf{X}})\end{pmatrix}^{T}\begin{pmatrix}\mathbf{0} & \boldsymbol{F}_{\boldsymbol{ct}}\\ \boldsymbol{F}_{\boldsymbol{tc}} & \boldsymbol{F}_{\boldsymbol{tt}}\end{pmatrix}\begin{pmatrix}\mathbf{c}^{\mathbf{Y}}(\omega_{\mathbf{Y}})\\ \mathbf{t}'^{\mathbf{Y}}(\omega_{\mathbf{Y}})\end{pmatrix}\Bigg\}.\end{aligned} \tag{4.47}$$

However, for the calculations of the static property, the approximation in the response function is not absolutely necessary as the property does not depend on the frequency. The use of this approximation will only deviate the value of the ic-MRCC-LR property further from the one obtained using the finite differences of energies.

The final formulation of the linear response theory for ic-MRCC has emerged here by evolving through two different approximations, involving in each of the response equations and expression of the response function. While this formulation will be used to calculate the dynamic second order properties for ic-MRCC in the forthcoming Chap. 6, the overall merit of these approximations will also be analyzed. However, in the static limit, an additional formulation will be used that does not involve any approximations and uses the response equations in Eq. 4.44 and the response function in Eq. 4.46. Static properties obtained from this formulation would exactly match the finite field calculation of the properties done without relaxing the orbitals or the metric matrix $\mathbf{X}$.

4.6 Excitation Energies from the Response Theory

The poles of the linear response function appear whenever the frequency of the external field approaches the electronic excitation energies of a molecular system. Thus, in the response theory the excitation energies are obtained by finding these poles. The singularity of the linear response function at the poles is linked to the singularity of the solution of the response equations at that frequency. The condition of singularity for the response equations, therefore, leads to the well-known eigenvalue problem. Now, following the fact that the response equations lead to the coupling between first order wave function parameters of opposite frequencies, as discussed in Sec. 4.4, one can show that pairs of solutions exist with corresponding eigenvalues ω_X and $-\omega_X$, respectively. This also causes singularities in $\mathbf{c}^X(\omega)$ and $\mathbf{t}'^X(\omega)$ at both of these eigenvalues.

Therefore, following the approximation that has been made while solving the response equations in Sec. 4.4, the eigenvalue problem can be derived from Eq. 4.43. The eigenvalue problem now has the form [P1]:

$$\left[\begin{pmatrix} \mathbf{A}_{\bar{c}c} & \mathbf{A}_{\bar{c}t} \\ \mathbf{A}_{\lambda c} & \mathbf{A}_{\lambda t} \end{pmatrix} - \omega \begin{pmatrix} \mathbf{1} & \mathbf{0} \\ \mathbf{0} & \mathbf{\Sigma}_{\lambda t} \end{pmatrix} \right] \begin{pmatrix} \mathbf{r}_c \\ \mathbf{r}'_t \end{pmatrix} = \mathbf{0}. \tag{4.48}$$

So, the matrix $\boldsymbol{A}$, as defined in Eq. 4.35, has been diagonalized to get the excitation energies ω. The eigenvector has two components: $\boldsymbol{r}_c$ in the space of the reference coefficients and $\boldsymbol{r}'_t$ in the space of the cluster amplitudes. Here the exclusion of the coupling term $\boldsymbol{B}_{\boldsymbol{\lambda c}}$ decouples the solutions for positive and negative eigenvalues. The dimension of the eigenvalue problem is also reduced by half compared to the coupled eigenvalue problem.

It is worth mentioning that the terms $\mathbf{A}_{\bar{c}t}$ and $\mathbf{A}_{\lambda t}$ can be rewritten by expanding the derivative of the similarity transformed Hamiltonian as [P1]:

$$\begin{aligned} \frac{\partial \bar{H}_0}{\partial \boldsymbol{t}'^{(0)}} &= \frac{\partial e^{-\hat{T}}}{\partial \boldsymbol{t}'^{(0)}} \hat{H}_0 e^{\hat{T}^{(0)}} + e^{-\hat{T}^{(0)}} \hat{H}_0 \frac{\partial e^{\hat{T}^{(0)}}}{\partial \boldsymbol{t}'^{(0)}} \\ &= [\bar{H}_0, e^{-\hat{T}^{(0)}} \frac{\partial e^{\hat{T}^{(0)}}}{\partial \boldsymbol{t}'^{(0)}}] = [\bar{H}_0, \tilde{\boldsymbol{\tau}}'], \end{aligned} \tag{4.49}$$

where $\tilde{\boldsymbol{\tau}}'$ is defined according to

$$\begin{aligned} \tilde{\boldsymbol{\tau}}' &= e^{-\hat{T}^{(0)}} \frac{\partial e^{\hat{T}^{(0)}}}{\partial \boldsymbol{t}'^{(0)}} \\ &= \hat{\boldsymbol{\tau}}' + \tfrac{1}{2}[\hat{\boldsymbol{\tau}}', \hat{T}^{(0)}] + \tfrac{1}{6}[[\hat{\boldsymbol{\tau}}', \hat{T}^{(0)}], \hat{T}^{(0)}] + \ldots. \end{aligned} \tag{4.50}$$

The new definition of

$$\hat{R} = \tilde{\boldsymbol{\tau}}' \mathbf{r}'_t = \boldsymbol{\tau} \tilde{\mathbf{r}}_t \tag{4.51}$$

gives us the freedom to follow another way to solve Eq. 4.48 by choosing $\tilde{\mathbf{r}}_t$ as the variable and truncating it in a similar way as the cluster operator. The resulting equation will then have an EOM-like structure containing the commutator $[\bar{H}_0, \hat{R}]$. The same $\hat{R}$ will appear in the term containing ω and will turn $\boldsymbol{\Sigma}_{\lambda t}$ into a unit matrix according to its definition in Table 4.1. This alternative EOM approach to get excitation energies will be discussed in a more rigorous way in the forthcoming chapter 7 of this thesis.

While solving the eigenvalue problem, the response vector

$$\mathbf{r}_0 = \begin{pmatrix} \mathbf{c} \\ \mathbf{0} \end{pmatrix}, \tag{4.52}$$

would be a valid solution with the eigenvalue $\omega = 0$ for the final states with the same spatial and spin symmetry as the initial state. This solution is a redundant one as it gives back the initial state. Considering that the response vector is nonorthogonal to $\mathbf{r}_0$,

$$\mathbf{r} = \mathbf{r}^{\perp} + x\mathbf{r}_0, \quad \text{with} \quad x = \mathbf{r}_0 \cdot \mathbf{r}, \tag{4.53}$$

the component parallel to $\mathbf{r}_0$ does not change the eigenvalue due to $\mathbf{A}\mathbf{r}_0 = \mathbf{0}$:

$$(\mathbf{A} - \omega\boldsymbol{\Sigma})\mathbf{r} = (\mathbf{A} - \omega\boldsymbol{\Sigma})\mathbf{r}^{\perp} - x\omega\mathbf{r}_0. \tag{4.54}$$

Therefore, both the term $\mathbf{A}\mathbf{r}$ and the response vector $\mathbf{r}$ are orthogonalized to $\mathbf{r}_0$ in each iteration while solving the eigenvalue problem in order to avoid the trivial solution $\omega = 0$. This is equivalent to solving the equation

$$\mathbf{X}^{\dagger}(1 - \mathbf{r}_0\mathbf{r}_0^{\dagger})(\mathbf{A} - \omega\boldsymbol{\Sigma})\mathbf{r}^{\perp} = \mathbf{0} \tag{4.55}$$

which will give $\mathbf{r}^{\perp}$ instead of $\mathbf{r}$ as eigenvectors, but the correct excitation energies. A similar issue also occurs in Mk-MRCC response theory and the problem is dealt with in the same manner [64].

5 | Results: First Order Properties

The expression to calculate the first order properties for the ic-MRCC theory, Eq. 4.21, has been derived in Sec. 4.3. The overall formulation gives two variants, ic-MRCC(1) and ic-MRCC(2), depending on which of the lambda equations, 4.19 and 4.20, are solved to obtain the Lagrange multipliers, respectively. As the first order properties obtained from both of these formulations do not include the effect of the perturbation on the molecular orbitals, the results obtained here are 'unrelaxed' in nature.

The main implementation for solving the lambda equation and subsequent evaluation of the first order properties are done in the General Contraction Code (GeCCo) program. This program has been used for the development and implementation of the ic-MRCC and allied methods [18, 25, 26, 118, 119]. The previous implementations and corresponding applications of ic-MRCC were mainly done using the spin-orbital formalism. However, a recent implementation of the spin-adapted ic-MRCC allows the use of properly spin-adapted solutions of the equations while other spin components are projected out from the solutions. All the calculations in this chapter are done using this spin-adapted version of the ic-MRCC theory. The current implementation of the formulation is restricted in using single and double excitation operators for ic-MRCC. While solving all the equations involved in the property calculations, all commutator expansions have been truncated up to their quadratic terms.

In this chapter, first the merit of the unrelaxed approximation is assessed by comparing the results it provides with the relaxed properties. The differences in results between the formulations ic-MRCC(1) and ic-MRCC(2) are also compared alongside. The formulation is then applied to calculate different first order properties and the accuracy of these results are compared with those from other highly accurate quantum chemical methods. Both of the spin-independent properties, namely dipole moment, quadrupole moment, electric field gradient, and spin-dependent properties, like isotropic and anisotropic hyperfine coupling constants (HFCC) are calculated in this regard.

5.1 Effect of Different Approximations on Dipole Moments

TABLE 5.1: Dipole moments of sample molecules as obtained for ic-MRCCSD using different approaches. The unrelaxed values are the generalized expectation values as given in Eq. 4.21 where the corresponding lambda equations are solved using Eqs. 4.19 and 4.20 for ic-MRCCSD(1) and ic-MRCCSD(2), respectively. The relaxed values are obtained by doing finite field calculations. The values denoted as relaxed($\mathbf{X}$) are obtained by doing the finite field calculations using fixed orbitals, obtained from a CASSCF calculation for the unperturbed system. The another set of finite field calculations, with orbitals optimized for the respective field, gives the values listed under relaxed($\mathbf{X}$,$\mathbf{C}$). The ic-MRCCSD(2) value and all relaxation contributions are given as increments upon the unrelaxed ic-MRCCSD(1) value. Atomic units are used throughout.

Molecule(State)	CAS	Basis	unrelaxed		relaxed($\mathbf{X}$)	relaxed($\mathbf{X}$,$\mathbf{C}$)
			ic-MRCCSD(1)	ic-MRCCSD(2)		
LiH($^1\Sigma^+$)	(2,2)	aug-cc-pVDZ	2.316748	-0.000060	+0.000001	-0.000163
		aug-cc-pVTZ	2.297557	-0.000035	+0.000006	-0.000101
		aug-cc-pVQZ	2.292855	-0.000017	+0.000006	-0.000040
BH($^1\Sigma^+$)	(2,2)	aug-cc-pVDZ	0.508498	+0.004718	-0.000017	+0.001913
		aug-cc-pVTZ	0.534220	+0.000438	+0.000011	-0.019379
		aug-cc-pVQZ	0.538832	+0.000485	+0.000006	-0.010669
CH_2($^1A_1$)	(2,2)	aug-cc-pVDZ	0.645982	+0.000226	+0.000017	-0.000596
		aug-cc-pVTZ	0.652833	+0.000153	+0.000018	-0.000893
		aug-cc-pVQZ	0.656458	+0.000131	+0.000018	-0.001251
HF($^1\Sigma^+$)	(2,2)	aug-cc-pVDZ	0.712876	-0.004209	-0.000045	-0.004914
		aug-cc-pVTZ	0.712962	-0.001646	-0.000051	-0.002986
		aug-cc-pVQZ	0.715583	-0.000918	-0.000041	-0.002610
LiF($^1\Sigma^+$)	(2,2)	aug-cc-pVDZ	2.518980	-0.000289	-0.000013	+0.003377
		aug-cc-pVTZ	2.499795	-0.000159	+0.000001	+0.002995
		aug-cc-pVQZ	2.498166	-0.000129	+0.000000	+0.002239
CN($^2\Sigma^+$)	(5,6)	aug-cc-pVDZ	0.571625	-0.004052	-0.002328	-0.008866
		aug-cc-pVTZ	0.577816	-0.003112	-0.001380	-0.008012
		aug-cc-pVQZ	0.586043	-0.002782	-0.001017	-0.007760
BO($^2\Sigma^+$)	(5,6)	aug-cc-pVDZ	0.888180	-0.004256	+0.000125	+0.000875
		aug-cc-pVTZ	0.899560	-0.002378	+0.000133	+0.006636
		aug-cc-pVQZ	0.905347	-0.001723	+0.000177	+0.008341
CH_2($^1A_1$)	(6,6)	aug-cc-pVDZ	0.643191	-0.000999	+0.000389	-0.003275
		aug-cc-pVTZ	0.647858	-0.000409	+0.000630	-0.002060
		aug-cc-pVQZ	0.650672	-0.000099	+0.000685	-0.001716

As discussed in Sec. 4.3, the expression for the first order properties is obtained for ic-MRCC without considering the relaxation effect of the perturbation on both the MO

coefficients, **C**, and the transformation matrix, **X**. These relaxation effects are included when the first order properties are calculated numerically as finite differences of energies obtained for different field-strengths. Comparisons of the 'unrelaxed' first order properties with the corresponding numerical results of 'relaxed' properties provide scope to see the extent to which the current formulation can recover the effect of additional relaxation coming from **C** and **X**. In the finite differential technique, the orbitals involved in the calculations are optimized for different field-strengths, as opposed to the use of fixed orbitals for calculations involving the current formulation. The same is also true regarding the use of the transformation matrix **X**. However, it is possible to do the numerical differentiation by fixing both **C** and **X** to their unperturbed values. This numerical calculation then exactly reproduces the first order properties obtained following the ic-MRCC(1) formulation (use of ic-MRCC(2) formulation will produce a small error here). But in this section, the focus is mainly to obtain the relaxed values of the first order properties using the finite differential technique and then to compare those results with the unrelaxed properties obtained using ic-MRCC(1). The effects of the other approximation, which leads to the formulation ic-MRCC(2) after excluding the term $B_{\lambda c}$ from the lamda equations, is also studied through comparisons between the results obtained from both the ic-MRCC(1) and ic-MRCC(2) variants.

In order to show the separate effects of the relaxation coming individually from **C** and **X**, two different ways of getting numerical derivatives are used here. In the first set of calculations only the **X** is relaxed for different field-strengths while keeping **C** the same. In the second set of calculations, both **C** and **X** are relaxed to a get a fully relaxed dipole moment for ic-MRCC. Properties obtained using these two types of numerical differentiation are represented as relaxed(**X**) and relaxed(**X**,**C**), respectively, in the rest of this chapter.

Dipole moments as obtained from ic-MRCCSD by using different levels of approximation involved in the current formulation are summarized in Tab. 5.1. The dipole moments are calculated for states of several molecules, namely the singlet ground states of Lithium Hydride (LiH), Boron Hydride (BH), Methylene radical (CH_2), Hydrogen Fluoride (HF) and Lithium Fluoride (LiF); and the doublet ground states of Cyanide (CN) and Boron oxide (BO) radicals. An active space of (2e,2o) is used for all the singlet states and CAS(5e,6o) is used for the doublets. Additional calculations are done for CH_2 using the CAS(6e,6o). Comparisons of dipole moments for all of these molecular states are made using aug-cc-pVDZ, aug-cc-pVTZ and aug-cc-pVQZ basis sets in order to analyze the effect of the basis set size on the relaxation of dipole moments. The geometries of all the singlet states are obtained through numerical optimization with the use of the CAS(2e,2o) and ic-MRCCSD/aug-cc-pVDZ level of method. For the doublet states, the geometries are obtained by doing the optimization with the use of a CAS(1e,1o) and the

same level of method. The exact geometries of all these molecules are given in the appendix A.1. Dipole moments presented here are calculated by correlating all the electrons in the molecules.

The values of the relaxed(**X**) dipole moments do not change significantly from corresponding unrelaxed counterparts when they are calculated using the active space of (2e,2o). The maximum deviation in the dipole moment, for this kind of relaxation, is an underestimation by 0.03% for the HF. As **X** is dependent on the reference coefficients c_μ's through Eqs. 3.15 and 3.16, the reason for these small deviations can be attributed to the small change in these c_μ's with the change of the external field. Increasing the size of the basis set does not affect the results much either. Use of a larger active space, on the other hand, introduces more configurations which cause greater relaxation of **X** and thus contributes to a larger difference between the unrelaxed and relaxed(X) properties. For CN, this difference is 0.4% with the aug-cc-pVDZ basis and it decreases while going to triple- and quadruple-zeta basis sets. The deviations in the results when using larger active spaces are 0.01% and 0.13% for BO and CH_2, respectively.

However, the effect on the dipole moments is much more pronounced when the orbitals are also relaxed. The relaxation effect is least pronounced for the ground state of LiH, with the maximum change in the dipole moment being 0.4%. The relaxation effect is greatest for BH and HF with the change in the dipole moment being around 3% compared to the one obtained from the expectation value. While this change is about 1.5% for CN, the relaxed values of dipole moments deviate by less than 1% for LiF, BO and CH_2.

These results for ic-MRCCSD can be compared to the differences between expectation values and relaxed first-order properties obtained in ic-MRCI or CASPT2 calculations. Results for these methods, which are calculated using the Molpro program package [120, 121] are added in Tabs. A.2-A.3 of the supplemental. Both of these methods work with internally contracted doubly external configurations, using reference coefficients fixed at the values of the initial internal CI (normally coinciding with the coefficients of the preceding CASSCF computation), but without further relaxation during later steps. The corresponding results show that relaxation of the coefficients has sizable effect on the first order properties, particularly for CASPT2. This effect is larger than the contribution from **X** discussed above for ic-MRCCSD. This relaxation of the reference function is, however, fully accounted for in the ic-MRCCSD first-order properties.

The orbital relaxation contributions are also significantly larger at the CI or CASPT2 level. For instance, the ic-MRCI relaxed and unrelaxed dipole moments of CN deviate by nearly 6 per cent, while this deviation is below 1.5 per cent for ic-MRCCSD. For

CASPT2, the impact of orbital relaxation is even larger for CN, but partially cancels with the effect from the relaxation of the reference.

The dipole moments, as obtained from the ic-MRCC(2) variants of the formulation, are presented in Tab. 5.1 as errors with respect to the ic-MRCC(1) variant. These results show that the magnitudes of these errors are always less than the errors introduced due to the 'unrelaxed' approximation in our formulation. The differences between the dipole moments obtained from these two variants also diminish with an increase in the size of the basis set.

To conclude ic-MRCC unrelaxed properties deviate only slightly from the fully orbital-relaxed values, as it is the case in single-reference coupled-cluster theory [54]. The additional approximation of neglecting the complicated inner derivative due to the transformation of the internally contracted basis has a negligible effect, compared to orbital relaxation.

5.2 Spin-Independent Properties

5.2.1 Different First Order Properties: BH

The current formalism is employed to calculate different spin-independent first order properties, namely the electric dipole moment (μ), the traceless electric quadrupole moment (Θ) and the electric field gradient at the nuclei (q) for the Boron Monohydride (BH) molecule. A benchmark of all these properties using different perturbation and coupled-cluster methods, along with full CI, was done by Halkier *et. al.* [122]. In this section, the results obtained using ic-MRCCSD are compared to those from CCSD(T) and CCSDT, as in Ref. [122], by calculating the error in these first order properties with respect to corresponding full CI results. All of the results from the coupled cluster theories are obtained after relaxing the orbitals. As BH is a linear molecule, only the Z-component of the dipole moment (μ_z) is non-trivial. Similarly, only the ZZ component is significant for both Θ and q as the other diagonal components are redundant following the relation $p_{zz} = -2p_{yy} = -2p_{xx}$, with p=$\Theta$, q. So, from here on, μ, Θ and q simply refer to μ_z, Θ_{zz} and q_{zz}, respectively.

The experimental bond length of BH, 2.3289 a_0 [123], is used to calculate all the properties. An active space of (2e,4o) is used for all the ic-MRCCSD calculations. The 4 active orbitals consist of all the $2p$-orbitals of B and a fourth orbital which is a combination of $2s$(B) and $1s$(H). Calculations of all the first order properties are done using both the

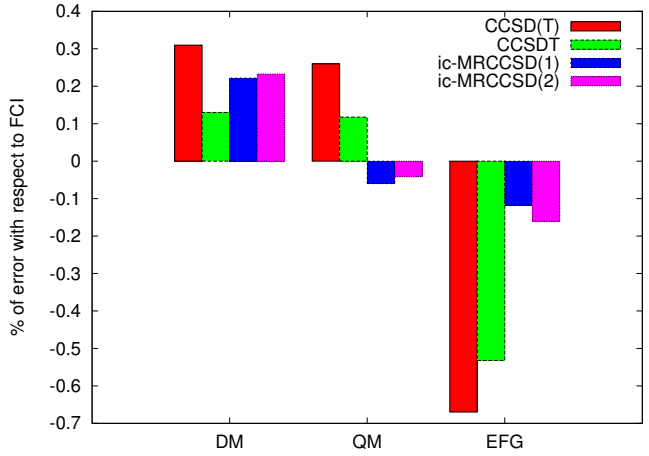

FIGURE 5.1: Errors in different first order properties (DM=dipole moment, QM=quadruple moment, EFG=electric field gradient on B) for BH using the d-aug-cc-pVQZ basis. ic-MRCCSD calculations are done using CAS(2e,4o). Properties for the coupled cluster methods are obtained from Ref. [122] and they include the relaxation effects of orbitals.

variants of ic-MRCCSD. Tabs. A.4-A.6 of the appendix contain all of these calculated values along with those of CCSD(T), CCSDT and FCI where a collection of basis sets are used following Ref. [122]. These basis sets are aug-cc-pVXZ, d-aug-cc-pVXZ and aug-cc-pCVXZ (X=D,T,Q). All calculations are done after keeping the $1s$ orbital of B frozen. An additional calculation is also done correlating all the electrons while using aug-cc-pCVDZ basis set. These calculations show that all of these first order properties obtained using different types of basis, aug-cc-pVXZ, d-aug-cc-pVXZ and aug-cc-pCVXZ, do not change much for a particular X. That is why, as a prototype, the results obtained using the d-aug-cc-pVQZ basis are analyzed here.

Fig. 5.1 graphically presents different first order properties calculated using d-aug-cc-pVQZ. These values are presented as the percentage error with respect to corresponding properties for full CI. The difference between the results from both variants of ic-MRCCSD is always very small compared to the deviations they have with CCSD(T) and CCSDT results, and thus both of these results will be referred to collectively as ic-MRCCSD results in the rest of this section. For the dipole moment, ic-MRCCSD produces an accuracy that lies between the CCSD(T) and CCSDT results, whereas it predicts both Θ and $q(B)$ more accurately than CCSD(T) and CCSDT. Among these three first order properties, the quadrupole moment operator is quadratic in the electronic coordinates (r_i) and demands a good description of the diffuse region of the molecule. The operator for the electric field gradient at a nucleus, on the other hand, is inversely cubic in r_i demanding an accurate description of the inner valence region. That is why a good description of the electronic density in different regions of the molecule is required for a method to

predict equally accurate values of these molecular properties. ic-MRCCSD proves to give a reasonably good description in both of these regions and seems to work reliably while predicting first order properties of different kinds.

5.2.2 Dipole Moment Curve of Lithium Fluoride

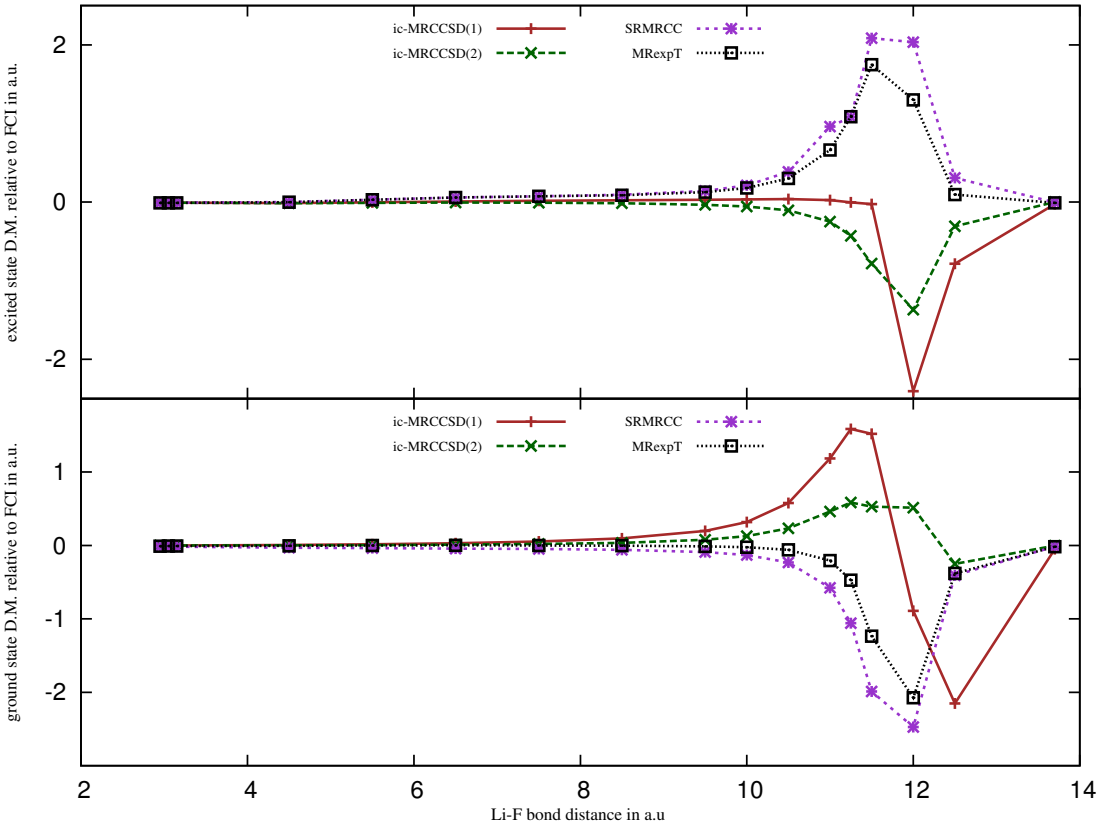

FIGURE 5.2: Errors in the dipole moments with respect to FCI for the ground state and first excited state for the bond breaking model of LiF. The basis set and the dipole moment of methods other than ic-MRCC are obtained from the Ref. [124]. The term ic-MRCCSD(1) and ic-MRCCSD(2) correspond to solving lambda equation with and without the $B_{\lambda c}$ term.

The two lowest lying $^1\Sigma^+$ states of Lithium Fluoride are very important systems for testing multireference theories. At the equilibrium, the ground state $X^1\Sigma^+$ has mainly ionic character, while the excited state $1^1\Sigma^+$ is more covalent. While dissociating the Li-F bond, the molecule goes through a neutral-ionic curve crossing, which requires a balanced description of static and dynamic correlation. While several single-reference [125–127] and multireference methods [124, 128, 129], along with ic-MRCC [18, 119], have been involved in describing the potential energy curve of LiF, a recent study by

Hanrath [124] also used multireference methods to get the dipole moment curve along the same coordinate. In the current work the dipole moment curves for both these states are calculated using ic-MRCCSD and compared to the results for the SRCC based state specific ansatz (SRMRCC) of Oliphant *et. al.* [130] and Piecuch *et. al.* [131] and the MRexpT ansatz of Hanrath [20, 132] along with the results from FCI.

The dipole moments have been calculated using both variants of solving the lambda equations, as denoted by ic-MRCCSD(1) and ic-MRCCSD(2) earlier. Fig. 5.2 shows the dipole moments for different multireference methods as errors with respect to FCI dipole moments for both the ground and excited states of LiF. The ic-MRCCSD calculations are done using the orbitals and reference coefficients as obtained from a state-averaged ($X^1\Sigma^+$ and $1^1\Sigma^+$) CASSCF calculation using an active space of (2e,2o). The basis used for these calculations is the same as was used in Ref. [124] containing $(9s5p)/[4s2p]$ functions for Li and $(9s6p1d)/[4s3p1d]$ functions for F. The $1s$ orbital of lithium and $1s$ and $2s$ orbitals of flourine are kept frozen in order to compare all these results with those of the FCI. The total energies of both these states, obtained using all the methods described here, are presented in Tabs. A.7 and A.8 of the appendix. Corresponding details about the dipole moments are presented in Tabs. A.9 and A.10.

The avoided crossing between these two $^1\Sigma$ states, as predicted by the FCI and all the other multireference methods, is around 12 a.u. Due to the near degeneracy between these two states at this avoided curve crossing, the energies of both states, calculated by MRexpT and ic-MRCCSD, show the largest deviation from FCI. For ic-MRCCSD, as argued in Ref. [119], this deviation can be attributed to the lack of mixing between these two states in the vicinity of the avoided crossing due the state-specific nature of the theory. The dipole moments calculated from all of these multireference methods also show, in Fig. 5.2, largest errors with respect to FCI around the avoided curve crossing.

The dipole moments calculated for the ground state are going to be discussed here first. Near the equilibrium, dipole moments, calculated by all of these multireference methods, are within an error of 10^{-3} a.u. to FCI results. The values of the dipole moments for this region are presented in Tab. A.9 of the appendix. In this region, the dipole moments obtained from ic-MRCCSD are ten times more accurate than those form both the SRMRCC and MRexpT methods. Near the avoided curve crossing, both SRMRCC and MRexpT underestimate the dipole moment by about 2.5 a.u. and 2 a.u. respectively. The behaviour of the ic-MRCCSD(1), which includes the $B_{\lambda c}$ term while solving the lambda equations, is also very erratic near the avoided crossing. The errors, as obtained for ic-MRCC(1), also have a discontinuity as they move from overestimating the dipole moment by 1.5 a.u. to underestimating it by 2 a.u. on either side of this avoided curve crossing. However, the use of ic-MRCCSD(2), by excluding the $B_{\lambda c}$ term while solving

the lambda equations, makes the results less erratic. ic-MRCSSD(2) also produces more consistent dipole moment near the avoided crossing, and is the most accurate among all the methods shown here with the maximum error being an overestimation of about 0.5 a.u.

For the excited state, ic-MRCCSD predicts the dipole moments at equilibrium with almost the same accuracy as compared to both SRMRCC and MRexpT, as evident from Tab. A.10. Around the avoided curve crossing, SRMRCC and MRexpT both overestimate the dipole moment by 2 a.u. and 1.7 a.u. respectively, where ic-MRCCSD(1) and ic-MRCCSD(2) underestimate it by 2.5 a.u. and 1.5 a.u. respectively. Though the dipole moments obtained from ic-MRCCSD(1) are worse in terms of accuracy, they are not as erratic as they were for the ground state.

It is clear that the inclusion of $B_{\lambda c}$ while solving the lambda equations compromises the accuracy of the dipole moments near the avoided curve crossing. However, as mentioned in Sec. 4.5, the term $B_{\lambda c}$ vanishes in the FCI limit and its effects are largest when the excitation classes are truncated in lower ranks making it a more severe approximation. On the other hand, exclusion of this term, by using ic-MRCCSD(2), emerges as a better method to get first order properties for the systems with near degeneracy. The ic-MRCCSD(2) results show a definite improvement over its counterpart in terms of both the nature of the dipole moment curve and its accuracy.

5.3 Spin-Dependent Properties: Hyperfine Coupling Constant

The hyperfine coupling constant is a measure of the hyperfine splitting in electron paramagnetic resonance spectra which is caused by the coupling between the electronic and nuclear magnetic moments. The hyperfine coupling tensor $\mathbf{A}$ is obtained from the spin Hamiltonian describing the coupling between the electron spin $\mathbf{s}$ and the nuclear spin $\mathbf{I}$ as $\hat{H}_{SI} = \mathbf{s} \cdot \mathbf{A} \cdot \mathbf{I}$. The contribution to the hyperfine coupling tensor for a particular nucleus 'K' comes mainly from: a) the isotropic Fermi Contact (FC) and b) the anisotropic Spin-Dipole (SD) interaction terms:

$$\mathbf{A}^{(K)} = \mathbf{A}^{(K;c)} + \mathbf{A}^{(K;d)}; \tag{5.1}$$

with the isotropic FC tensor $\mathbf{A}^{(K;c)}$:

$$\mathbf{A}^{(K;c)}_{kl} = \delta_{kl} \frac{8\pi}{3} \frac{g_e g_K \beta_e \beta_K}{2S} \sum_{pq} {}^3\Gamma^q_p \langle \chi_p | \delta(r_{iK}) | \chi_q \rangle, \tag{5.2}$$

and the anisotropic SD tensor $\mathbf{A}^{(K;d)}$:

$$\mathbf{A}_{kl}^{(K;d)} = \frac{g_e g_K \beta_e \beta_K}{2S} \sum_{pq} {}^3\Gamma_p^q \langle \chi_p | r_{iK}^{-5} (r_{iK}^2 \delta_{kl} - 3 r_{iK;k} r_{iK;l}) | \chi_q \rangle. \tag{5.3}$$

Here, χ_ps are the molecular orbitals. The components of the one-particle spin-density, ${}^3\Gamma_p^q$, are calculated following their definition given in Eq. 4.25. The indices k, l, in the definition of the above tensors, denote the spatial components x, y, z. g_e and β_e are respectively the g-factor and the Bohr magneton of electrons, where g_K and β_K are the corresponding counterparts for the K'th nucleus. The total spin of the system is denoted here by S with r_{iK} denoting the distance between the i'th electron and K'th nucleus.

The accuracy of these HFCCs, as calculated using Eqs. 5.2 and 5.3, depends on an accurate description of spin-density throughout a molecule. In this work, HFCCs for the doublet ground states of BeH are calculated first to see how these properties change with an increase in the size of the active space. Both of the HFCCs are then calculated for the doublet ground states of BO, CO^+, CN and AlO radicals and compared with the results from other multireference methods. The spin-adapted version of ic-MRCCSD, that has been used in this whole work, is more relevant in these calculations as it keeps the total spin of the doublet states intact.

5.3.1 BeH

The accuracy of the energies obtained using a multireference method increases with the increase in the size of the active space as the corresponding number of configurations also increases. However, this might not be the same for the properties as they require a good description of the charge or spin density in the different region of a molecule depending on the nature of the properties. To check how the change in the size of the active space affects the accuracy of the spin-dependent properties, both the FC and SD terms are calculated using ic-MRCC for the doublet ground state of BeH. The bond distance of Be-H that is used here is 1.356 Å, with the bond being along the z-axis. These calculations are done for different active spaces and then the accuracy of the results for are measured with respect to the FCI results. The aug-cc-pCVDZ basis set is employed for these calculations as the use of a larger basis set was not possible here due to the lack of corresponding FCI results. Similar trends in the CASSCF and the uncontracted multireference configuration interaction (MRCI) methods are also calculated and discussed here.

Four different active spaces are used for the calculations of the HFCCs. The active orbitals used for respective active spaces are presented in Tab. 5.2. This hierarchy of active spaces is obtained by sequentially adding the orthogonal 2p orbitals ($2p_x$ and $2p_y$)

and the core 1s orbitals of Be on top of a minimal active space of (3e,3o). It is expected that an increase in the size of the active spaces would increase the accuracy of the energy and properties of molecules. The outcomes of the calculations are presented graphically in Fig. 5.3 for ic-MRCC, MRCI and CASSCF. More of the data used in this discussion can be found in Tab. A.11 of appendix A.

TABLE 5.2: Description of the different active spaces used for BeH

active space	active orbitals
(3e,3o)	Be: 2s2p$_z$ H: 1s
(3e,5o)	Be: 2s2p$_z$2p$_x$2p$_y$ H: 1s
(5e,4o)	Be: 1s2s2p$_z$ H: 1s
(5e,6o)	Be: 1s2s2p$_z$2p$_x$2p$_y$ H: 1s

For ic-MRCCSD, the accuracy of the results of HFCCs do not increase with increasing size of the active space except for the FC term of Be. For the FC term of Be, ic-MRCCSD produces the best result using the largest active space of (5e,6o). But for all the other HFCCs, the results move away from those of FCI after including the orthogonal p orbitals (p$_x$ and p$_y$) though the error decreases after including the core 1s orbital of Be. Values of some other first order properties, such as dipole moment, quadrupole moment and electric field gradient, along with the energy of this state are presented in Tab. A.11 of the appendix. These data also show that these first order properties also do not converge to the FCI results while increasing the active space, although the energy does converge to the FCI energy.

The values of HFCCs obtained from MRCI are not as accurate as those of ic-MRCC. However, for MRCI, the error with respect to FCI results decreases when the orthogonal p-orbitals are included in the active space, although this error increases when the (5e,4o) active space is used, which has the core 1s orbital of Be included. Fig. 5.3 also presents the values of HFCCs from CASSCF as both ic-MRCCSD and MRCI calculations are done taking the orbitals and CI coefficients from CASSCF.

5.3.2 BO, CO^+, CN and AlO

The FC and SD terms of BO, CO^+, CN and AlO radicals were evaluated recently by Yanai *et. al.* [133, 134] using different suite of methods, such as DFT, coupled cluster

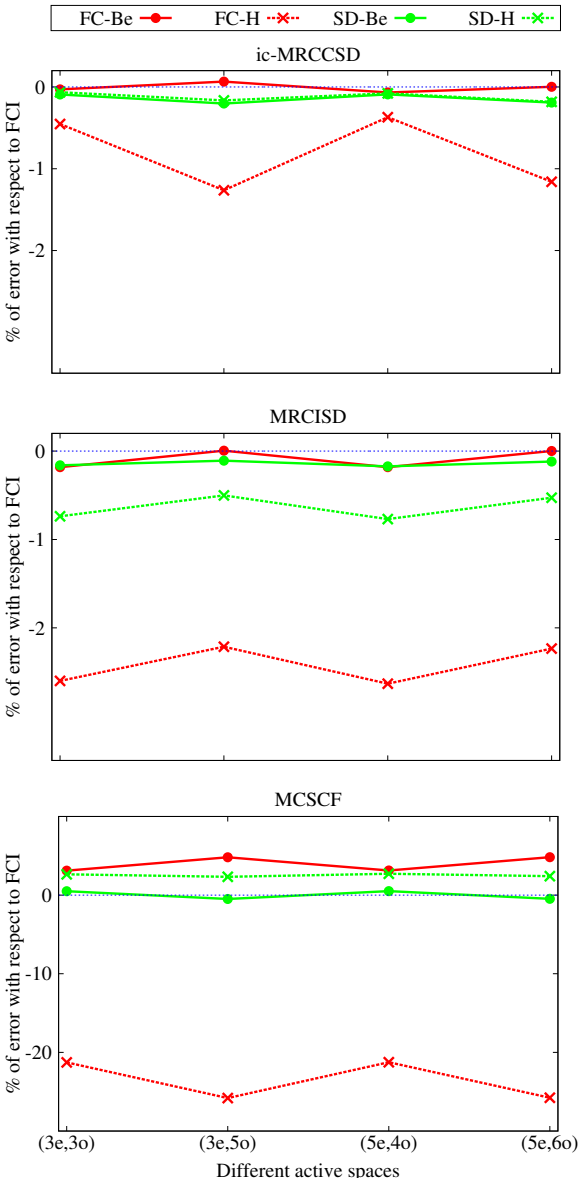

FIGURE 5.3: Percentage of errors in the isotropic HFCC (FC) and anisotropic HFCC (SD) with respect to the FCI results for the $^2\Sigma$ ground states of the BeH. Results are obtained for ic-MRCCSD , uncontracted MRCI and MCSCF using aug-cc-pVDZ. The errors are presented with a different scale for MCSCF than ic-MRCCSD and MRCI.

level of methods, CASPT2 and density matrix renormalization group (DMRG) methods. In this work, the values of these HFCCs are calculated using ic-MRCC and the results are compared with those obtained from Ref. [133, 134]. Experimental measurements of HFCCs done in gas-phase are mostly used as the reference for these comparisons, however sometime measurements in Ne or Ar matrices are also used as the reference.

The geometries for all the $^2\Sigma$ diatomic radicals are adopted from the experimental measurements [135] as in Ref. [133]. The bond lengths that are used here are 1.2049 Å, 1.1500 Å, 1.1718 Å and 1.6176Å for the BO, CO^+, CN and AlO radicals respectively. The basis EPR-III is used to calculate both of the HFCCs. Yanai *et. al.* [133] showed that the basis set error in EPR-III is negligible for these molecules as it gives results comparable to the uncontracted ANO-L-TZP basis. Choice of the active space for the ic-MRCCSD calculations is also a significant contributor to the accuracy of the spin-densities calculated here. Three different types of active spaces: (1e,1o), (5e,6o), and (9e,8o) are employed for the ic-MRCCSD calculations of BO, CO^+ and CN radicals here, and corresponding calculations for AlO radicals are done using (1e,1o) and (7e,6o) active spaces. CAS(1e,1o) has the singly occupied orbital as the active orbital and thus contains only one reference function in the space. While the CAS(5e,6o) includes the 2p-orbitals of its constituent elements as the active orbitals, the CAS(9e,8o) has 9 electrons distributed over all the valence orbitals of the elements. The active orbitals for the (7e,6o) CAS for AlO are obtained from the set of [Al:3p,O:2p] orbitals by replacing the unoccupied $3p_z$ with the occupied 3s orbital.

The (1e,1o) CASSCF is equivalent to a ROHF calculation and the HFCCs obtained from ic-MRCCSD thereafter differ from the CCSD results mainly due the spin-adaptation that has been used. All the electrons are correlated while calculating HFCCs. All the ic-MRCCSD results presented here are obtained by using the ic-MRCCSD(1) variant of the method. For the BO, CO^+ and CN radical, the results of both the HFCCs have been presented in Figs. 5.4 and 5.5 as a percentage of deviations compared to the experimental results. The results for the AlO radical have been presented in Tab. 5.3 which also contains some additional results obtained using CASPT2 calculations. These results are presented elaborately in tabular forms in appendix(A.13-A.16).

5.3.2.1 Isotropic HFCC

The FC term of the less electro-negative counterpart of the molecules under study have been analyzed first. For this analysis the experimental gas phase results are used as the reference to compare to the theoretical results. For the discussions, the main comparison of the ic-MRCCSD results are made with the results obtained from the DMRG methods.

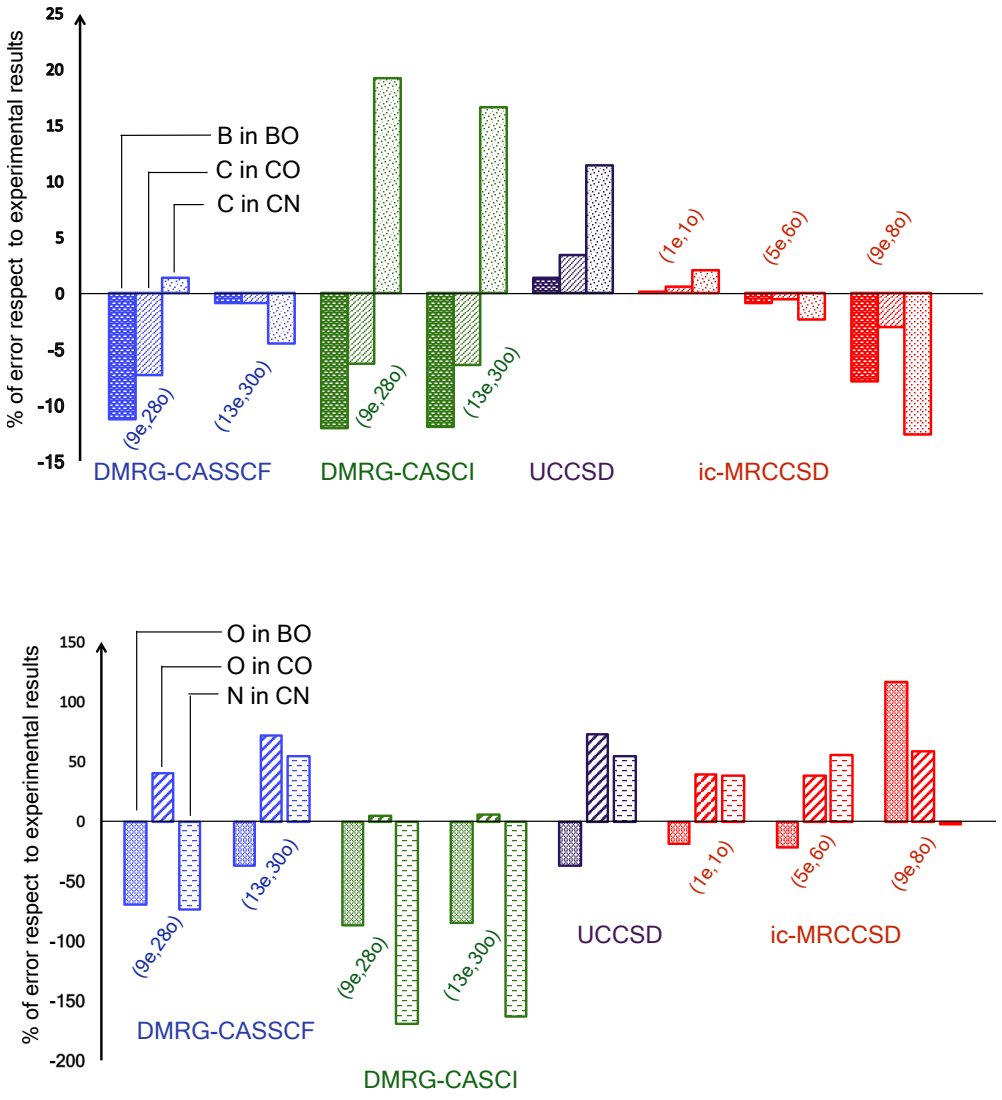

FIGURE 5.4: Percentage of errors in the isotropic HFCC with respect to the gas-phase experimental results for the $^2\Sigma$ ground states of the radicals CO^+, BO and CN. The EPR(III) basis set is used for all the calculation and all the results, except the ones for ic-MRCCSD, are obtained from Ref. [133].

The DMRG methods [136–138] have been established in recent years to be an efficient way to include the static correlation while still using a very large active space. These methods have also been extended to their orbital optimized form (DMRG-CASSCF) [139, 140] and have also been proven to be accurate while predicting spin densities of complex molecules [133, 141]. DMRG results obtained without the orbital optimization are denoted here as DMRG-CASCI. All the results for different DMRG methods are obtained from Ref. [133] and those calculations are done mainly using the active spaces of (9e,28o) and (13e,30o), where the latter also includes the core electrons and orbitals as a part of the active space.

For the B atom in BO, the best result for the FC term among all of the DMRG methods, is obtained from optimizing the orbitals for the active space of (13e,30o) producing an error of 0.87%. DMRG-CASSCF with a (9e,28o) active space and DMRG-CASCI for both of the active spaces underestimate the FC term by almost 12%. ic-MRCCSD while using (1e,1o) gives the FC term with an overestimation of the experimental result by only 0.09%. The value decreases and it underestimates the experimental value by 0.84% when a larger active space of (5e,6o) is used. The magnitude of error increases for the CAS(9e,8o) to -7.8%

For the C atom in CO^+ the calculated values for the FC term follow the same trend as the last example. DMRG-CASSCF(13e,30o) produces an accuracy of 1.37% while the other DMRG methods underestimate the experimental value by almost 7%. ic-MRCCSD(1e,1o) is very accurate, overestimating the experimental value by only 0.64%. With the increase of the active space, ic-MRCCSD underestimates the experimental value giving errors of 0.47% and 3% for (5e,6o) and (9e,8o) respectively.

For the C atom in the CN radical, CCSD overestimates the experimental value of the FC term in an Ar matrix by 11.39%. Inclusion of perturbative triples lowers the value below the experimental one with the error now being 5.43%. DMRG-CASCI calculations largely overestimate the experimental value while DMRG-CASSCF reduces the error. With the active space of (9e,28o) DMRG-CASSCF overestimates the experimental value by 1.44%, but with the enlargement of the active space to (13e,30o) DMRG-CASSCF goes on to underestimate it by 4.43%. For ic-MRCCSD, the value of the FC term decreases with increases in the active space, the error with respect to the experimental value being 2.04% and -2.37% for the active spaces (1e,1o) and (5e,6o) respectively. The error increases to -12.6% for the CAS(9e,8o).

Theoretical prediction of HFCCs for AlO is difficult as the spin density of the radical is extremely sensitive to the way the electronic structure method treats the two main configurations $Al^{2+}O^{2-}$ and $Al^{+}O^{-}$. The unpaired electron resides in the Al *s* orbital for the first configuration and in the O *sp* hybrid orbital for the latter. This difficulty

in getting the HFCCs is reflected in the value obtained for the FC term of Al here while using different methods. The experimental value in the gas phase has been used as the reference here. The experimental value in a Ne matrix differs significantly from the gas phase one. Single-reference methods CCSD and CCSD(T) fail measurably to produce the experimental value with the error being -34.7% and -23.4% respectively. For DMRG-CASSCF, the results depends heavily on the choice of the active space. Here the best result with an error of -3.43% is obtained with a huge active space of (21e,36o). In this case, all the core electrons and the Al $4d$ polarization orbitals are added to the active space. Individual inclusion of either of these orbitals lead to errors of 20.19% and -22.35% respectively. ic-MRCCSD, however, produces the values with good accuracy even with smaller active spaces. With the active space of (1e,1o) it overestimates the experimental value only by 6.15%, whereas use of the larger active space of (7e,6o) produces an error of -2.8%.

It is difficult to measure the HFCC experimentally in the gas-phase for the electro-negative atoms in each of these radicals. So, the results from experiments done in the noble gas matrix has been used as the reference for the comparison between the theoretical results. The errors in predicting the HFCCs by different methods are very high in general for the electro-negative atoms which could be attributed to the absence of any good experimental references and also the fact that absolute values of these HFCCs are quite low. For the B atom in the BO radical, DMRG-CASSCF is giving the best results with an error of -37.11% using active space of (13e,30o). All the other DMRG calculations are giving a very low value and these are not at all comparable to the experimental one. For ic-MRCCSD, the best result with an underestimation of 18.63% is obtained using the active space of (1e,1o) whereas CAS(9e,8o) gives the poorest result. For the O atom in CO^+, ic-MRCCSD overestimates the experimental result by about 39% for both the active spaces of (1e,1o) and (5e,6o). DMRG-CASSCF(13e,30o) gives an overestimation of 71.6% where DMRG-CASCI produces an accurate result within 5% of the experiment. For O in AlO radical, the experimental value of the isotropic HFCC is very low (2 MHz) and only DMRG-CASCI can predict a value close to this experimental value and also when the active space includes the core electrons. This agreement could also be due to fortuitous error cancellation [133]. ic-MRCCSD overestimates the experimental results by 6.20 MHz and 5.7 MHz while using the active spaces of (1e,1o) and (7e,6o) respectively. The reason for this poor agreement can be attributed to the lack of balance while treating the two main configurations as described earlier.

For the N atom in the CN radical, the errors are also quite big. The best result obtained from DMRG are with CASSCF (13e,30e) which still overestimate it by 54.9%. For ic-MRCCSD, the best result is obtained for the largest active space (9e,8o) with an underestimation of 2%. ic-MRCCSD, otherwise, overestimates the FC term by 38.3%

and 55% while using the (1e,1o) and (5e,6o) active spaces respectively.

5.3.2.2 Anisotropic HFCC

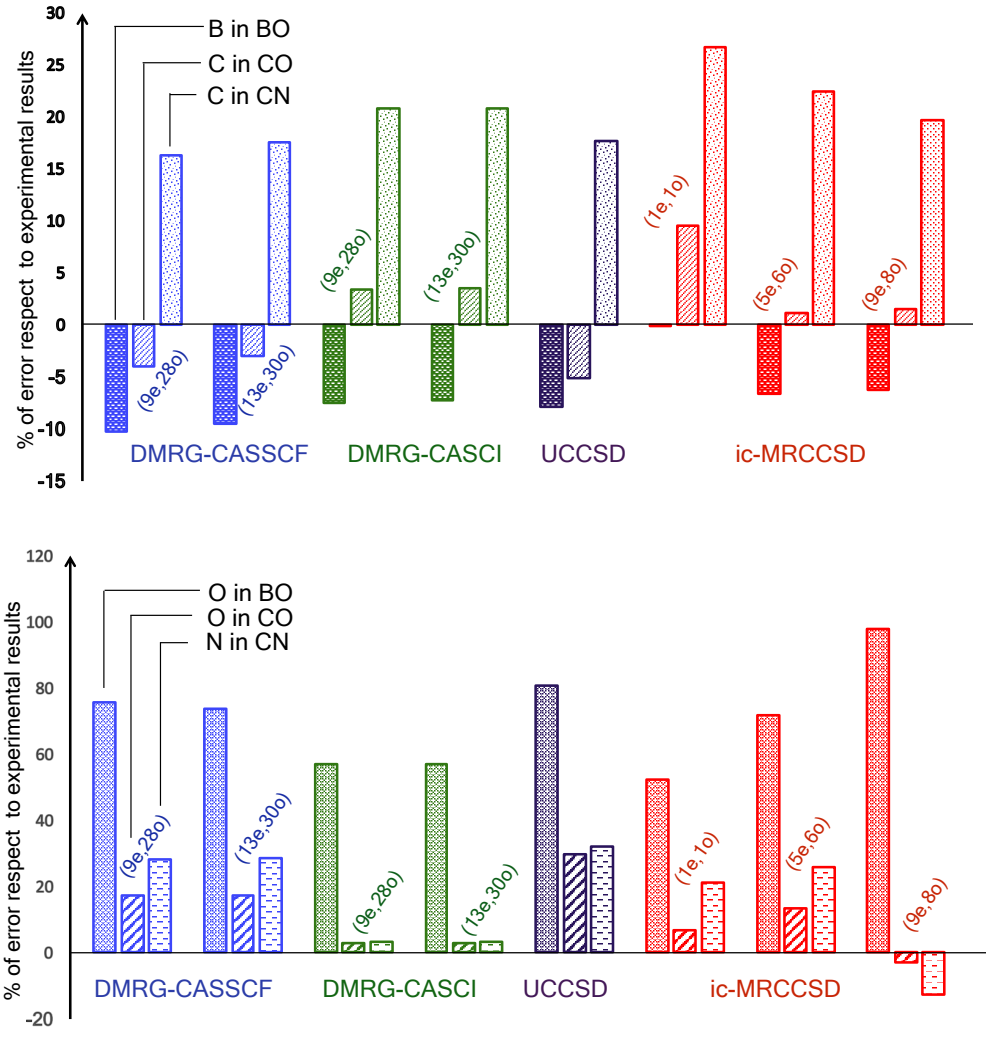

FIGURE 5.5: Percentage of errors in the anisotropic HFCC with respect to the gas-phase experimental results for the $^2\Sigma$ ground states of the radicals CO^+, BO and CN. The EPR(III) basis set is used for all the calculation and all the results, except the ones for ic-MRCCSD, are obtained from Ref. [133].

Due to the linear structure of all these molecules the anisotropic HFCC matrix is diagonal in nature and the diagonal elements follow the relation $A_{33}^{K,d} = -2A_{11}^{K,d} = 2A_{22}^{K,d}$. Therefore the component $A_{33}^{K,d}$ will be mainly discussed here and will be referred as $A^{K,d}$ from here.

The analysis of the results for the SD term is first done here for the less electronegative atoms of the free radicals. A general trend observed here is that neither the use of optimized orbital nor the inclusion of core electrons inside the active space have much effects on the results for DMRG. The best of the results obtained for ic-MRCCSD are more accurate than those obtained from DMRG methods for all but the C center in CN. The full valence active space, (9e,8o), gives results comparable to that of the (5e,6o) active space for these cases. Use of the CAS(1e,1o) gives an accuracy of 0.1% for B in BO where the accuracy reduces when the higher active spaces are used. But for C in CO^+ and CN, ic-MRCCSD produces a better accuracy with the higher active spaces of (5e,6o) and (9e,8o). For Al in AlO, the best results are obtained from the CASPT2 calculation that uses the (9e,8o) active space, and optimizes both the orbitals and reference coefficients giving an error of only -1.0% with respect to the experimental result. ic-MRCCSD provides the SD term with an error of 1.3% using the (1e,1o) active space.

TABLE 5.3: Isotrpoic ($A^{K,c}$) and anisotropic ($A^{K,d}$) hyperfine coupling constants (in MHz) for the ^{2}AlO radical obtained using EPR-III basis sets. DMRG-CASSCF, DMRG-CASCI, CCSD and CCSD(T) results are taken from Ref. [133]. CASPT2 results are taken from Ref. [134].

	^{27}Al		^{17}O	
Methods	$A^{K,c}$	$A^{K,d}$	$A^{K,c}$	$A^{K,d}$
DMRG-CASCI(9e,21o)	727.98	94.63	-0.71	-85.13
DMRG-CASCI(15e,28o)	670.79	92.73	-2.07	-91.28
DMRG-CASCI(21e,31o)	682.79	92.79	1.57	-90.95
DMRG-CASCI(15e,33o)	702.8	92.83	-3.16	-90.51
DMRG-CASCI(21e,36o)	708.32	92.99	1.61	-90.28
DMRG-CASSCF(15e,28o)	629.25	106.27	-42.28	-98.4
DMRG-CASSCF(21e,31o)	887.02	105.97	-28.35	-92.94
DMRG-CASSCF(15e,33o)	573.08	109.62	-57.34	111.09
DMRG-CASSCF(21e,36o)	712.65	108.31	-35.04	-104.4
CASPT2(9e,8o), unrelaxed	998.8	106.6	-0.5	68.8
CASPT2(9e,8o), relaxed	788.3	111.6	13.4	105.2
CCSD	482.02	114.26	18.14	-127.71
CCSD(T)	565.3	112.4	19.3	-117.8
ic-MRCCSD(1e,1o)	783.35	114.23	8.20	-97.42
ic-MRCCSD(7e,6o)	717.28	105.04	7.74	-111.13
ic-MRCCSD(7e,7o)	694.23	106.18	16.50	-112.31
expt - gas phase	738	112.8	-	
expt - Ne matrix	766	106	2	-100

The errors with respect to the experimental results are again very large when the SD terms for the electronegative atoms of all the radicals are considered as the experimental

references are obtained in Ne matrix instead of the gas phase. For these examples, DMGRG-CASCI provides better results than DMRG-CASSCF and for O in CO^+, and N in CN, these results are even better than results obtained from ic-MRCCSD. The best of the ic-MRCCSD results are obtained using the active space of (1e,1o) for O in BO, and AlO and (9e,8o) for O in CO^+ and N in CN. For AlO, ic-MRCCSD(1e,1o) gives the anisotropic HFCC to within an error of 3% where this accuracy is only matched while using DMRG-CASSCF while using a huge CAS of (15e,28o).

To summarize, ic-MRCCSD consistently provides good agreement of both the HFCCs to the experimental result even with an active space of (1e,1o). In most of the cases, these results are better than the best obtained from DMRG. With the enlargement of the active space to (5e,6o), the accuracy of the results decreases a little, but even then it is better than that from DMRG for most of the cases. Use of the full valence active space (9e,8o), however, gives the poorest results among all these active space for most of the examples. This shows that HFCCs, especially the singular Fermi contact term, appear to be very difficult to converge with an increasing size of active space which is also discussed for BeH in Sec. 5.3.1.

6 | Results: Second Order Properties

The linear response formalism for the ic-MRCC theory, as presented in Sec. 4.5, provides the expression for the linear response function. In the current chapter, this formalism has been applied to calculate static and dynamic polarizabilities of several molecular systems which are obtained as the values of this linear response function at corresponding frequencies. the linear response formalism also provides, in Sec. 4.4, the response equations which need to be solved to obtain first order wave function parameters $c_\mu^{(1)}$ and $t'_\rho{}^{(1)}$. These parameters are then used to calculate the linear response functions. However, both of the final expressions for the response function and response equations are obtained through respective approximations during their formulations. Both of these two approximations are required in order to get rid of the unphysical second order poles of the linear response function which are otherwise inherent to the ic-MRCC theory. The approximation introduced in the response equations ensures this by removing the coupling between the first order wave function parameters of different frequencies. The same is achieved through the approximation made in the linear response function as it removes the terms which are quadratic in the wave function parameters of the same frequency. In the first part of this chapter, these two approximations are assessed numerically through direct comparison between the results obtained with and without the use of each of these approximations. In the latter part of this chapter, the approximated version of the linear response theory is used to show the accuracy of the method, by comparing the second order properties that it provides with the FCI results. Different components of the polarizabilities are also calculated for *p*-benzyne and pyridyne to show that no additional spurious poles appear in the linear response function from the use of this response formalism of the ic-MRCCSD method, unlike some other multireference methods.

6.1 Avoiding the Second Order Poles: Assessment of the Approximations

The linear response theory for ic-MRCC is developed following two different approximations. While the approximation dealing with the response equations has been presented in Sec 4.4, the approximation in the response function has been discussed in Sec. 4.5. Both of these approximations ensure that there is no term present in the expression of the linear response function which could potentially lead to any second order pole. In this section, the individual contributions of these two approximations towards the removal of the second order poles are going to be be analysed. The errors arising due to the individual uses of these two approximations are also presented here to show how much these approximations can change the values of the second order properties. To analyse these effects, electrical polarizabilities at different frequencies are calculated for CH_2 and BH molecules and plotted against the frequencies. The actual structure of the linear response function can be understood, however, by inverting the plots of electrical polarizabilities as they have opposite signs following the relation given in Eq. 2.46. For CH_2, the calculations are done assuming c_{2v} symmetry with the coordinates for C(0,0,-0.188174), and H(0,$\pm$1.630065,1.120279) in Bohr and using the cc-pCVTZ basis set. The active space of (2e,2o) comprising the orbitals $3a_1$ and $1b_1$ are used for these calculations. The calculations for BH are done using the TZP basis and a bond distance of 2.4648 Å. The minimal active space of (2e,2o) is also used for BH where the σ and σ^* orbitals corresponding to the BH bond are the ones used as the active orbitals. All the electrons are correlated in the calculations for both of these molecules. The polarizabilities of the components ZZ (α_{ZZ}) and XX (α_{XX}) are calculated for CH_2, whereas only the ZZ component (α_{ZZ}) is calculated for BH. These are the only components for these two molecules which require contributions from first order reference coefficients, and thus making these approximations non-trivial.

Four different variants of the ic-MRCC-LR appear depending on which of these two approximations are used. The descriptions of all these four ways of formulating the ic-MRCC-LR variants are presented in Tab. 6.1. To study the effects of these two approximations individually, different components of polarizability are calculated using variants of ic-MRCC-LR which differ in one of these approximations. This study is done in the following sections by first analyzing the effect of the approximation in the response function, as it produces the main contribution in the appearance of second order poles of the linear response function. An analysis of the approximation made in the response equation will then follow.

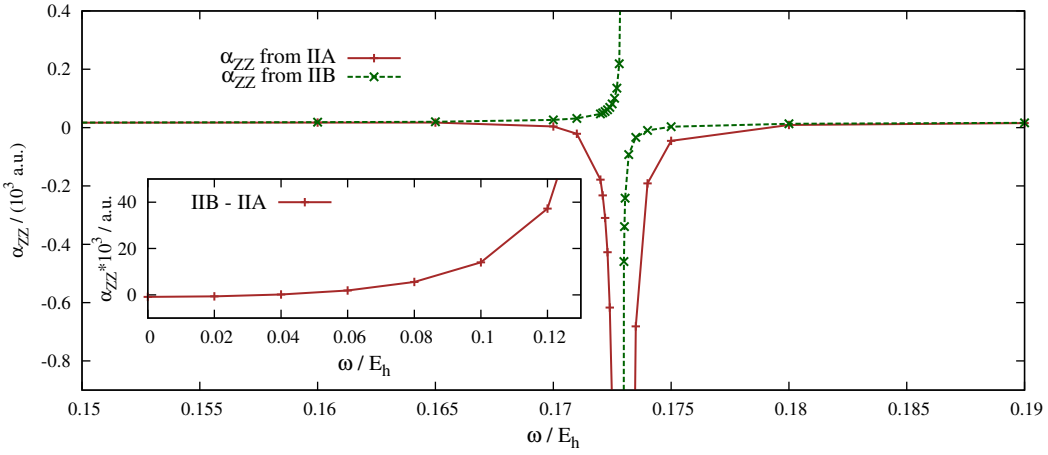

(a) α_{ZZ} of CH_2

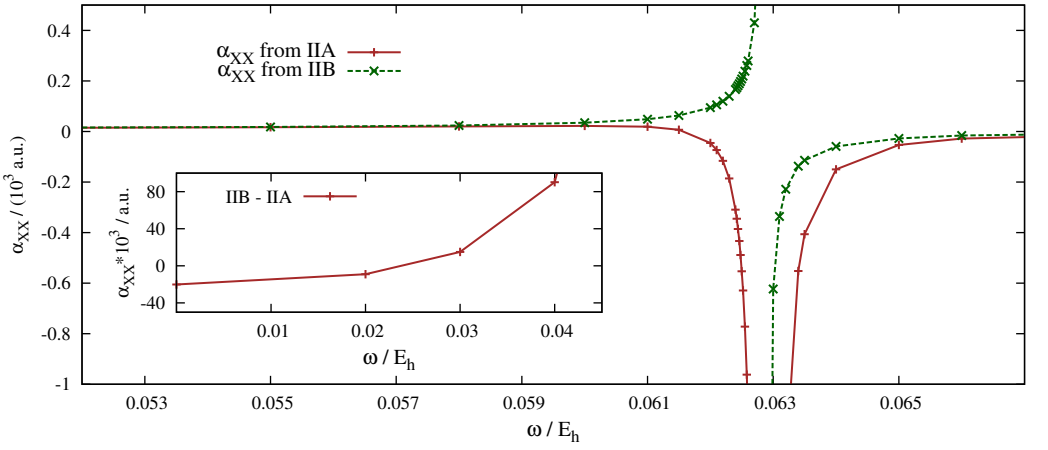

(b) α_{XX} of CH_2

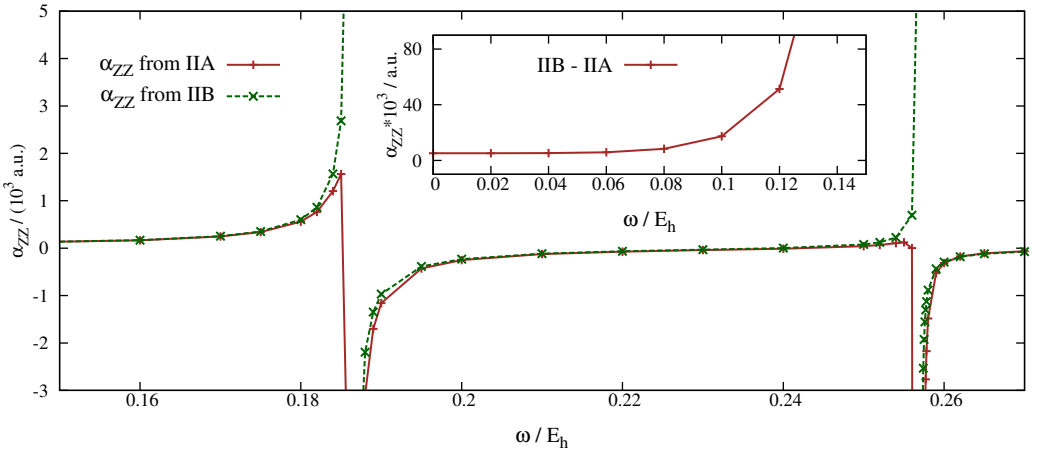

(c) α_{ZZ} for BH

FIGURE 6.1: These plots show the change in the numerical results due to the approximation in the response function. Components of electrical polarizability are plotted against frequencies for three different cases (a-c). The main parts of each plot have polarizabilities from ic-MRCC calculated with (ic-MRCC-LR-IIB) and without (ic-MRCC-LR-IIA) the approximation in the response functions. The plots in the inset show the differences between these two methods. The ranges of the frequencies in the X-axis and polarizabilities in the Y-axis differ for the main part and inset of each of the plots.

TABLE 6.1: Introduction of the labels for the different levels of the ic-MRCC-LR methods depending on the approximations being used. (✓) is used in this table to denote the use of the original expression/equation where (✗) denotes the use of the approximated one.

ic-MRCC-LR variants	use of Response Equation[1]	use of Response Function[2]
IA	✓	✓
IB	✓	✗
IIA	✗	✓
IIB	✗	✗

[1] Original: Eq. 4.34, approximated: Eq. 4.43.
[2] Original: Eq. 4.46, approximated: Eq. 4.47.

6.1.1 Approximation in the Response Function

The full expression of the linear response function, presented in Eq. 4.46, is split into four components, where the terms belonging to part IV are quadratic in the same first order wave function parameters when $X = Y$ ($\omega_Y = -\omega_X$). These contributions potentially lead to a second order pole structure for the diagonal component of linear response function. These two terms appear, along with the term in III, due to the presence of reference function in the projection manifold, in place of its bi-orthogonal conjugate, in the expression for the time-dependent Lagrangian. To get a correct pole structure, a new linear response function, as given in Eq. 4.47, is formulated by removing the terms in III and IV of Eq. 4.46. However, the second order properties as obtained from this approximated linear response function are prone to errors from removing those terms. The magnitude of these properties needs to be considered only near the static limit as near the poles these errors also diverge. In this section, this approximation in the form of the linear response function is assessed by looking into the change in the corresponding pole structure, and also by evaluating the magnitude of errors it introduces in the second order properties. With that aim, electrical polarizabilities for ic-MRCC are calculated using the variants IIA and IIB which use the full and approximated expressions for the linear response function, respectively. The approximated response equations are solved to get the first order wave function parameters for both of these cases, which removes any possible contributions to the second order pole structure coming from the response equations. The polarizabilities obtained from both of these formulations are plotted against a range of frequencies in Figs. 6.1a-6.1c along with the difference between these two results. Where absolute polarizabilities obtained from both of the formulations are plotted for frequencies closer to the poles, the difference between these two results is plotted to show

the error in the region closer to the static limit. A detailed look into the values of these polarizabilities can be found in Tabs. B.2-B.4 of appendix B.

The plots of different components of polarizability, obtained using both the variants IIA and IIB, clearly show that the second order nature of the poles of the linear response function is successfully circumvented through the approximation in its expression. The second order nature of the poles obtained from the variant IIA is obvious from the plots in Fig. 6.1a-6.1c, as the linear response function approaches the singularity by diverging to $+\infty$ and then comes out of it also from $+\infty$. The variant IIB, on the other hand, produces a simple first order pole as plotted in Fig. 6.1. The errors introduced through this approximation are the total magnitudes of the terms in III and IV of Eq. 4.46. These errors are only meaningful close to the static limit as these terms diverge at the poles. At the static limit, variant IIB, which uses the approximated linear response function, underestimates the α_{XX} of CH_2 by 0.2% with respect to the one obtained from variant IIA. Corresponding errors for α_{ZZ} are -0.006% and 0.01% for CH_2 and BH, respectively. However, for CH_2, the variant IIB starts overestimating both α_{XX} and α_{ZZ} with an increase in frequency of the external field before they diverges to $+\infty$ at the poles. These errors are within 10% for α_{XX} and α_{ZZ} untill the frequency reaches 0.055 a.u. and 0.16 a.u. respectively. α_{ZZ} for BH is overestimated by the approximation throughout its spectrum with the error being within 10% untill the frequency of 0.18 a.u. The errors introduced through the approximations are very high even after the poles, though for both of the variants polarizabilities start from$-\infty$ after the singularity. This, in fact also broadens the width of the second order poles, compared to the first order ones. However, the difference between these two variants decreases between two consecutive poles. Between the two poles of $\langle\langle Z; Z\rangle\rangle$ for BH, shown in Fig. 6.1c, the difference reduces to $\sim$8%, whereas at the end of the observed spectra, this difference reduces to $\sim$2% and $\sim$3% for CH_2 and BH respectively.

Overall, the approximation made in the formulation of the linear response function for ic-MRCC gives the correct first order pole structure. The errors introduced by this approximation are very small near the static limit. A further study has shown that the main two contributions, the terms in III and IV of Eq. 4.46, cancel the effect of each other through opposite signs. This keeps the overall errors for the approximation smaller and also independent of the size of the active space.

6.1.2 Approximation in the Response Equations

The response equations as derived for ic-MRCC in Eq. 4.34 couple $\mathcal{X}$ and $\mathcal{Y}$ which are the vectors containing the first order wave function parameters for ω, and $-\omega$, respectively.

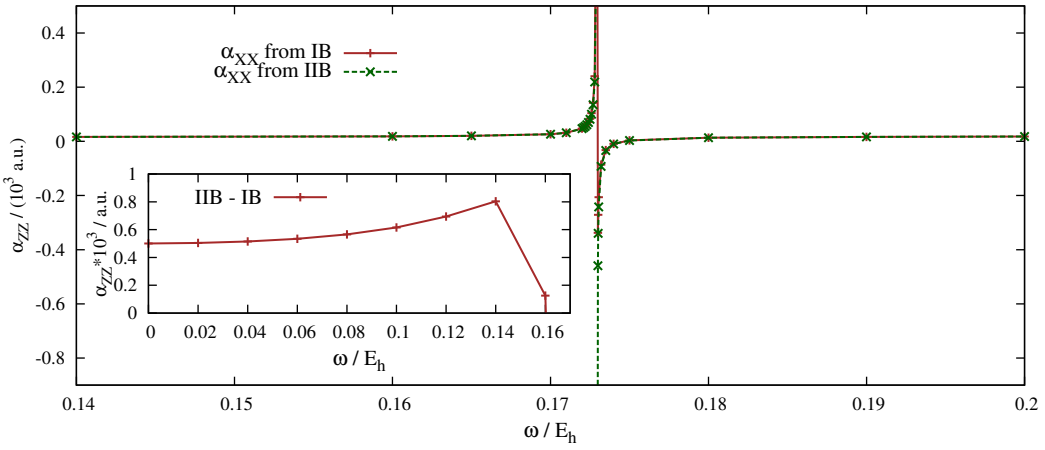

(a) α_{ZZ} of CH_2

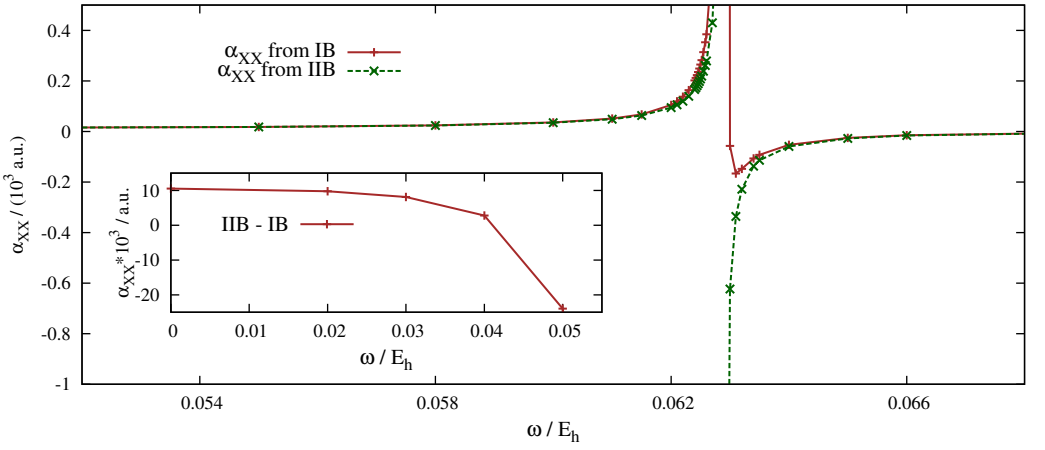

(b) α_{XX} of CH_2

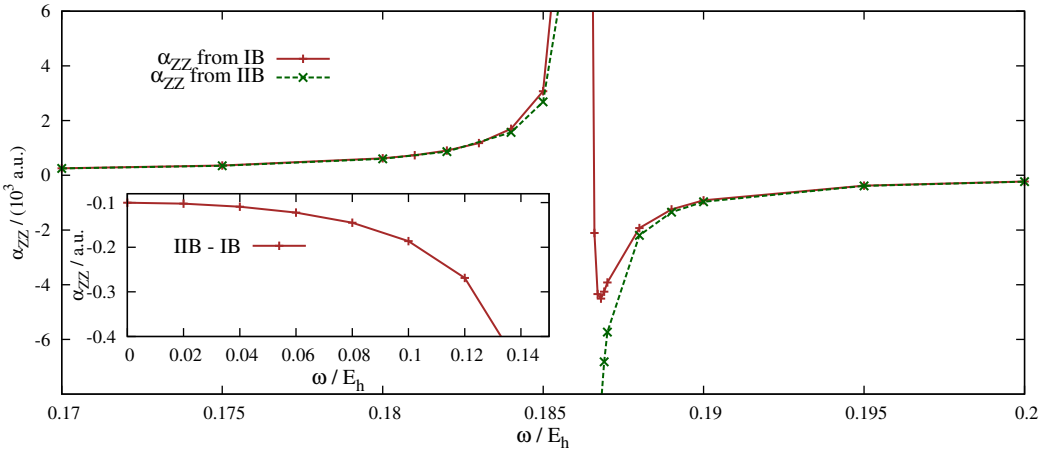

(c) α_{ZZ} for BH

FIGURE 6.2: Plots of different components of electrical polarizability against frequency for three different cases: (a-c). Polarizabilities are obtained by solving the response equations formulated in two different ways: I) in Eq. 4.34 which includes the coupling between first order parameters corresponding to the frequencies of opposite signs (the IB variant), and II) in Eq. 4.43 which excludes the coupling mentioned earlier (IIB variant). The main part of each of the plot has the polarizabilities from both IB and IIB plotted individually. The inset has the differences between the results of these two methods. The ranges of the frequencies in the X-axis and polarizabilities in the Y-axis differ for the main part and inset of each of the plots.

The full vector forms of both $\mathcal{X}$ and $\mathcal{Y}$ are defined in Eqs. 4.38, and 4.39, respectively. The coupling between $\mathcal{X}$ and $\mathcal{Y}$ leads to the simultaneous divergence of both of them near the poles of the linear response function. Through term II in the Eq. 4.46, the singularities of these parameters contribute to the second order poles of the linear response function. A Tamm-Dancoff inspired approximation produces the alternative response equations (Eq. 4.43) which decouple $\mathcal{X}$ and $\mathcal{Y}$ and thus remove the contribution to the second order poles coming through the response equations. However, this approximation also introduces errors in the values of the second order property which is calculated using the solutions of these equations. To see the extent to which these values deviate due to the approximation, electrical polarizabilities are calculated for a range of frequencies while solving the response equations with and without this approximation. To remove any further contribution to the second order poles, the approximated expression of the response function, as given in Eq. 4.47, is used for calculating these polarizabilities. So, the IB and IIB variants of ic-MRCC-LR, defined in Tab. 6.1, are used here to calculate the polarizabilities. These results from each of these variants and also the difference between them are plotted in Fig. 6.2a-6.2c. Similarly to the discussion of the results in the previous section, for the approximation in the response function, the values of polarizabilities from both the variants are plotted for the frequencies near the poles, whereas their differences are plotted close to the static limit. The results used in these plots are presented in Tabs. B.5-B.7 of appendix B.

The plots of polarizabilities obtained from the variant ic-MRCC-LR-IB, which uses the coupled response equations, show the second order poles of the linear response function, albeit the second order nature of the poles are not as prominent as those obtained from the the variant ic-MRCC-LR-IIA presented in in Sec. 6.1.1. Figs. 6.2a-6.2c clearly show that the second order nature of the poles obtained from the IB variant of ic-MRCC-LR is removed through the approximation in the response equations as it appear in the variant IIB. To show how the simultaneous divergence of $\mathcal{X}$ and $\mathcal{Y}$ affect the nature of the poles, the first order reference coefficients, $\mathbf{c}^Z(\omega)$ and $\mathbf{c}^Z(-\omega)$, have been plotted against the frequencies in Fig. 6.3 corresponding to the α_{ZZ} of BH. The reference coefficients corresponding to the first configuration in the active space are plotted here. The solution vector $\mathbf{c}^Z(\omega)$ from both of the response equations attain the singularity at the poles of the response function as it has the main contribution to the corresponding excited state. The vector $\mathbf{c}^Z(-\omega)$, on the other hand, should not have any singularity as de-excitation from the ground state is not possible. However, through the coupling with $\mathbf{c}^Z(\omega)$, $\mathbf{c}^Z(-\omega)$ diverges when obtained by solving the coupled response equations. This leads to a second order pole of the response functions.

The error introduced in the second order properties by these well-behaved response equations is significant only close to the static limit as this error, like the one coming

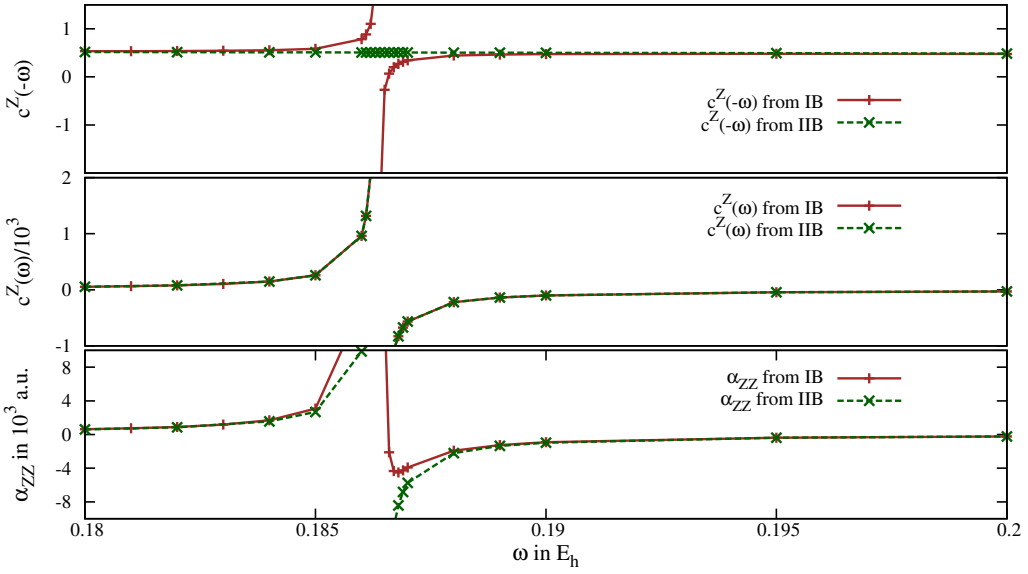

FIGURE 6.3: Polarizabilities and the first order reference coefficients $\mathbf{c}^Z(\omega)$ and $\mathbf{c}^Z(-\omega)$ are plotted near the poles of the response function $\langle\langle Z; Z\rangle\rangle_\omega$. Polarizabilities are calculated from the IB and the IIB variants of the ic-MRCC-LR methods which differ in the response equations used for solving the first order response wave function parameters. The reference coefficients plotted here correspond to the first configuration in the active space. Note that the two plots of the reference coefficients use different scales for presenting the values in the Y-axis.

from the well-behaved response function, also attains singularity at the poles of the response function. Whereas the errors at the static limit are positive for CH_2 with the approximation overestimating α_{ZZ} and α_{XX} by 0.004% and 0.1% respectively, it is -0.2% for the α_{ZZ} of BH. The larger error for the BH molecule can be ascribed to its higher multireference character (with -0.9238 and 0.3827 being the coefficients of the two dominant configurations) compared to that of CH_2 (-0.9803 and 0.1972). Away from the static limit, this error does not increase much. For α_{ZZ} and α_{XX} of CH_2 these errors are within 1% untill the frequencies reach 0.172 a.u. and 0.058 a.u. respectively. For BH, the error is within 1% untill the frequency of 0.17 a.u.. This study also shows that the approximation involving the response equations is less erroneous than the one made in the response function.

Therefore, through the approximations, made in both the response equations and the linear response function, the variant IIB emerges as the final formulation of ic-MRCC-LR theory which is free of any second order poles. The errors introduced through each of these approximations are also shown to be very small near the static limit. This formulation, denoted as ic-MRCC-LR from now on, is going to be used to calculate the second order properties, if not mentioned otherwise.

6.1.3 Effect of the Approximations on the Static Properties

Two different formulations of the ic-MRCC-LR can be used to calculate the static second order properties. As the approximations in both the response equations and the response function are made to correct the second order pole structures, they are not necessary for calculating the second order properties in the static limit. So, the variant IA, as described in Tab. 6.1, can be used to calculate static properties. The values of the second order property obtained from this variant match the properties calculated from the finite differences of the energies when they are obtained without relaxing the orbitals and the metric matrix. Static properties can also be obtained, on the other hand, as the static limit of the final ic-MRCC-LR formulation, i.e. the variant IIB, which includes both the approximations required for the response equations and the response function. In this section, values of the static properties calculated using both of these variants are compared.

TABLE 6.2: An comparison between the values of the static properties as obtained using the initial (IA) and final (IIB) formulations of ic-MRCC-LR for different chemical system. While the IIB variant uses both the approximated versions of the response equations and the response function, the IA variant uses both of the original ones without invoking any approximation.

Molecule/CAS	Property	ic-MRCCSD-LR		Full CI
		IA	IIB	
CH_2/(2e,2o)	α_{XX}	10.0379	10.0250	
	α_{ZZ}	13.9539	13.9536	
CH_2/(6e,6o)	α_{XX}	10.0130	10.0146	
	α_{YY}	15.1272	15.1550	
	α_{ZZ}	13.9392	13.9375	
BH/(2e,2o)	α_{ZZ}	52.4962	52.3718	52.568[1]

1. The FCI result is obtained from [64].

Apart from the systems mentioned earlier in this section, static polarizabilities are calculated additionally for CH_2 using an active space of (6e,6o). This active space contains all the valence orbitals of CH_2. The values of the static polarizability are presented in the Tab. 6.2 for the components with non-trivial errors coming from this approximation.

The difference between the static polarizabilities, as obtained from the two formulations of ic-MRCC-LR, should be of similar magnitude to the cumulative errors coming from the individual approximations used in the response equations and the response function. An analysis of the results for the lower active space also indicates the same when compared with the results presented for the individual approximation in Secs. 6.1.1 and 6.1.2. For CAS(2e,2o) a comparatively larger deviations between results for the IA and IIB variants of ic-MRCC-LR can be attributed to the higher contribution from the reference determinants to the first order wave function parameters, affecting mostly the response equations. Similarly, an increase in the size of the active space naturally increases the contribution of the reference determinants to the first order wave function. This is also reflected in the results for CH_2 when the larger active space is used. But, even though the active space is substantially increased, by including all the valence orbitals, the change in the errors due to this approximation is not that significant. This can be explained by small changes in the results for the approximation made in the response function, and also the fact that the main two terms contributing to this error, terms III and IV in Eq. 4.46, cancel each other. It is also important to note that, by comparing the results with the FCI results available for BH, it is evident that the ic-MRCC-LR formulation gives more accurate results when it does not include any approximation.

6.2 Comparison to FCI Results: BH

In this section, the linear response formulation of ic-MRCCSD is used to calculate the parallel component of the electrical polarizability, $\alpha_{||}$, for the singlet ground state of BH. This second order property is calculated for frequencies close to the static limit and then the results are compared with CCSD, Mk-MRCCSD and full CI results. This study allows us to assess the accuracy of the ic-MRCC-LR formalism for calculating second order properties even after introducing the necessary approximations in the response equations and the response function. The CCSD, Mk-MRCCSD and FCI results are obtained from a previous study by Jagau *et al.* [64]. The length of the B-H bond used here is 2.4648 Å which is twice the experimental bond distance [123]. The larger bond distance is used for these calculations as it provides higher multireference character for the electronic state. The TZP basis set [142] is used while correlating all the electrons in these calculations. An active space of (2e,2o), comprising the bonding ($3\sigma^+$) and antibonding ($4\sigma^+$) orbitals as the active ones, is used for all the multireference calculations. The values of $\alpha_{||}$ calculated using all of these methods are plotted against frequencies of the external field in Fig. 6.4 while the errors with respect to the FCI results are plotted in the inset of the the same figure. The exact values of polarizability, used in this plot, can be found in Tab. B.14 of appendix B.

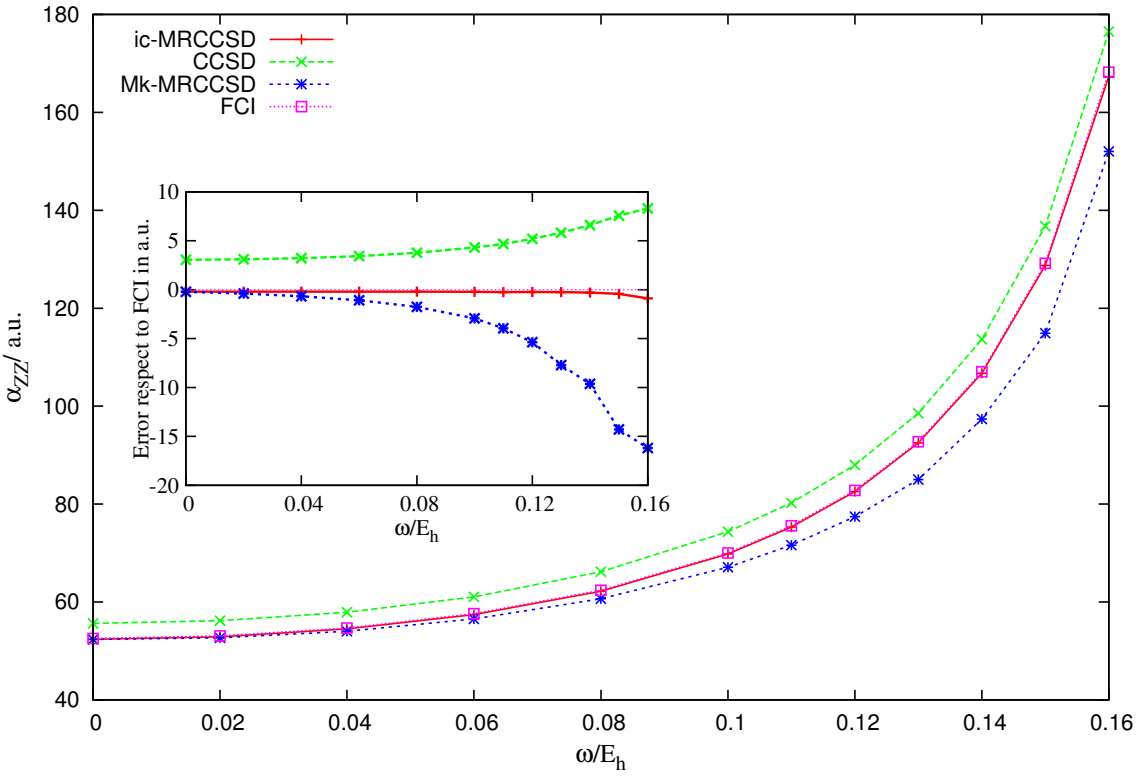

FIGURE 6.4: $\alpha_{||}$ for the singlet ground state of BH computed using ic-MRCCSD, CCSD, Mk-MRCCSD and full CI. Values for each of the methods are plotted in the main part of the plot. The differences of the results for ic-MRCCSD, CCSD and Mk-MRCCSD with respect to the FCI results are plotted in the inset.

It is clear from Fig. 6.4 that ic-MRCCSD provides polarizabilities with better accuracy compared to both CCSD and Mk-MRCCSD throughout the range of frequencies used in the study. Both of the ic-MRCCSD and Mk-MRCCSD results are quite accurate near the static limit while the CCSD results are far away from the FCI results in that region. At the static limit, ic-MRCCSD underestimates the $\alpha_{||}$ for FCI by 0.36%, whereas the corresponding errors for CCSD and Mk-MRCCSD are 5.8% and -0.4% respectively. With increasing frequency, the errors in the Mk-MRCCSD results exceed those of the CCSD results, although the polarizabilities obtained from ic-MRCCSD do not differ significantly from the FCI results. Within the frequency range used in this study, the highest error in $\alpha_{||}$ values for ic-MRCCSD is 0.52% for the frequency 0.16 a.u., whereas the errors for Mk-MRCCSD are as high as 11%. The position of the first pole as obtained from ic-MRCCSD is at 0.1864 a.u. and it is much closer to the FCI value of 0.1859 a.u. than those obtained using CCSD (0.1930 a.u.) and Mk-MRCCSD (0.1877 a.u.). The higher errors for Mk-MRCCSD, mainly near the poles, have been attributed to the wrong pole structure of the corresponding linear response function [64] arising due to the presence of linear-dependencies in its excitation manifold.

Therefore, even though there are errors coming from the approximations involved in the linear response theory of ic-MRCC, they do not seem to affect the accuracy of the method much in predicting second order properties. This holds true even for frequencies close to the poles producing better accuracy compared to results from other quantum chemical methods.

6.3 *p*-benzyne and 2,6-Pyridyne

In this section, electrical polarizabilities of different components and frequencies are studied for *p*-benzyne and 2,6-pyridyne. For both of these molecules, calculations are done for their singlet ground states which are both multireference in nature. Jagau *et al.* [64] studied the same while calculating the polarizabilities using the Mk-MRCCSD method and comparing it with single-reference methods CCSD and CCSD(T). Polarizabilities as calculated from ic-MRCCSD-LR are compared with all of the results from this previous study. Whereas both of the variants of ic-MRCCSD-LR, IA and IIB, are used here for evaluating different components of static polarizability, only the final formulation of ic-MRCCSD-LR (i.e. the IIB variant) is used for their dynamic counterparts. The geometries used for calculating polarizabilities of both these molecules are taken from the Ref. [64] and also presented in Tab. B.1. For both of the molecules, the lines connecting the dehydrogenated carbon atoms are parallel to the Y axis, while the molecular planes are perpendicular to Z and X axes for *p*-benzyne and 2,6-pyridyne respectively. The aug-cc-pCVDZ basis set is used for these calculations following Ref.[64] with all the electrons present in the molecules being correlated. The multireference calculations, Mk-MRCCSD and ic-MRCCSD, are done by using a (2e,2o) active space. Under the symmetries of D_{2h} and C_{2v}, used for the respective calculations of *p*-benzyne and 2,6-pyridyne, the active orbitals for *p*-benzyne are of a_g and b_{3u} symmetries, while those for 2,6-pyridyne are of a_1 and b_2 symmetries. The active space of (2e,2o) consists of two determinants, with each having the respective active orbitals doubly filled. The reference coefficients c_1 and c_2 corresponding to these two determinants, as obtained from ic-MRCCSD calculations, are 0.5264 and -0.8502 for *p*-benzyne, and -0.9183 and 0.3959 for 2,6-pyridyne, respectively. This also shows the strong multireference character of these two states.

The results for the different components of polarizability are first discussed for the static limit. Tab. 6.3 presents the static polarizability tensors as obtained using CCSD, CCSD(T), Mk-MRCCSD and the two variants of ic-MRCCSD for both of the *p*-benzyne and 2,6-pyridyne molecules. Among the two variants, the IA variant of the ic-MRCCSD uses the response equations and the response function without making any approximations, i.e. Eqs. 4.34 and 4.46 respectively. The second variant, IIB, on the other hand,

TABLE 6.3: Static polarizability tensors in atomic units for *p*-benzyne and 2,6-pyridyne obtained using different single-reference [CCSD and CCSD(T)] and multireference [Mk-MRCCSD and ic-MRCCSD] methods are presented here. The aug-cc-pCVDZ basis set is used for all the calculations. For the ic-MRCCSD results the variants IA and IIB of the linear response formulation are used which also shows the error introduced through the approximations made in both of the response equations and the response function.

Property	CCSD	CCSD(T)	Mk-MRCCSD	icMRCCSD-LR	
				IA	IIB
			p-benzyne		
α_{XX}	79.661	77.910	79.552	79.062	79.062
α_{YY}	85.359	64.840	73.113	77.386	78.413
α_{ZZ}	42.631	42.377	42.498	42.493	42.493
			2,6-Pyridyne		
α_{XX}	39.358	39.046	39.121	39.031	39.031
α_{YY}	77.578	69.048	72.529	73.541	74.557
α_{ZZ}	70.998	69.048	70.839	70.263	70.267

TABLE 6.4: First order reference coefficients in the presence of static electric fields of different components for the molecules *p*-benzyne and 2,6-pyridyne. The (2e,2o) active space has been used for these calculations with u and v representing the active orbitals. Two different variants of ic-MRCCSD are as defined in Tab 6.1.

Molecule	property	configurations	ic-MRCCSD-IA		ic-MRCCSD-IIB	
			$c_1^{(1)}$	$c_2^{(1)}$	$c_1^{(1)}$	$c_2^{(1)}$
p-benzyne	α_{YY}	$u_\alpha v_\beta$, $u_\beta v_\alpha$	-3.4599	3.4599	-3.4397	3.4397
2,6-Pyridyne	α_{YY}	$u_\alpha v_\beta$, $u_\beta v_\alpha$	-3.9574	3.9574	-3.9083	3.9083
	α_{ZZ}	$u_\alpha u_\beta$, $v_\beta v_\alpha$	0.2645	0.6135	0.2639	0.6119

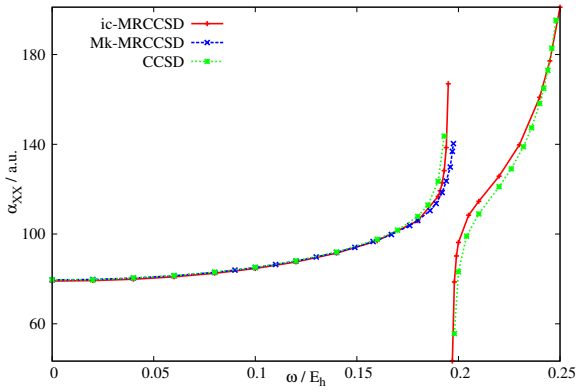

(a) α_{XX} for p-benzyne. Convergence could not be achieved beyond $\omega = 0.197\ E_h$ for Mk-MRCCSD linear response equations [64].

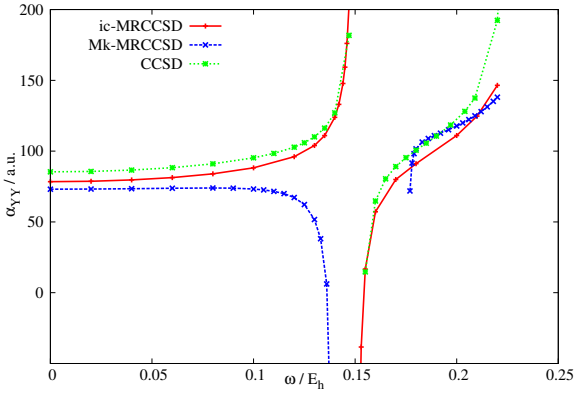

(b) α_{YY} for p-benzyne. Convergence could not be achieved between $\omega = 0.14\ E_h$ and $\omega = 0.177\ E_h$ for Mk-MRCCSD linear response equations [64].

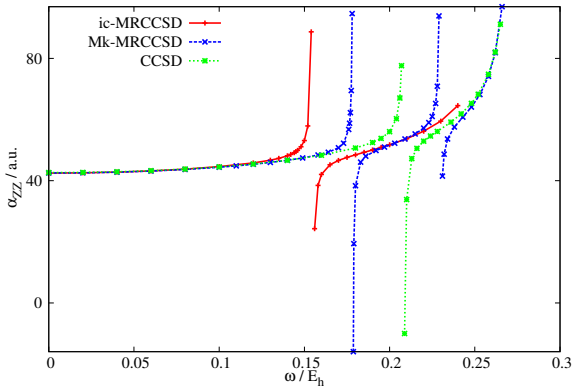

(c) α_{ZZ} for p-benzyne.

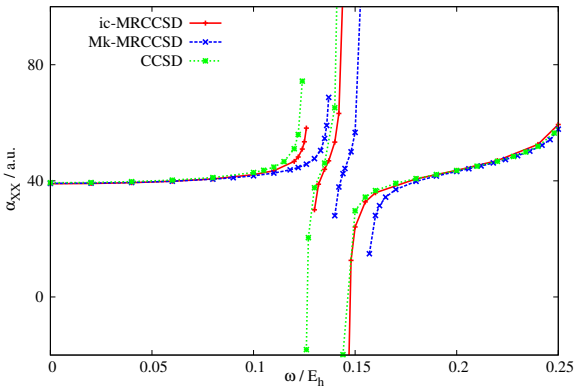

(d) α_{XX} for 2,6-Pyridyne.

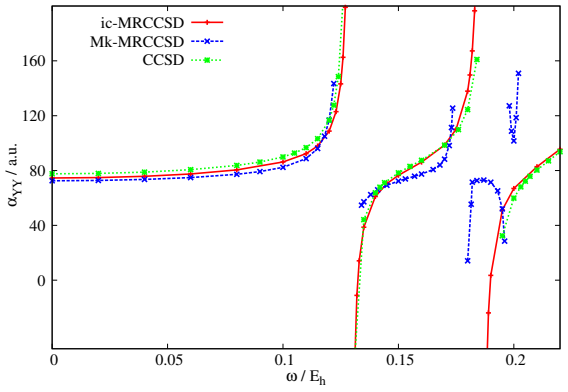

(e) α_{YY} for 2,6-Pyridyne.

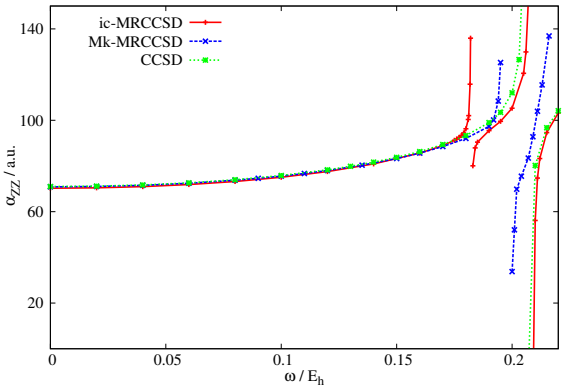

(f) α_{ZZ} for 2,6-Pyridyne.

FIGURE 6.5: Dynamic polarizability tensors in atomic units for p-benzyne and 2,6-pyridyne obtained using the CCSD, Mk-MRCCSD and ic-MRCCSD methods are presented here. The aug-cc-pCVDZ basis set is used for all the calculations while correlating all the electrons. For the ic-MRCCSD results the final variant IIB of the linear response formulation is used which removes any second order contribution to the structure of the poles.

uses the approximated equations: Eq. 4.43 for the response equations and Eq. 4.47 for the response function. Different components of the polarizability tensors can be categorized into two types. For α_{XX} and α_{ZZ} of p-benzyne, and α_{XX} of 2,6-pyridyne, there is no contribution coming from the first order reference coefficients in the multireference framework using the CAS(2e,2o). This also leads to a smaller changes in their values as obtained from the single-reference theories compared to those obtained using the multireference theories. The two different formulations of ic-MRCCSD also give the same values for these components of polarizability. However, the differences between the results from these two approaches is non-trivial for the components α_{YY} of p-benzyne, and α_{YY} and α_{ZZ} of 2,6-pyridyne because of the non-trivial contributions from the first order reference coefficients in these cases. Through the approximations in the linear response formalism of ic-MRCC, α_{YY} is overestimated by $\sim$1.4% for both of the molecules, while α_{ZZ} changes by only 0.25%. The magnitude of these errors is mainly governed by the magnitude of the first order wave function parameters, especially the first order reference coefficients. These first order reference coefficients for the calculations using both of the variants of ic-MRCCSD-LR are presented in Tab. 6.4. The magnitude of these first order coefficients is larger for the coefficients contributing to the α_{YY} for both the molecules. Thus, the terms quadratic in these coefficients, which are the main difference between these two variants of ic-MRCCSD-LR, produces larger errors for the α_{YY} values. The smaller contributions of the first order reference coefficients to α_{ZZ} of 2,6-pyridyne is also the reason behind the smaller change in its values where going from single-reference methods to the multireference methods, with the differences being within 1 a.u.. Corresponding changes in the values of α_{YY} are as high as $\sim$14 a.u. for p-benzyne and $\sim$4.5 a.u. for 2,6-pyridyne. The overall smaller effect of multireference theories on the results for 2,6-pyridyne can be attributed to its comparably smaller multireference character [64].

Different components of the dynamic polarizability tensor for the ground states of both p-benzyne and 2,6-pyridyne are plotted against frequency in Fig. 6.5. Dynamic polarizibilities calculated using the linear response formulation of the ic-MRCCSD method are compared with the corresponding results obtained for CCSD and Mk-MRCCSD from the Ref. [64]. The values of these dynamic polarizibilities, which are used to generate the plots, are given in Tabs. B.8-B.13 of appendix B. As both the states used here are strongly multireference in nature, the CCSD method can predict neither the dynamic polarizabilities nor the position of the corresponding poles accurately, demanding a multireference description of these states. However, even though the Mk-MRCC method gives more accurate polarizabilities, it is prone to produce unphysical spurious poles and wrong pole structures as discussed in Ref. [64]. Thus, it is important here to investigate how ic-MRCCSD behaves to predict the polarizabilities and the corresponding poles for these multireference systems. Therefore, the position of the poles for the linear response

function is also studied further for both Mk-MRCC and ic-MRCC in the context of obtaining excitation energies from the linear response formalism in Sec. 7.1.2 and also in the Ref. [P1].

For the α_{XX} component of the polarizability of both the molecules, the curves from all the three methods are almost identical. For *p*-benzyne, the positions of the poles of the linear response function $\langle\langle X; X\rangle\rangle$ are within 2 mE_h for all these methods which is also evident from the data presented in Tab. B.8. For 2,6-pyridyne, the positions of both the poles for ic-MRCCSD are within 3 mE_h of the ones for CCSD, while the Mk-MRCCSD predicts both the poles shifted by about 15 mE_h towards higher frequencies from the CCSD ones. The positions of the poles corresponding to the response function $\langle\langle Z; Z\rangle\rangle$ differ significantly for these three methods. For *p*-benzyne, ic-MRCCSD produces the pole at 50 mE_h lower in frequency compared to that from CCSD. Mk-MRCCSD, however, produces two different poles in the same region. However, this additional pole for Mk-MRCCSD is not a spurious one as the corresponding excited state can also be obtained for both CCSD and ic-MRCCSD but at a higher frequency (see Tab. 7.2 using a slightly different basis sets). For 2,6-pyridyne, ic-MRCCSD produces two poles for $\langle\langle Z; Z\rangle\rangle$ where both CCSD and Mk-MRCCSD produces only one pole in the same frequency range. The first pole of ic-MRCCSD is shifted by 24 mE_h towards lower frequencies compared to the pole of CCSD.

The most significant changes between the curves of polarizability obtained from Mk-MRCCSD and ic-MRCCSD appear for the α_{YY} for both *p*-benzyne and 2,6-pyridyne. However, for both of the cases, the poles of the linear response function $\langle\langle Y; Y\rangle\rangle$ as obtained for ic-MRCCSD lie within $\sim$3 mE_h of the corresponding CCSD poles. For *p*-benzyne, Mk-MRCCSD produces two very close poles in this region, where one of these is spurious and has no physical counterpart. The position of these two poles cannot be obtained here as the response equations do not converge for Mk-MRCCSD in the frequency range 0.14-0.177 E_h [64]. However, the appearance of this redundant excited state of Mk-MRCCSD is also analysed in the forthcoming Sec. 7.1.2. For 2,6-pyridyne a similar spurious pole also appears for the Mk-MRCCSD linear response function as can be seen in Fig. 6.5e. Another important aspect of these spurious poles is their corresponding structures, which look second order in nature, as similar pole structure has been analyzed for the initial variants of ic-MRCC-LR in Sec. 6.1.

7 | Excitation Energies from ic-MRCC

The linear response formulation of ic-MRCC (ic-MRCC-LR) produces the eigenvalue equation (Eq. 4.48) which gives the excitation energies of molecular systems, as discussed in Sec. 4.6. In the first part of this chapter, excitation energies of different chemical systems are calculated using this ic-MRCC-LR formulation. Alternatively, equation for getting excitation energies can also be obtained following an equation of motion (EOM) like formulation. This formulation is developed in the second part of this chapter and it leads to two different working equations. Though this approach produces Eq. 4.48 as one of these, it also presents an alternative equation, alongside, to solve the excited states and to get a different excitation energy using ic-MRCC. This new formulation is denoted here as ic-MRCC-EOM. Finally, differences between the LR and EOM formulations for ic-MRCC are analyzed theoretically as well as using numerical results in the last part of this chapter.

7.1 Application of ic-MRCC-LR

The ic-MRCC-LR method is applied first to investigate vertical excitation energies for a variety of states of singlet methylene (CH_2). The performance of the ic-MRCCSD-LR method of getting accurate excitation energies for single- and double-excitation dominated states is the main focus of this study. Being sufficiently small, the CH_2 molecule allows to compare these results with excitation energies obtained from full CI. Excitation energies are calculated for the prominent multireference system of *p*-benzane with the aim of showing that no spurious roots appear from the ic-MRCCSD-LR theory, unlike the Mk-MRCC-LR theory. The excited states which have dominant contributions within the model space can also be targeted directly using ic-MRCC. Therefore, energies of the excited states obtained directly through ic-MRCCSD are compared with the energies obtained as excitation energies from a specified ground state using ic-MRCCSD-LR. These calculations are done for the singlet-triplet spitting of the methylene molecules and some lower lying excited states of *p*-benzyne.

7.1.1 Methylene

Methylene is an important molecular system for benchmarking excitation energies as it has several lower-lying excited states dominated by both single- and double-excitations with respect to the singlet ground state. Among the states studied in this context, 2^1A_1, 2^1B_1, 3^1B_1, 2^1B_2 and 2^1A_2 are the ones dominated by the double excitations where the remaining states are single-excitation dominated [143]. The excitation energies of these states obtained from the ic-MRCCSD-LR theory are compared [P1] with those of the full CI and single-reference coupled-cluster methods as previously calculated by Koch *et al.* [143].

The calculations for CH_2 are done using the C_{2v} point-group symmetry with the coordinates for C and H being (0, 0, 0) and (0, $\pm$1.644403, 1.32213), respectively, in Bohr. The basis set employed for these calculations is the cc-pVDZ from Dunning [144] where the basis set uses the spherical Gaussians and it is also augmented with diffuse functions. The augmentation consists of one s function with exponent 0.015 for C and one s function with exponent 0.025 for H. All orbitals are included in the correlated methods. Two active spaces, CAS(2e,2o) and CAS(6e,6o), are used for the ic-MRCCSD and subsequent linear response calculations. While the minimal active space is comprised of the orbitals $3a_1$ and $1b_1$, the full-valence active space includes in addition the orbitals $2a_1$, $4a_1$, $1b_2$ and $2b_2$. The impact of the commutator approximation [i.e. the truncation of the residual equations, Eqs. 3.7 and 4.7, at the commutator level N_{com}] are demonstrated here by doing ic-MRCCSD calculations for both $N_{\mathrm{com}} = 2$ and $N_{\mathrm{com}} = 3$. For the larger active space of (6e,6o), the results are obtained for two choices of the threshold η which is used to discard the small metric eigenvalues.

The results are presented in Tab. 7.1. The excitation energies for the states dominated by single-excitations are accurately described by both of the single-reference CCSD and CC3 methods, with errors being below 0.02 eV. The latter method produces comparatively better results, as it is seen from Tab. 7.1, because it includes the leading terms of the triply excited clusters in perturbation theory[145]. The excitation energies for these states are less accurate when obtained from the ic-MRCC-LR method using the default choice of $N_{\mathrm{com}} = 2$ and $\eta = 10^{-5}$ [P1]. In particular for the larger active space these errors go up to 0.1 eV (for the 4 A_1 state). However, inclusion of the threefold commutators ($N_{\mathrm{com}} = 3$) reduces these errors significantly to 0.03 eV. This suggests the importance of using higher commutator terms in the ic-MRCCSD wave function while getting excitation energies for the singly excited states. Additionally, the excitation energies are also improved significantly with an increase in the threshold η to 10^{-4} while using of the larger active space of (6e,6o). Notably, use of $\eta = 10^{-4}$ brings down the errors close to

TABLE 7.1: Vertical excitation energies for CH_2, given in eV (published in Ref. [P1]). The structure [C(0,0,0), H(0,±1.644403,1.32213)] and the basis set (cc-pVDZ augmented with one s function with exponent 0.015 for C and one s function with exponent 0.025 for each H) are taken from Ref. [143].

State	Type[1]	FCI[2]	CCSD[2]	CC3[2]	ic-MRCCSD					
					CAS(2e,2o)		CAS(6e,6o)			
					N_{com}=2	N_{com}=3	N_{com}=2		N_{com}=3	
							η=10^{-5}	η=10^{-4}	η=10^{-5}	η=10^{-4}
$2\,^1A_1$	d	4.656	6.112	5.127	4.835	4.834	4.721	4.725	4.705	4.718
$3\,^1A_1$	s	6.514	6.509	6.509	6.485	6.496	6.449	6.486	6.503	6.505
$4\,^1A_1$	s	8.479	8.460	8.474	8.438	8.450	8.375	8.434	8.447	8.457
$1\,^1B_1$	s	1.793	1.780	1.788	1.799	1.797	1.803	1.798	1.800	1.798
$2\,^1B_1$	d	8.906	10.705	9.478	9.607	9.600	9.332	9.362	9.220	9.360
$3\,^1B_1$	d	10.553	12.376	11.168	11.327	11.321	11.055	11.100	10.954	11.100
$1\,^1B_2$	s	7.704	7.714	7.720	7.688	7.699	7.647	7.687	7.706	7.708
$2\,^1B_2$	d	8.016	9.619	8.533	8.342	8.349	8.136	8.142	8.125	8.141
$1\,^1A_2$	s	5.853	5.859	5.859	5.839	5.838	5.870	5.857	5.867	5.857
$2\,^1A_2$	d	9.410	11.826	10.583	10.635	10.634	10.063	10.129	10.081	10.142
Difference with respect to FCI										
$2\,^1A_1$	d		1.456	0.471	0.180	0.178	0.065	0.069	0.049	0.062
$3\,^1A_1$	s		−0.005	−0.005	−0.030	−0.019	−0.065	−0.029	−0.011	−0.009
$4\,^1A_1$	s		−0.019	−0.005	−0.041	−0.029	−0.104	−0.045	−0.032	−0.022
$1\,^1B_1$	s		−0.014	−0.005	0.006	0.004	0.008	0.004	0.007	0.005
$2\,^1B_1$	d		1.799	0.571	0.701	0.694	0.426	0.456	0.314	0.454
$3\,^1B_1$	d		1.823	0.615	0.774	0.769	0.502	0.548	0.402	0.548
$1\,^1B_2$	s		0.011	0.016	−0.016	−0.005	−0.057	−0.016	0.003	0.005
$2\,^1B_2$	d		1.603	0.517	0.325	0.333	0.120	0.126	0.108	0.124
$1\,^1A_2$	s		0.005	0.005	−0.014	−0.015	0.017	0.004	0.014	0.003
$2\,^1A_2$	d		2.416	1.173	1.225	1.225	0.653	0.720	0.671	0.732
RMSE[3]	s		0.012	0.009	0.025	0.017	0.061	0.025	0.017	0.011
RMSE[3]	d		1.849	0.717	0.739	0.737	0.420	0.457	0.381	0.461

[1] Character of excitation with respect to the Hartree-Fock determinant: s = single-excitation dominated, d = double-excitation dominated.
[2] Ref. [143]
[3] Root mean square error.

those obtained with CCSD and CC3 for the single excitation dominated transitions. This is also supported by the root mean square errors computed for these states.

The excitation energies for the states dominated by double-excitations, on the other hand, can not be predicted as accurately by the single-reference methods, CCSD and CC3. For CCSD, the errors in excitation energies for these states are in the range of 1.5-2.4 eV, whereas they are in the range of 0.5-1.2 eV for CC3. The lesser accuracy of both of these methods for the doubly excited states can be understood following the analysis by Hald *et al.* [146]. They have shown that the excitation energies obtained from different truncation levels of single-reference coupled cluster hierarchy are correct up to certain order in the perturbation theory. While for the single-excitation dominated states CC3 can give excitation energies which are correct through the third order in perturbation theory, an equally good description of the double-excitation dominated states needs at least the use of quadruple excitations.

In ic-MRCC-LR, however, main contributions to these excited states come from either excitations involving active orbitals (semi-internal excitations) or by a response of the reference function. Due to the involvement of these effectively lower rank excitations in both of the cases, one can expect an increased accuracy of ic-MRCCSD over CC3 for double-excitation dominated states. This is also followed in the results presented for these states in Tab. 7.1. In comparison to the excitation energies obtained from the single-reference methods for these states, the ic-MRCCSD-LR method gives more accurate results, with the errors being of the range 0.2–1.2 eV for CAS(2e,2o) and 0.05–0.7 for CAS(6e,6o). While inclusion of threefold commutators (N_{com}) does not change the results significantly for both of the choice of active spaces, an increase in the threshold η decrease the accuracy of the results. However, for the low-lying doubly excited state 2^1A_1, the error using the larger active space of (6e,6o) is even as small as for the singly exited states. The accuracy of the excitation energies for the higher lying doubly excited states decreases which can be attributed to the involvement of more semi-internal or external excitations as the dominant contributions of these states instead of the internal excitation vector $\mathbf{r}_c$. A larger active space or perturbative inclusion of higher body cluster operators can give a better description for these states.

7.1.2 Excited Singlet States of *p*-benzyne

The ground state of *p*-benzyne is the most prominent multireference system among all the three isomers of benzyne. Due to this high multireference character, *p*-benzyne has been used extensively for benchmarking multireference methods with the main focus being the singlet-triplet splitting of the molecule [147–157]. A recent study by Jagau and

Gauss has reported vertical excitation energies for several excited states obtained with Mk-MRCCSD-LR [65]. These results have shown the occurrence of spurious poles due to the overcomplete space of excited configurations of Mk-MRCCSD.

TABLE 7.2: Vertical singlet excitation energies of *p*-benzyne, given relative to the ^1A_g ground state in eV, using the structure from Ref. [65] and the cc-pCVTZ basis set (published in [P1]). The CAS(2,2) in the MRCC calculations comprises the active orbitals $6a_g$ and $5b_{3u}$. The Hartree-Fock reference function in CCSD corresponds to the dominant configuration in the active space, $\phi_2 = |5b_{3u}\alpha\, 5b_{3u}\beta\rangle$.

State	CCSD[1]	Mk-MRCCSD-LR[1]			ic-MRCCSD-LR		
		ΔE	LR vectors dominated by		ΔE	LR vectors dominated by	
$2\,^1A_g$	6.082	5.089	$r_c(\phi_1)$	0.834^2	4.489	$r_c(\phi_1)$	0.712^2
			$r_c(\phi_2)$	0.521^2		$r_c(\phi_2)$	0.449^2
$3\,^1A_g$	8.566	9.009	$1b_{3g}/5b_{3u} \rightarrow 6a_g/1a_u(\phi_2)^3$	0.473	7.882	$1b_{3g}/5b_{3u} \rightarrow 6a_g/1a_u{}^3$	0.418
			$1b_{3g}/5b_{3u} \rightarrow 1a_u/6a_g(\phi_2)^3$	0.226		$1b_{3g}/5b_{3u} \rightarrow 1a_u/6a_g{}^3$	0.206
$1\,^1B_{2u}$	5.355	5.417	$1b_{2g} \rightarrow 1a_u(\phi_2)$	0.466	5.368	$1b_{2g} \rightarrow 1a_u$	0.535
			$1b_{3g} \rightarrow 2b_{1u}(\phi_2)$	−0.322		$1b_{3g} \rightarrow 2b_{1u}$	0.390
			$1b_{2g} \rightarrow 1a_u(\phi_1)$	−0.272			
			$1b_{3g} \rightarrow 2b_{1u}(\phi_1)$	0.206			
$2\,^1B_{2u}$	⋯	8.188	$3b_{1g} \rightarrow 5b_{3u}(\phi_1)$	0.657	7.339	$3b_{1g} \rightarrow 5b_{3u}$	0.855
			$3b_{2u}/6a_g \rightarrow 5b_{3u}/5b_{3u}(\phi_1)^4$	0.130^4		$3b_{2u} \rightarrow 6a_g$	−0.402
						$1b_{3g} \rightarrow 2b_{1u}$	0.252
						$1b_{2g} \rightarrow 1a_u$	−0.171
$3\,^1B_{2u}$	7.192	7.525	$1b_{3g} \rightarrow 2b_{1u}(\phi_2)$	0.406	7.608	$3b_{1g} \rightarrow 5b_{3u}$	0.640
			$4b_{2u} \rightarrow 6a_g(\phi_2)$	0.306		$1b_{3g} \rightarrow 2b_{1u}$	−0.385
			$1b_{2g} \rightarrow 1a_u(\phi_2)$	0.288		$4b_{2u} \rightarrow 6a_g$	0.344
			$1b_{3g} \rightarrow 2b_{1u}(\phi_1)$	−0.248		$1b_{2g} \rightarrow 1a_u$	0.270
$4\,^1B_{2u}$	8.582	9.321	$3b_{2u} \rightarrow 6a_g(\phi_2)$	0.619	9.126	$3b_{2u} \rightarrow 6a_g$	0.633
$1\,^1B_{3u}$	4.046	3.827	$5b_{3u} \rightarrow 6a_g(\phi_2)$	0.487	4.159	$r_c(\|6a_g\alpha\, 5b_{3u}\beta\rangle)$	0.592
			$6a_g \rightarrow 5b_{3u}(\phi_1)$	−0.272		$r_c(\|6a_g\beta\, 5b_{3u}\alpha\rangle)$	−0.592
			$1b_{2g} \rightarrow 2b_{1u}(\phi_2)$	−0.256		$5a_g \rightarrow 5b_{3u}$	0.359
						$1b_{2g} \rightarrow 2b_{1u}$	−0.149
$^1B_{3u}{}^5$	⋯	4.831	$6a_g \rightarrow 5b_{3u}(\phi_1)$	0.522	⋯	⋯	
			$5b_{3u} \rightarrow 6a_g(\phi_2)$	0.309			
			$5a_g \rightarrow 5b_{3u}(\phi_1)$	0.211			
$2\,^1B_{3u}$	6.710	6.711	$1b_{3g} \rightarrow 1a_u(\phi_2)$	0.500	6.661	$1b_{3g} \rightarrow 1a_u$	0.604
			$1b_{3g} \rightarrow 1a_u(\phi_1)$	−0.312		$1b_{2g} \rightarrow 2b_{1u}$	−0.295
			$1b_{2g} \rightarrow 2b_{1u}(\phi_2)$	0.278			
$1\,^1B_{1g}$	6.514	7.150	$3b_{1g} \rightarrow 6a_g(\phi_2)$	0.659	6.754	$3b_{1g} \rightarrow 6a_g$	0.744
$2\,^1B_{1g}$	8.180	8.864	$5b_{3u} \rightarrow 5b_{2u}(\phi_2)$	0.635	8.596	$5b_{3u} \rightarrow 5b_{2u}$	0.762

$1\,^1\mathrm{B}_{1u}$	$\cdots$	4.836	$1b_{2g} \rightarrow 5b_{3u}(\phi_1)$	0.666	4.120	$1b_{2g} \rightarrow 5b_{3u}$	1.107
						$1b_{1u} \rightarrow 6a_g$	0.323
$2\,^1\mathrm{B}_{1u}$	$\cdots$	7.641	$6a_g \rightarrow 2b_{1u}(\phi_1)$	0.642	6.776	$6a_g \rightarrow 2b_{1u}$	1.062
$3\,^1\mathrm{B}_{1u}$	5.728	6.365	$1b_{1u} \rightarrow 6a_g(\phi_2)$	0.595	7.451	$1b_{1u} \rightarrow 6a_g$	0.689
			$1b_{2g}/5b_{3u} \rightarrow 6a_g/6a_g(\phi_2)$	0.304		$1b_{2g} \rightarrow 5b_{3u}$	-0.488
$4\,^1\mathrm{B}_{1u}$	8.604	8.616	$3b_{1g} \rightarrow 1a_u(\phi_2)$	0.559	8.688	$3b_{1g} \rightarrow 1a_u$	0.640
			$3b_{1g} \rightarrow 1a_u(\phi_1)$	-0.340			
$1\,^1\mathrm{B}_{3g}$	3.133	3.754	$1b_{3g} \rightarrow 6a_g(\phi_2)$	0.669	3.496	$1b_{3g} \rightarrow 6a_g$	0.784
$2\,^1\mathrm{B}_{3g}$	4.370	5.068	$5b_{3u} \rightarrow 1a_u(\phi_2)$	0.665	4.900	$5b_{3u} \rightarrow 1a_u$	0.776
$1\,^1\mathrm{B}_{2g}$	2.941	3.556	$1b_{2g} \rightarrow 6a_g(\phi_2)$	0.671	3.234	$1b_{2g} \rightarrow 6a_g$	0.767
$2\,^1\mathrm{B}_{2g}$	5.401	6.094	$5b_{3u} \rightarrow 2b_{1u}(\phi_2)$	0.664	5.849	$5b_{3u} \rightarrow 2b_{1u}$	0.764
$^1\mathrm{B}_{2g}$[5]	$\cdots$	6.578	$1b_{2g}/6a_g \rightarrow 5b_{3u}/5b_{3u}(\phi_1)$	0.498	$\cdots$	$\cdots$	
			$1b_{1u} \rightarrow 5b_{3u}(\phi_1)$	0.456			
$3\,^1\mathrm{B}_{2g}$	$\cdots$	$\cdots$			8.338	$1b_{1u} \rightarrow 5b_{3u}$	1.138
$1\,^1\mathrm{A}_u$	8.413	4.917	$1b_{3g} \rightarrow 5b_{3u}(\phi_1)$	0.674	4.516	$1b_{3g} \rightarrow 5b_{3u}$	1.223
$2\,^1\mathrm{A}_u$	$\cdots$	7.034	$6a_g \rightarrow 1a_u(\phi_1)$	0.655	6.502	$6a_g \rightarrow 1a_u$	1.180
$^1\mathrm{A}_u$[5]	$\cdots$	9.142	$1b_{3g}/5b_{3u} \rightarrow 6a_g/6a_g(\phi_2)$	0.609	$\cdots$		
$3\,^1\mathrm{A}_u$	9.058[4]	9.162[4]	$1b_{2g} \rightarrow 5b_{2u}(\phi_2)^4$	0.562[4]	9.138	$1b_{2g} \rightarrow 5b_{2u}$	0.642
			$1b_{2g} \rightarrow 5b_{2u}(\phi_1)^4$	-0.327[4]			

[1] Ref. [65].

[2] Note that the true response vector $\mathbf{r}_c$ may be shifted along the direction of the ground state vector $\mathbf{c}$.

[3] The corresponding distribution of spin functions is $\alpha/\beta \rightarrow \alpha/\beta$.

[4] Ref. [158].

[5] Artificial root arising in Mk-MRCCSD due to the problem of overcompleteness of excited space.

In this study, the structure of *p*-benzyne is taken from the Ref. [65]. This geometry has been obtained by optimizing the ground state at the Mk-MRCCSD/cc-pCVTZ level of theory. The same orbital basis, cc-pCVTZ, is used for the calculation while correlating all the electrons to compare the results with Mk-MRCCSD-LR. An active space of (2e,2o) are used to do the multireference calculations with the active orbitals being $6a_g$ and $5b_{3u}$ (the molecule is oriented such that the z axis is perpendicular to the molecular plane and the x axis runs through the radical centers). The CI coefficients of the configurations within the active space, $\phi_1 = |6a_g\alpha\, 6a_g\beta\rangle$ and $\phi_2 = |5b_{3u}\alpha\, 5b_{3u}\beta\rangle$, are $c_1 = -0.53$ and $c_2 = 0.85$, according to the ic-MRCCSD theory. Tab. 7.2 compares the results from the methods CCSD-LR, Mk-MRCCSD-LR and ic-MRCCSD-LR. The elements of the ic-MRCCSD response vectors are presented in the original basis of excitation operators (not the orthogonalized basis). Within each spatial symmetry, the states are ordered according to their ic-MRCC excitation energies. The excitation energies from CCSD and

Mk-MRCC are then assigned for each of these states after comparing the response vectors. Note that this way of assigning the CCSD and Mk-MRCC roots leads to some changes in the energetic ordering of the Mk-MRCC states in the symmetries B_{2u}, B_{1u} and A_u.

$1\,^1B_{2u}$, $2\,^1B_{3u}$, $4\,^1B_{1u}$, $3\,^1A_u$ are the excited states for which the dominant configurations are achieved through excitations involving no active orbitals. For these excited states, the excitation energies lie within 0.1 eV for all three methods, CCSD, Mk-MRCCSD and ic-MRCCSD. Among those roots where the dominant contributions come from core-to-active or active-to-virtual excitations, there are significant differences between the results from Mk-MRCC-LR and ic-MRCC-LR. Whenever the dominant excitations are defined with respect to the first reference function (i.e. the one with the smaller weight) in Mk-MRCCSD ($2\,^1B_{2u}$, $1\,^1B_{1u}$, $2\,^1B_{1u}$, $3\,^1B_{2g}$, $1\,^1A_u$, $2\,^1A_u$), the excitation energies obtained from ic-MRCC-LR are about 0.4–0.9 eV lower than the corresponding Mk-MRCCSD excitation energies. However, no particular trend is observed for states where the dominant excitations are with respect to the second reference function. While for most of these states the methods agree within 0.5 eV, two notable exceptions exist: for the states $3\,^1A_g$ and $3\,^1B_{1u}$, the excitation energies differ by more than 1 eV.

The ic-MRCC-LR calculations of *p*-benzyne do not produce any additional root. This is also expected, because the set of excited functions in the ic-MRCC theory are non-redundant. Among all the additional roots in Mk-MRCC-LR pointed out by Jagau and Gauss [65], some are also recognized as additional by the current work. Those states which are recognized as additional root in Mk-MRCC-LR are denoted by leaving a blank space in the beginning of a row in Tab. 7.2. However, there are some roots which are assigned as additional in Ref. [65] but they are found to be proper roots within the limit of this study.

One root of each of the symmetries B_{3u}, B_{2g} and A_u is assigned as additional root in Mk-MRCCSD-LR. These roots come in pairs (due to the choice of the active space) and the ones closer in energy to the ic-MRCC roots are considered here as 'proper' and the other one as 'spurious'. The pair of corresponding roots with B_{3u} symmetry is dominated by a single excitation from one active orbital to the other and vice versa. The reason for the appearance of a spurious root for Mk-MRCC-LR in this case is that the model space response is described by internal excitation operators rather than by a response of the reference function. This is done in order to prevent a symmetry-conditioned decoupling between closed-shell and open-shell determinants through the eigenvalue equations [65]. In ic-MRCC-LR, however, such an obstacle in describing this state as the response of the CI coefficients does not exists. The additional roots of both B_{2g} and A_u symmetry, on the other hand, get their main contributions from double excitations and those are linearly dependent with single excitations acting on the other reference function. A higher

contribution of double excitations in describing these additional roots is likely the reason for the much higher energies of these roots compared to their counterparts.

In Ref. [65], the roots assigned here as $2\,^1B_{2u}$, $1\,^1B_{1u}$, $2\,^1B_{1u}$ and $2\,^1A_u$ have also been reported to be spurious roots. However, ic-MRCC-LR calculations recognize each of these roots as proper ones [P1]. Detailed look into the response vectors with those of other roots of the same symmetry suggests that they indeed describe distinct physical states. These roots have been mainly considered as spurious because of the absence of corresponding roots in the CCSD-LR calculations [65]. It is likely that the CCSD counterparts of these roots are much higher in energy, since the main contributing excitations for each of these states are single excitations with respect to the first reference function and thus correspond to double excitations with respect to the Hartree-Fock determinant.

In conclusion, ic-MRCC-LR avoids the difficulties due to spurious roots as encountered in Mk-MRCC-LR and is certainly also more accurate than the corresponding single-reference treatment of di-radical systems such as *p*-benzyne.

7.1.3 Direct ic-MRCC vs. Linear Response approach

Any state possible to describe within the model space may either be obtained directly by solving the ic-MRCC equations, or it may be obtained by using ic-MRCC-LR starting from a different initial state. In the following, both of these approaches are compared, focusing on those low-lying states of methylene and *p*-benzyne that can be described within the same CAS(2,2) as the initial states $1\,^1A_1$ and $1\,^1A_g$, respectively. Tab. 7.3 compares the ic-MRCCSD-LR method with the direct (state-specific) methods ic-MRCCSD and ic-MRCCSD(T)[25] and also reports results from CASSCF and the traditional EOM-CC approaches CCSD and CC3. The same structures and basis sets as in the previous sections have been employed for these calculations.

In case of methylene, Tab. 7.3 shows very small deviations (< 0.1 eV) between ic-MRCCSD-LR and a direct ic-MRCCSD treatment when based on the orbitals of the $1\,^1A_1$ reference state (i.e. without orbital relaxation). Although orbital relaxation produces only a minor effect on the ic-MRCC energies in contrast to the large differences observed between CASSCF and CASCI, the use of state-specific CASSCF orbitals brings the direct ic-MRCCSD excitation energies significantly closer to the FCI results. The best results are achieved here by using the perturbative triples correction, proposed in Ref. [25], yielding errors within 0.01 eV. This example slightly favors the direct ic-MRCCSD method over its linear response extension in terms of accuracy. This behaviour might be partially related to the circumstance that the overall contributions from dynamical correlation to

TABLE 7.3: Comparison of vertical ic-MRCCSD-LR excitation energies (in eV) with those obtained using direct (state-specific) ic-MRCC and selected conventional methods (published in [P1]). Those states of CH_2 and *p*-benzyne are considered, which can be described within the same CAS(2,2) as the reference state in the linear response treatment, i.e. $1\,^1A_1$ and $1\,^1A_g$, respectively. Structures and basis sets are the same as in Tabs. 7.1 and 7.2. Values given in parentheses are based on the CASSCF orbitals of the reference state and thus do not contain orbital relaxation effects.

State	CASSCF	(CASCI)	CCSD	CC3	FCI	ic-MRCC / CAS(2,2)				
						SD-LR	direct SD		direct SD(T)	
methylene										
$2\,^1A_1$	5.320	(14.677)	6.112[1]	5.127[1]	4.656[1]	4.835	4.670	(4.745)	4.646	(4.646)
$1\,^1B_1$	2.026	(8.815)	1.780[1]	1.788[1]	1.793[1]	1.799	1.805	(1.783)	1.795	(1.757)
$1\,^3B_1$	−0.091	(3.021)			−0.082	−0.068	−0.077	(−0.097)	−0.081	(−0.115)
p-benzyne										
$2\,^1A_g$	8.13	(11.788)	6.082[2]	4.245[3]		4.489	4.949	(5.027)	4.105	(3.932)
$1\,^1B_{3u}$	7.366	(11.595)	4.046[2]	3.622[3]		4.159	4.593	(4.730)	3.843	(3.724)
$1\,^3B_{3u}$	0.082	(0.123)				0.261	0.237	(0.241)	0.285	(0.284)

[1] Ref. [143].

[2] Ref. [65].

[3] Computed with the program package CFOUR (Ref. [159]).

the discussed transition energies (i.e. the differences between CASSCF and FCI) are rather small. This is much different in the case of *p*-benzyne, for which the CASSCF and CC3 excitation energies to the states $2\,^1A_g$ and $1\,^1B_{3u}$ each differ by as much as 4 eV. In these cases, the ic-MRCCSD-LR method agrees much better with CC3 compared to the direct ic-MRCCSD scheme, which gives excitation energies higher by up to 0.5 eV. A possible explanation for this is that the linear response ansatz gives a more flexible parameterization for the description of differential correlation effects, whereas the quality of the ic-MRCCSD results depends heavily on whether the chosen active space is still sufficient for the excited states under consideration. The ic-MRCCSD(T) results, on the other hand, is less sensitive to the size of the active space and yields much lower excitation energies. The same trend also holds for the excitation energies of the triplet state $1\,^3B_{3u}$, with the ic-MRCCSD-LR result lying halfway between the ic-MRCCSD and ic-MRCCSD(T) values. The absolute values of these excitation energies, however, are an order of magnitude smaller than in the case of the other two states, certainly due to the similarity of electron correlation effects in the $1\,^1A_g$ and $1\,^3B_{3u}$ states.

In the above study of CH_2, the reference state in the linear response treatment ($1\,^1A_1$) is not the system's ground state ($1\,^3B_1$) at the equilibrium. The remainder of this section will be spent to demonstrate that ic-MRCC theory allows one to perform a linear response

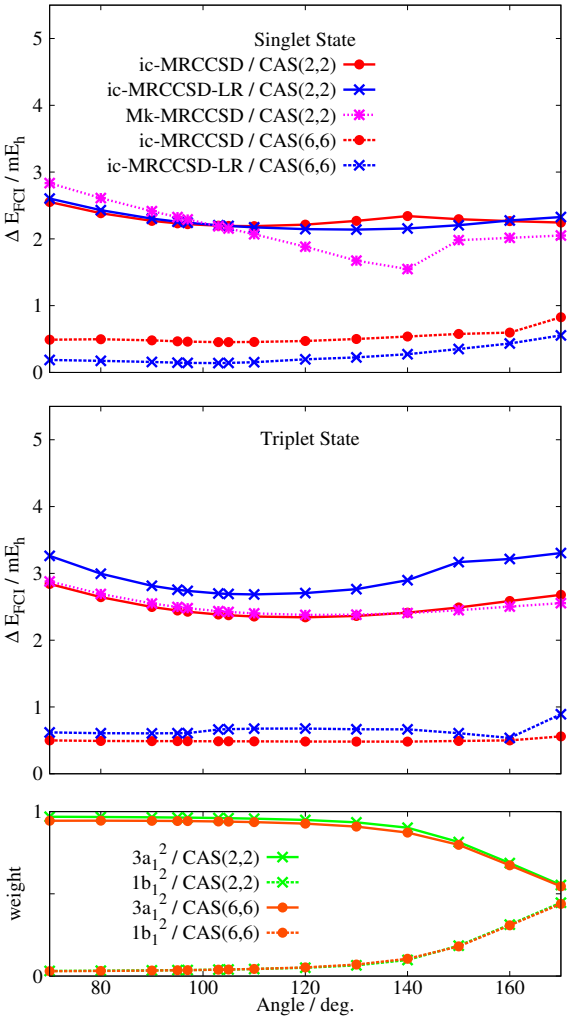

FIGURE 7.1: Top and middle: Energy difference with respect to full CI for the singlet state ($^1A_1$) and triplet state ($^3B_1$) of CH_2 for different MRCC methods, see text for details. Bottom: Weights of the dominant model space configurations for the singlet state, according to ic-MRCCSD (published in [P1]).

treatment starting from either state, without a loss of accuracy in regions of changing multireference character. The triplet state of methylene is energetically more stable than the singlet state at its equilibrium bond angle of about 130°. These two potential energy surfaces, however, cross at a bond angle of about 100°, close to the equilibrium structure of the singlet state. Both these states of methylene have been studied by Yamaguchi and coworkers[160] with the spin-orbital-based Mk-MRCC method, and by Mukherjee and coworkers[85, 161] using a spin-adapted variant of Mk-MRCC theory, UGA-SSMRCC. Following Ref. [85], the cc-pVDZ basis set has been used and the C-H bond length has been fixed at 2.11 a_0, while changing the bond angle in the range from 70° to 170°. The $1\,^1A_1$ state essentially has single-reference character up to a bond angle of about 130°. However, the weight of a second configuration (with the $1b_1$ orbital doubly occupied instead of the

$3a_1$ orbital) in the wave function rapidly increases with the molecule approaching the linear structure, as shown at the bottom of Fig. 7.1.

For two choices of active spaces, CAS(2,2) and CAS(6,6), ic-MRCCSD energies of the states $1\,^1A_1$ and $1\,^3B_1$ have been calculated both directly and through a response from the other state with the ic-MRCCSD-LR method. In case of the excitation from $1\,^1A_1$ to $1\,^3B_1$, the spin-flip symmetry of the response vector is constrained to that of a triplet-adapted excitation operator, thus removing any contamination from singlet or quintet states. Therefore, the ic-MRCC-LR approach leads to a spin-pure description of the triplet state and to identical energies for the $M_s = 0$ and $M_s = 1$ components. The ic-MRCC method in its present spin-orbital-based formulation, however, produces a slight spin contamination while computing the $1\,^3B_1$ state directly. The magnitude of this spin contamination is of about 10^{-4} for the expectation value of $\hat{S}^2$ at the linear order, i.e. when the spin expectation value is calculated for the function $\hat{T}|\Psi_0\rangle$. The present results are obtained for the $M_s = 0$ component of the triplet state. The differences with respect to FCI results are reported in Tabs. C.1-C.2 of the appendix C, and are plotted in Fig. 7.1. In case of the CAS(6,6), the tables in the appendix C contain results for both $\eta = 10^{-5}$ and $\eta = 10^{-4}$, whereas the plots only show the curves for $\eta = 10^{-4}$. The ic-MRCC results are compared here with those from spin-orbital-based Mk-MRCC theory[85]. For the CAS(2,2), both ic-MRCCSD and ic-MRCCSD-LR yield excitation energies with errors of similar magnitude as those of Mk-MRCCSD. However, the ic-MRCC based methods produce smoother curves for the singlet state and a smaller non-parallelity error (NPE=0.4–0.5 mE_h) than Mk-MRCCSD (NPE=1.3 mE_h). The results from ic-MRCCSD-LR agree with the direct ic-MRCCSD solutions within 0.7 mE_h ($\approx$ 0.02 eV). The same is also true for the larger active space CAS(6,6). Use of this larger active space mainly reduces the absolute errors from more than 2 mE_h down to about 0.5 mE_h and also decreases the NPE for the triplet state.

7.2 Equation of Motion Based Approach: an alternative Formulation for the Excitation Energy

In the context of the single-reference CC theory, linear response theory (CC-LR) [32, 52, 53, 66, 67] and equation-of-motion theory (CC-EOM) [68–70] produce the identical equations which lead to an unique solution for the excitation energies obtained for SRCC. The uniqueness of these equations follow from the fact that the excitation operators used in the single-reference framework are commutative with themselves which leads to the

relation:

$$\frac{\partial \bar{H}_0}{\partial \mathbf{t}} = [\bar{H}_0, \hat{\boldsymbol{\tau}}]. \tag{7.1}$$

The expressions in the left-hand side and the right-hand side of this relation appear in the CC-LR and CC-EOM equations respectively and thus these equations reduce to be the same one. Now, because the same relation does not hold for ic-MRCC as the corresponding excitation operators are not commutative, an EOM-fashioned theory for ic-MRCC is not bound to give the same equation as ic-MRCC-LR. The investigation of an equation-of-motion approach is attempted for ic-MRCC in this section.

The EOM approach starts from the Schrödinger equations of both the ground and the excited states. Here the ground state and the corresponding energy are denoted by $|\Psi_g\rangle$ and E_g, respectively, whereas the same for the excited state are denoted by $|\Psi_f\rangle$ and E_f, respectively. For the ic-MRCC ground state $|\Psi_g\rangle$, defined in the Eq. 3.1, the Schrödinger equation can be written as:

$$\hat{H}_0 e^{\hat{T}} |\Psi_0\rangle = E_g e^{\hat{T}} |\Psi_0\rangle, \tag{7.2}$$

where a pre-multiplication with $e^{-\hat{T}}$ changes it to:

$$\bar{H}_0 |\Psi_0\rangle = E_g |\Psi_0\rangle. \tag{7.3}$$

In the Equation of Motion approach the final excited state is defined from the ground state with an operator, say R, acting on it. Here, the final state is described as a perturbation $\delta T = \hat{\boldsymbol{\tau}}' \cdot \boldsymbol{\delta}\mathbf{t}'$ of the cluster operator T and $\delta\mathbf{c}$ of the reference coefficient $\mathbf{c}$:

$$|\Psi_f\rangle = \left(\frac{\partial}{\partial \mathbf{t}'}\boldsymbol{\delta}\mathbf{t}' + \frac{\partial}{\partial \mathbf{c}}\boldsymbol{\delta}\mathbf{c}\right)|\Psi_g\rangle = \frac{\partial e^{\hat{T}}}{\partial \mathbf{t}'}\boldsymbol{\delta}\mathbf{t}'|\Psi_0\rangle + e^{\hat{T}}|\boldsymbol{\Phi}\rangle\boldsymbol{\delta}\mathbf{c}. \tag{7.4}$$

Some shorthand notation are introduced in the equation above. Here, $|\boldsymbol{\Phi}\rangle$ and the $\hat{\boldsymbol{\tau}}'$ are the row vectors comprising the reference determinants and the excitation operators, respectively. $\mathbf{c}$ and $\mathbf{t}'$ are the column vectors of corresponding wave function parameters. The first part of the right hand side of Eq. 7.4 can be written as a product of $e^{\hat{T}}$ and an operator $\hat{R}_t$:

$$\frac{\partial e^{\hat{T}}}{\partial \mathbf{t}'}\boldsymbol{\delta}\mathbf{t}' = e^{\hat{T}}\hat{R}_t, \tag{7.5}$$

where the operator $\hat{R}_t$ is represented in the form of the following commutator expansion:

$$\hat{R}_t = \delta\hat{T} + \frac{1}{2}[\delta\hat{T}, \hat{T}] + \frac{1}{6}[[\delta\hat{T}, \hat{T}], \hat{T}] + \ldots. \tag{7.6}$$

The commutators, in the definition of $\hat{R}_t$, are appearing because of the non-commutativity

of the cluster operators for ic-MRCC. This is unique for the MRCC theories. A generalization to the single-reference coupled-cluster theory would omit these commutators leading to a simpler form of $\hat{R}_t$. However, this definition of $\hat{R}_t$ can be realized in two different ways:

$$\hat{R}_t = \tilde{\boldsymbol{\tau}}' \boldsymbol{r}'_{\boldsymbol{t}} = \boldsymbol{\tau}' \tilde{\boldsymbol{r}}'_{\boldsymbol{t}}, \tag{7.7}$$

where,

$$\tilde{\boldsymbol{\tau}}' = \boldsymbol{\tau}' + \frac{1}{2}[\boldsymbol{\tau}', \hat{T}] + \frac{1}{6}[[\boldsymbol{\tau}', \hat{T}], \hat{T}] + \ldots, \tag{7.8}$$

$$\boldsymbol{r}'_{\boldsymbol{t}} = \boldsymbol{\delta}\mathbf{t}', \tag{7.9}$$

and,

$$\tilde{\boldsymbol{r}}'_{\boldsymbol{t}} = \boldsymbol{\delta}\mathbf{t}' + \frac{1}{2}[\boldsymbol{\delta}\mathbf{t}', \hat{T}] + \frac{1}{6}[[\boldsymbol{\delta}\mathbf{t}', \hat{T}], \hat{T}] + \ldots. \tag{7.10}$$

These two alternative definitions lead to subsequent ways to solve the final equation to get the excitation energy. This are going to be discussed at a latter part of this section. The final state can now be written in a standard form for an EOM approach:

$$|\Psi_f\rangle = e^{\hat{T}}(\hat{R}_t + \hat{R}_c)|\Psi_0\rangle = e^{\hat{T}}\hat{R}|\Psi_0\rangle. \tag{7.11}$$

Here $\hat{R}_c$ is defined as:

$$\hat{R}_c = |\boldsymbol{\Phi}\rangle\langle\Psi_0|\frac{\boldsymbol{r_c}}{\langle\Psi_0|\Psi_0\rangle}; \quad \boldsymbol{r_c} = \boldsymbol{\delta}\mathbf{c}. \tag{7.12}$$

Now, use of Eq. 7.11 into the Schrödinger equation for the final state and pre-multiplication of both sides with e^{-T} give:

$$\bar{H}_0\hat{R}_t|\Psi_0\rangle + \bar{H}_0|\boldsymbol{\Phi}\rangle\boldsymbol{r_c} = E_f\hat{R}_t|\Psi_0\rangle + E_f|\boldsymbol{\Phi}\rangle\boldsymbol{r_c}. \tag{7.13}$$

Following the EOM approach, pre-multiplication of Eq. 7.3 with $\hat{R}$ yields,

$$\hat{R}_t\bar{H}_0|\Psi_0\rangle + \frac{\langle\Psi_0|\bar{H}_0|\Psi_0\rangle}{\langle\Psi_0|\Psi_0\rangle}|\boldsymbol{\Phi}\rangle\boldsymbol{r_c} = E_g\hat{R}_t|\Psi_0\rangle + E_g|\boldsymbol{\Phi}\rangle\boldsymbol{r_c}. \tag{7.14}$$

By subtracting Eq. 7.14 from Eq. 7.13, one can obtain:

$$[\bar{H}_0, \hat{R}_t]|\Psi_0\rangle + (\bar{H}_0 - E_g)|\boldsymbol{\Phi}\rangle\boldsymbol{r_c} = \omega\hat{R}_t|\Psi_0\rangle + \omega|\boldsymbol{\Phi}\rangle\boldsymbol{r_c}, \tag{7.15}$$

where $\omega = E_f - E_g$ and $\frac{\langle\Psi_0|\bar{H}_0|\Psi_0\rangle}{\langle\Psi_0|\Psi_0\rangle} = E_g$. The equation for $\boldsymbol{r_c}$ can be obtained by projecting Eq. 7.15 onto $\langle\boldsymbol{\Phi}|$:

$$\langle\boldsymbol{\Phi}|[\bar{H}_0, \hat{R}_t]|\Psi_0\rangle + \langle\boldsymbol{\Phi}|(\bar{H}_0 - E_g)|\boldsymbol{\Phi}\rangle\boldsymbol{r_c} = \omega\boldsymbol{r_c}. \tag{7.16}$$

The equation for $\hat{R}_t$ follows from the projection of Eq. 7.15 onto $\langle\Psi_0|\boldsymbol{\tau'}^{\dagger}$:

$$\langle\Psi_0|\boldsymbol{\tau'}^{\dagger}[\bar{H}_0, \hat{R}_t]|\Psi_0\rangle + \langle\Psi_0|\boldsymbol{\tau'}^{\dagger}\bar{H}_0|\boldsymbol{\Phi}\rangle\boldsymbol{r_c} = \omega\langle\Psi_0|\boldsymbol{\tau'}^{\dagger}\hat{R}_t|\Psi_0\rangle. \tag{7.17}$$

Now, as $\hat{R}_t$ can be realized using two alternative definitions as presented in Eq. 7.7, an eigenvalue equation can be derived to solve each of the parameters $\boldsymbol{r'_t}$ and $\tilde{\boldsymbol{r}}_{\boldsymbol{t}}$. The use of the first definition $\hat{R}_t = \tilde{\boldsymbol{\tau}}'\boldsymbol{r'_t}$ leads to an Eigenvalue equation, for solving r'_t and r_c, of the form:

$$\left[\begin{pmatrix} \langle\boldsymbol{\Phi}|(\bar{H}_0 - E_g)|\boldsymbol{\Phi}\rangle & \langle\boldsymbol{\Phi}|[\bar{H}_0, \tilde{\boldsymbol{\tau}}']|\Psi_0\rangle \\ \langle\Psi_0|\boldsymbol{\tau'}^{\dagger}\bar{H}_0|\boldsymbol{\Phi}\rangle & \langle\Psi_0|\boldsymbol{\tau'}^{\dagger}[\bar{H}_0, \tilde{\boldsymbol{\tau}}']|\Psi_0\rangle \end{pmatrix} - \omega \begin{pmatrix} \mathbf{1} & \mathbf{0} \\ \mathbf{0} & \mathbf{S_t} \end{pmatrix}\right] \begin{pmatrix} \mathbf{r}_c \\ \boldsymbol{r'_t} \end{pmatrix} = 0, \tag{7.18}$$

where the metric matrix is defined as:

$$\mathbf{S_t} = \langle\Psi_0|\boldsymbol{\tau'}^{\dagger}(\boldsymbol{\tau'} + \frac{1}{2}[\boldsymbol{\tau'}, \hat{T}] + \frac{1}{6}[[\boldsymbol{\tau'}, \hat{T}], \hat{T}] + \dots)|\Psi_0\rangle. \tag{7.19}$$

Eq. 7.18 is the same as that was derived earlier as ic-MRCC-LR in Eq. 4.48. The correspondence of these two equations would be clear after using the expression of the derivative of the similarity transformed Hamiltonian [P1]

$$\frac{\partial\bar{H}_0}{\partial t'} = [\bar{H}_0, \tilde{\boldsymbol{\tau}}'] \tag{7.20}$$

as shown also in Eq. 4.49. It is worth mentioning that the ic-MRCC-LR equation has been arrived here, starting from Schrödinger equation, without the appearance of the term $B_{\lambda c} = \langle\boldsymbol{\Phi}|\boldsymbol{\tau'}^{\dagger}\bar{H}_0|\Psi_0\rangle$ in our equation. A similar term appeared during the derivation of ic-MRCC-LR equation in Eq. 4.34 [P1] and was later removed in the spirit of Tamm-Dancoff approximation. The appearance of such term in the previous study seems to be an artifact of ic-MRCC.

The alternative definition $\hat{R}_t = \boldsymbol{\tau'}\tilde{\boldsymbol{r}}'_{\boldsymbol{t}}$ would give a different eigenvalue equation to solve $\tilde{\boldsymbol{r}}'_{\boldsymbol{t}}$:

$$\left[\begin{pmatrix} \langle\boldsymbol{\Phi}|(\bar{H}_0 - E_g)|\boldsymbol{\Phi}\rangle & \langle\boldsymbol{\Phi}|[\bar{H}_0, \hat{\boldsymbol{\tau}}']|\Psi_0\rangle \\ \langle\Psi_0|\boldsymbol{\tau'}^{\dagger}\bar{H}_0|\boldsymbol{\Phi}\rangle & \langle\Psi_0|\boldsymbol{\tau'}^{\dagger}[\bar{H}_0, \hat{\boldsymbol{\tau}}']|\Psi_0\rangle \end{pmatrix} - \omega \begin{pmatrix} \mathbf{1} & \mathbf{0} \\ \mathbf{0} & \mathbf{1} \end{pmatrix}\right] \begin{pmatrix} \mathbf{r}_c \\ \tilde{\boldsymbol{r}}'_{\boldsymbol{t}} \end{pmatrix} = 0. \tag{7.21}$$

This equation has a much simpler form compared to Eq. 7.18, as the metric matrix is an unit matrix here and also the commutator involves the simpler $\hat{\boldsymbol{\tau}}'$. This approach is named here as ic-MRCC-EOM.

Computationally ic-MRCC-EOM is less expensive compared to ic-MRCC-LR. ic-MRCC-EOM does not involve any metric matrix to be evaluated in each iteration while solving the eigenvalue equation. Moreover, the operator $\hat{\boldsymbol{\tau}}'$ involved in the commutator expression for the ic-MRCC-EOM is simply the cluster operator truncated at the doubles, while its counterpart in the ic-MRCC-LR, $\tilde{\boldsymbol{\tau}}'$, can be higher than two body following the definition in Eq. 7.8. Thus ic-MRCC-LR has a larger number of terms involved in its eigenvalue equation making it computationally more demanding. However, involvement of this higher body terms in ic-MRCC-LRT might also increase the accuracy and thus it has the potential to be more accurate than the EOM method, specially for excited state dominated by double excitations.

7.3 A Comparative Study of the LR and EOM Approaches

In this section the ic-MRCC-EOM method is compared with its LR counterparts in terms of numerical accuracy. Both of these methods are tested against the FCI results for the Beryllium triatomic cluster. Apart from an internal comparison between these two variants of ic-MRCC, an overall comparison is also made using the results obtained from the single-reference EOM methods that includes triples corrections. In another example, the relative ordering of the two lowest lying excited states of different trans-oligoenes is investigated using both of EOM and LR formulations of ic-MRCCSD.

7.3.1 Beryllium Triatomic Cluster

The Beryllium trimer (Be_3) is a prominent multireference system as the quasi-degeneracy of the 2s-2p orbitals of Be increases significantly with the formation of the trimer. Due to the same reason, there are several excited states of this system, dominated mainly by double excitations, appearing at relatively low energies. A good description of the ground state of Be_3 has been obtained using FCI [162], MRCI [163, 164] and also with the single-reference CCSDt methods [165]. Calculations of the excited state energies have also been attempted using single-reference EOM methods like CR-EOM-CCSD(T) and EOM-CCSDt [165] and compared with respect to available FCI results [166]. Both the EOM and LR variants of the ic-MRCCSD theory are applied here to calculate these excited states and the results are compared among each other and with the single-reference methods mentioned earlier.

TABLE 7.4: A comparison of vertical excitation energies (in eV) for several singlet states of Be_3 obtained using ic-MRCC-EOM, ic-MRCC-LRT, different variants of single-reference based EOMCC as a difference with respect to FCI.

State	type[1]	CR-EOMCCSD(T)[2]	EOMCCSDt[2]		ic-MRCCSD			
					CAS(6e,9o)		CAS(6e,12o)	
			(I)	(II)	EOM	LR	EOM	LR
$1E''$	s	-0.023	-0.012	0.008	0.001	-0.002	0.003	0.003
$1A_1''$	d		0.097	0.28	0.235	0.262	0.057	0.053
$1E'$	s	-0.052	-0.009	0.023	-0.006	-0.008	-0.003	-0.005
$2E''$	d		0.073	0.234	0.219	0.265	0.050	0.045
$2E'$	d	0.352	0.028	0.200	0.034	0.034	0.027	0.026
$1A_2'$	s	-0.100	-0.019	-0.019	0.004	0.005	0.005	0.004
$2A_1'$	s	-0.014	0.027	0.065	0.010	0.011	0.006	0.002
$3E''$	d	0.506	0.075	0.274	0.113	0.093	0.028	0.023
$3E'$	d	0.258	0.167	0.367	0.380	0.385	0.050	0.045
$1A_2''$	s,d	0.198	0.142	0.277	0.018	-0.001	0.007	0.016
$2A_1''$	d	0.291	0.129	0.317	0.228	0.281	0.034	0.028
$4E'$	d	0.153	0.061	0.263	0.392	0.395	0.010	0.010
$3A_1'$	d	0.393	0.206	0.348	0.325	0.316	0.037	0.012
$4E''$	d	0.054	0.118	0.312	0.184	0.254	0.041	0.034
$3A_1''$	s,d	-0.099	0.122	0.218	0.062	0.096	0.010	0.009
$2A_2''$	d	0.264	0.063	0.254	0.234	0.305	0.0042	0.060

1. Character of excitation with respect to the Hartree-Fock determinant: s = single-excitation dominated
d = double-excitation dominated

2. Ref. [165]

The ic-MRCC calculations to get excitation energies of the Be_3 molecule are done using the same geometry and ANO basis which have been used in Refs. [165, 166]. The original symmetry of Be_3, D_{3h}, is used here to assign its excited states, although the calculations are done using C_{2v} symmetry. Three core 1s orbitals of Be are kept frozen in order to compare the results with that of FCI. The results of the ic-MRCCSD excitation energies for both of the variants, along with the results obtained from the EOM-CCSD , CR-EOM-CCSD(T) and EOM-CCSDt calculations, are presented as differences with respect to the FCI results in Tab. 7.4. The ic-MRCCSD calculations are done using two different active spaces: (6e,9o) and (6e,12o). CAS(6e,9o) uses the lone 2s orbitals and the 2p orbitals residing in the molecular plane ($2p_x$ and $2p_x$ in this case) as the active orbitals. For CAS(6e,12o), on the other hand, the rest of the 2p orbitals ($2p_z$) of the system are added to the existing active orbitals of CAS(6e,9o). The orbitals involved in the ic-MRCCSD calculations are obtained from consecutive Hartree-Fock and CASSCF calculations with all the core 1s orbitals being frozen for the latter. This ensures that the

same orbital space is used while correlating electrons for all the calculations presented in Tab. 7.4. In the EOM-CCSDt method, the definition of the three body excitation operators needs the use of active orbitals. Among the two different variants of EOM-CCSDt used here, variant (I) has at least one active occupied and at least one active unoccupied spin-orbital indices in its definition of three body excitation operators. For the EOM-CCSDt(II), on the other hand, triple excitations contain at least two active occupied and two active unoccupied spin-orbitals thus spanning a relatively smaller space than the first variant. The EOM-CCSDt results, obtained from Ref. [165] and presented in Tab. 7.4, use the same active space of (6e,12o) as mentioned above to define the three body excitation operators.

The choice of the active space for ic-MRCCSD changes the accuracy of the excitation energies only for the doubly excited states. The results obtained using the active space of (6e,12o) are invariably more accurate for these states compared with those obtained for the CAS(6e,9o) as the former involves more configurations to describe the reference wave functions. The excitation energies do not change significantly between the use of the two variants of ic-MRCCSD. Though the differences between the results for EOM and LR are greater for the lower active active space, the highest among these differences is 0.05 eV obtained for the $2A_1''$ which is a doubly excited state.

Between the results of the two variants of EOM-CCSDt, the variant (I) provides excitation energies with better accuracy as it includes more configurations obtained through three-body excitations than the other variant. EOM-CCSDt(I) also provides better results than CR-EOM-CCSD(T) with the exceptions of two higher-lying excited states, $4E''$ and $3A_1''$. The ic-MRCCSD results obtained using either of the active spaces are better than the single-reference results for all the excited states dominated by single excitation. For the doubly excited states, ic-MRCCSD provides accuracy comparable to the EOM-CCSDt(II) when the multireference calculations are done using the lower active space of (9e,6o). For these states, ic-MRCCSD results are better than that of EOM-CCSDt(II) for all the states with an exception being the state $3A_1'$. However, by using the higher active space of (6e,12o), ic-MRCCSD produces excitation energies which are always more accurate even than those obtained for EOMCCSDt(I). The highest error in excitation energies with respect to FCI results is 0.057 for ic-MRCCSD/CAS(6e,12o) method, where EOM-CCSDt(I) produces an error as big as 0.2. Moreover, the errors in excitation energies obtained using ic-MRCCSD are always of similar magnitudes even for the higher lying states, where the magnitude of the errors increase for these states when the single-reference methods are used.

7.3.2 E-Oligoenes

Conjugated hydrocarbons are very important system in organic electronics, photonics, and biophysics [167]. The lowest singlet excited states of these molecules also provide a good test to theoretical methods [168–171]. The optically dark $2\,^1\mathrm{A}_g^-$ states of these hydrocarbons are doubly excited from the reference ground state and thus can not be described properly with the single-reference methods. On the other hand, the bright ionic $1\,^1\mathrm{B}_u^+$ states of these systems need an accurate treatment of the dynamic correlation and thus described poorly by the multireference perturbation theories like CASPT2. The $2\,^1\mathrm{A}_g^-$ state is lower in energy than the $1\,^1B_u^+$ state for the oligoenes beyond all-*E*-octatetraene. However, the order of these two states has been controversial for the shorter oligoenes and this phenomenon has been discussed quite often in the literature [172–175].

Here, the transitions from the $1\,^1\mathrm{A}_g^-$ ground state to these two states are studied for *E*-butadiene, all-*E*-hexatriene and all-*E*-octatetraene using both the EOM and LR variants of ic-MRCCSD. The structure and basis sets employed in this study are obtained from the work of Schreiber *et al.* [176–178]. All electrons have been correlated in the ic-MRCCSD calculations. However, a direct comparison with the experimental results is not followed here as it is not straightforward in this case. This is because excitation energies are calculated here following the Franck-Condon principle and also that smaller basis set, TZVP, is used here which cannot describe the $1\,^1\mathrm{B}_u^+$ states satisfactorily due to a lack of diffuse functions. Instead, the ic-MRCCSD results for both the EOM and LR variants are compared here with results CASPT2, CCSD and CC3 [176, 178], as well as with the most recent results from multireference equation-of-motion coupled-cluster theory (MREOM) [179]. These results are presented in Tab. 7.5.

The ic-MRCCSD calculations are done for two active spaces: a CAS(2e,2o), which includes the HOMO and LUMO inside the active space and thus allows a fair description of the double excitation between these two orbitals in the transition to the $2\,^1\mathrm{A}_g^-$ state; and another active space incorporating all the valence π orbitals, denoted here as CAS(n,n), where n is the number of the carbon atoms present in the polyene. The excitation energies obtained using these two active spaces differ by up to 0.1 eV for the $1\,^1\mathrm{B}_u^+$ state, but this difference increases to be of about 0.9 eV for the doubly excited $2\,^1\mathrm{A}_g^-$ state. Inspecting the response vector of the $2\,^1\mathrm{A}_g^-$ state for the larger active space, it is revealed that the contributions other than from HOMO to LUMO, such as from HOMO-1 to LUMO, or from HOMO to LUMO$+1$, are also significant in describing this state. Therefore, only the use of larger active space can properly account for these additional double excitations. The difference between the results from the EOM and LR formulations is significant only for the lower active space CAS(2e,2o). The use of the larger active space for each of the molecules leads to an agreement between the EOM and LR results within 0.05 eV which

TABLE 7.5: Energies of singlet states of all-*E*-oligoenes, given relative to the $^1A_g^-$ ground state in eV, using structures from Ref. [176] and the TZVP basis set from Ref. [142].

State	CASPT2[1] CAS(n,n)	CCSD[1]	CC3[1]	MREOM[2] CAS(n,n')	ic-MRCCSD CAS(2,2)		ic-MRCCSD CAS(n,n)	
					EOM	LR	EOM	LR
E-Butadiene ($n = 4$)								
$2^1A_g^-$	6.63	7.42	6.77	6.60	6.62	6.70	6.57	6.56
$1^1B_u^+$	6.47	6.72	6.58	6.66	6.56	6.55	6.65	6.60
all-*E*-Hexatriene ($n = 6$)								
$2^1A_g^-$	5.42	6.61	5.72	5.63	6.14	6.28	5.43	5.44
$1^1B_u^+$	5.31	5.72	5.58	5.78	5.60	5.68	5.68	5.66
all-*E*-Octatetraene ($n = 8$)								
$2^1A_g^-$	4.64	5.99	4.97		5.12	5.26	4.66	4.65
$1^1B_u^+$	4.70	5.07	4.94		4.94	4.99	5.06	5.05

1. Refs. [176, 178].
2. Ref. [179], using CAS(4,4) for *E*-butadiene and CAS(6,5) for all-*E*-hexatriene.

again decreases with the increase in the active space size for the larger polyenes. For the use of CAS(2e,2o), however, the EOM and LR results differ again mainly for the $2\,^1A_g^-$, although the differences are within 0.14 eV.

MREOM results are only available for *E*-butadiene and all-*E*-hexatriene and ic-MRCC results agree with these results within 0.2 eV, which highlights the close connection between the two methods. The ic-MRCC results match mostly with that of CASPT2 for the $2\,^1A_g^-$ states, while for the $1\,^1B_u^+$ states the results obtained from CC3 are the closest. The excitation from $1\,^1A_g^-$ to $2\,^1A_g^-$ is well described by most of the multireference level of theories, including CASSCF, as the main contributions here are included within the active space [170–173]. However, this is not the case for the $1\,^1B_u^+$ state and thus the multireference perturbation theories, such as CASPT2, tends to overshoot and becomes unreliable. For this single-excitation dominated state, the main contribution appears through the proper treatment of the dynamic correlation and thus CC3 provides a much better description of the state since it is correct up to the third order of perturbation theory [143, 146].

8 | Summary and Outlook

8.1 Summary

The main goal of this thesis is the development of the linear response (LR) method, based on the internally contracted multireference coupled cluster (ic-MRCC) framework, to calculate accurate molecular properties and excitation energies for molecular systems with prominent multireference character. The work done, towards achieving this goal, led to the following original contributions:

- A time-dependent Lagrangian, essential for the formulation of the linear response theory based on a non-variational method, is constructed for the ic-MRCC theory.
- The expression for calculating the first order molecular property from the ic-MRCC theory is derived. The equations for solving the zeroth order Lagrange multipliers, which are required to calculate the first order properties, are formulated
- The expression for the linear response function of the ic-MRCC theory is also derived. This is then used to calculate the static and frequency-dependent second order properties. As the linear response function depends on the first order wave function parameters, equations to solve these parameters are also formulated.
- In order to calculate excitation energies, ic-MRCC-LR and ic-MRCC-EOM have been formulated. These two formulations differ in the way the ansatz for the excited states are defined.

The main formulation of the LR theory on top of an ic-MRCC wave function is presented in Chap. 4. The time-dependent Lagrangian for ic-MRCC, constructed in this process, introduces the time-dependent Lagrange multipliers, $\boldsymbol{\lambda}$ and $\bar{\boldsymbol{c}}$, represented here as vectors. This Lagrangian also involves a non-unit metric matrix $\mathbf{S}_t$ arising due to the noncommutative property of the cluster operators used in the MRCC theories. The most important aspect of this Lagrangian, like its time-independent counterpart, is the

lack of bi-orthogonality in its form as one of the terms in this Lagrangian involves the adjoint of the reference function, $\langle\Psi_0|$, instead of its bi-orthogonal component, $\langle\overline{\Psi}_0|$. This makes ic-MRCC different from the single-reference CC method and other MRCC methods like Mk-MRCC. Presence of $\langle\Psi_0|$ in the Lagrangian, *i.e.* the reference coefficients $\mathbf{c}$ in the projection manifold of the Lagrangian, produces an additional term $B_{\lambda c}$ in the lambda equations, which give the solution for the zeroth order Lagrange multipliers, and the response equations, which produce the first order wave function parameters. Lack of bi-orthogonality particularly affects the frequency-dependent properties, as the presence of the term $B_{\lambda c}$ in the response equations causes the coupling between the first order parameters corresponding to frequencies of ω and $-\omega$. This coupling ensures a simultaneous divergence of the parameters corresponding to both the frequencies ω and $-\omega$ near the pole. As the linear response function depends on the product of these two parameters, the simultaneous divergence of them means appearance of an unphysical second order nature of its poles. Although $B_{\lambda c}$ vanishes in the FCI limit and is expected to be small in the truncated version of the ic-MRCC theory, its effect is not negligible. Thus the original response equations and response functions for ic-MRCC go through some approximations which remove the effect of the coupling and thus avoid the appearance of second order poles for the linear response function.

The approximation involved in the response equations, which is made in the spirit of the Tamn-Dancoff approximation, removes the term $B_{\lambda c}$ so that it decouples the solutions for the parameters corresponding to frequencies with opposite signs. Even though the response equations are now decoupled, the response function still has contributions for a second order pole due to the presence of term quadratic in the first order wave function parameters. This appears again due to the presence of $\langle\Psi_0|$, in the Lagrangian. So, the response function is approximated by removing all the terms which include the reference coefficients, $\mathbf{c}$, in the projection manifold. Therefore, complete removal of any contribution to the second order pole can only be done through the simultaneous use of these two approximations. Moreover, following the LR formalism, the eigenvalue equation for solving the excitation energies are obtained by extracting condition of singularity of the approximated response equations. These excited energies, therefore, correspond to the corrected first order poles of the linear response function.

In the static limit of the linear response function, however, these two approximations are not relevant. Also, the full formulations of the response equations and response function are essential in the static limit for the results to match the ones obtained from finite field method. The static second order properties obtained through the approximated formulation are significant only to avoid the discontinuity in the form of the linear response function, though the errors arising from these approximations are very small.

There is no direct effect of the term $B_{\lambda c}$, which also appears in the lambda equation, in the field independent first order properties. Thus, the term **c** is not removed from the main formulation of the lambda equation. However, an alternative formulation of removing this term is also made to study its effects on the first order properties. The more important aspect of the lambda equation is the way it is formulated. While the lambda equation represents a set of linear equations in the single-reference framework and other multireference methods such as Mk-MRCC, a similar set of equations are *homogeneous* in nature for the ic-MRCC theory. Thus, the non-trivial solutions for these equations are obtained by first casting the set of *homogeneous* linear equation as eigenvalue equation and then getting the eigenvector corresponding to the zero eigenvalue.

The linear response formulation developed in this work considers the effect of the perturbation only on the wave function parameters and corresponding Lagrange multipliers. Therefore, the calculated molecular properties do not account for any effect on the relaxation of the molecular orbitals. Moreover, for ic-MRCC, perturbations can cause an additional relaxation effect as it also affects the transformation matrix $\mathbf{X}$, used in the theory to obtain the linearly independent excitation manifold. The current formulation also ignores this additional relaxation effect on the properties. However, effect of leaving out these contributions of relaxations are not very large and this is shown through calculations of dipole moments for several molecules in Sec. 5.1.

For the ground state of BH, ic-MRCCSD produces the values of different first order properties as accurate as the CCSDT level of theory. This has been shown by calculating different first order electrical properties for the molecule, namely the dipole moment, quadrupole moment and electric field gradient, using a (2e,2o) active space. It proves that ic-MRCCSD provides reasonably good descriptions of the electronic density in different regions of space as this is essential for giving consistently good results for different kinds of properties. However, the main strength of the ic-MRCCSD theory is its effectiveness in describing a multireference situation. The two lowest lying $^1\Sigma^+$ states of LiF are perfect examples of such systems as these two states produce an avoided curve crossing while dissociating. The dipole moment curves for these two states, calculated using different MR methods, show that the ic-MRCCSD provides more accurate results compared to other methods, such as SRMRCC [130, 131] and MRexpT [20, 132]. These results has another significance as they show that inclusion of the disputed $B_{\lambda c}$ term in the ic-MRCC lambda equations introduces larger errors near the region of avoided curve crossing. The alternative formulation of excluding this particular term provides a definite improvement in the nature of the dipole moment curve and its accuracy.

Apart from the electrical first order properties, some spin-dependent first order properties, such as the Fermi contact (FC) and the spin-dipole (SD) interaction terms of hyperfine coupling constants, are also calculated using ic-MRCCSD. Calculations of these spin-dependent properties for the doublet ground state of BeH show that these properties do not converge to the corresponding FCI results with the increase in the size of the active space. This observation is also reflected when ic-MRCCSD is used to calculate the FC and SD terms for the doublet ground states of BO, CO^+, CN and AlO radicals, where the best results for ic-MRCCSD, when calculated using different size of active spaces, are often obtained with the lowest dimension in the CAS. However, these results are, for most of the cases, more accurate than the best results obtained from the highly accurate DMRG methods.

The first part of Chap. 6 focuses on showing the effectiveness of the approximations, involved in the response equations and in the response function, in removing any contribution to the second order pole of the linear response function. Different components of electrical polarizabilities for CH_2 and BH are plotted against frequencies to show individual contributions of these approximations in obtaining the regular first order poles of the linear response function. However, these approximations also introduce errors in the values of the polarizabillities. These errors are only meaningful close to the static limit as they diverge near the poles. A study of static polarizabilities and the dynamic polarizabilities near the static limit shows that these errors are very small and thus these approximations can be used together to give the final form of the ic-MRCC-LR method which can be used to calculate the second order molecular properties. When compared to the FCI results, available for the parallel component of polarizability of BH, the ic-MRCCSD-LR method provides very accurate results with a maximum deviation of 0.54% in contrast to that of Mk-MRCCSD being 11%. Different components of polarizabilities are also calculated for p-Benzyne and 2,6-Pyridyne and compared with the CCSD and Mk-MRCCSD results. This study shows that, unlike Mk-MRCC, ic-MRCC does not produce any additional spurious poles through the singularities in the linear response functions.

The vertical excitation energies as obtained using ic-MRCCSD-LR have the accuracy of the CC3 results for the single-excitation dominated states. For the double excitation dominated states, ic-MRCCSD-LR produces better accuracy in predicting the excitation energies than that of the CC3 results as the respective doubly excited configuration often lie inside the model space used for the ic-MRCCSD calculations. These observations are supported by calculations of excitation energies for methylene, beryllium trimer complex and several polyenes. The energies for excited states obtained from the ic-MRCCSD-LR calculations are compared with the ones obtained through a direct ic-MRCCSD calculation for the state. This comparison for the singlet to triplet excitations for methylene

shows that the differences between these two methods lie within the sub-mE_h regime.

The eigenvalue equation for solving the excitation energies is also achieved following a EOM-like derivation. However, these derivation shows an alternative to the eigenvalue equations that ic-MRCC-LR provides. This alternative, denoted as ic-MRCC-EOM, is stemming from different ways of representing the ansatz of the excited states in EOM. This is an unique feature of the MRCC methods and arises as cluster operators do not commute with each other. The differences between the results obtained from these two variants are larger for the doubly excited states, however, these differences diminish with an increase in the size of the active spaces.

Overall, the implementation of the linear response formalism for the ic-MRCC theory produces a reliable way of calculating molecular properties for systems with significant multireference character. This is indicated by some first applications of this formalism to obtain first order and second order molecular properties, and excitation energies. Even though there are approximations involved in this development, mainly to avoid the appearance of unphysical second order poles for the linear response function, the higher accuracy that the ic-MRCCSD theory provides is retained.

8.2 Future Outlook

The development of the linear response theory for ic-MRCC can further be extended in different directions. The current formalism is restricted to using only the single and double excitation operators in describing the zeroth order and first order wave functions of molecular systems. It is possible to include the triples perturbatively, in a way similar to how ic-MRCCSD(T) has been formulated [25] to calculate energies of molecular systems. Such an implementation will produce molecular properties and specifically excitation energies of very high accuracy.

In this thesis, properties are obtained within the realm of the linear response approach. An extension of the existing formulation in the context of the non-linear response theory will produce expressions for calculating third and higher order of molecular properties, such as dipole hyperpolarizabilities. Use of magnetic field as well as combination of electric and magnetic fields, on the other hand, will allow the existing linear response formulation of ic-MRCC to calculate some interesting properties, such as electronic g-tensor, which are of interest for understanding electron paramagnetic resonance (EPR) spectroscopy. Inclusion of the magnetic field inside the existing Hamiltonian, however, will require some modifications in the equations formulated in the current linear response approach.

In view of these future prospects, the work in this thesis has laid the foundation for developing a tool to calculate different sorts of molecular properties with higher accuracy and for strong multireference systems.

A | Data for the first order properties

TABLE A.1: Geometries of the molecules used for the calculations of dipole moments which are presented in Tab. II of the main paper and also Tabs. S2 and S3 of this supplemental.

Molecule	atoms (x,y,z)
LiH	Li (0.0, 0.0, 0.3760608001) H (0.0, 0.0, –2.6179589255)
BH	B (0.0, 0.0, –0.1984384020) H (0.0, 0.0, 2.1677065875)
CH_2	C (0.0, 0.0, –0.1933134200) H (0.0, 1.6445071385, 1.1508749235) H (0.0, –1.6445071385, 1.1508749235)
HF	H (0.0, 0.0 , 1.6578138390) F (0.0, 0.0, –0.0879435094)
LiF	Li (0.0, 0.0, 0.8014679850) F (0.0, 0.0, –2.1702680900)
CN	C (0.0, 0.0, 1.2055077943) N (0.0, 0.0, –1.0330655634)
BO	B (0.0, 0.0, 1.3580886010) O (0.0, 0.0, –0.9347728091)

TABLE A.2: MRCISD dipole moments of different molecules in atomic units as obtained by three different approaches. "Unrelaxed" is the expectation value of the CI wavefunction. "relaxed($\mathbf{c}_0$)" is obtained by determining the orbitals for the unperturbed system and a finite field approach in the subsequent CI calculation, such that the relaxation of the reference coefficients $\mathbf{c}_0$ is taken into account. The fully relaxed result ("relaxed($\mathbf{c}_0$,$\mathbf{C}$)") uses a finite field approach, where the orbitals are determined in the presence of the perturbation. All calculations are done using Molpro [120] and correlating all electrons. The "unrelaxed" result is given as the absolute value, for the other approaches the change relative to "unrelaxed" is reported.

Molecule (State)	CAS	Basis	unrelaxed	relaxed($\mathbf{c}_0$)	relaxed($\mathbf{c}_0$,$\mathbf{C}$)
LiH ($^1\Sigma^+$)	(2,2)	aug-cc-pVDZ	2.315153	+0.000375	+0.001783
		aug-cc-pVTZ	2.290690	+0.001125	+0.008111
		aug-cc-pVQZ	2.284040	+0.001267	+0.010200
BH ($^1\Sigma^+$)	(2,2)	aug-cc-pVDZ	0.531784	-0.004241	-0.010401
		aug-cc-pVTZ	0.558770	-0.000444	+0.009262
		aug-cc-pVQZ	0.568245	-0.000188	-0.032181
CH_2 ($^1A_1$)	(2,2)	aug-cc-pVDZ	0.648754	+0.000081	-0.003013
		aug-cc-pVTZ	0.655152	+0.000400	-0.002287
		aug-cc-pVQZ	0.658302	+0.000522	-0.001891
HF ($^1\Sigma^+$)	(2,2)	aug-cc-pVDZ	0.706774	+0.004850	+0.003598
		aug-cc-pVTZ	0.709717	+0.002599	+0.003271
		aug-cc-pVQZ	0.712608	+0.002671	+0.003605
LiF ($^1\Sigma^+$)	(2,2)	aug-cc-pVDZ	2.529038	+0.001780	+0.001211
		aug-cc-pVTZ	2.510752	+0.000912	-0.000178
		aug-cc-pVQZ	2.511312	+0.000809	-0.001513
CN ($^2\Sigma^+$)	(5,6)	aug-cc-pVDZ	0.673026	+0.002049	-0.032568
		aug-cc-pVTZ	0.720313	+0.002901	-0.040292
		aug-cc-pVQZ	0.742430	+0.003984	-0.042039
BO ($^2\Sigma^+$)	(5,6)	aug-cc-pVDZ	0.905959	+0.001115	-0.010885
		aug-cc-pVTZ	0.923684	+0.000891	-0.007385
		aug-cc-pVQZ	0.930796	+0.001717	-0.007347
CH_2 ($^1A_1$)	(6,6)	aug-cc-pVDZ	0.641727	+0.000604	-0.003043
		aug-cc-pVTZ	0.645576	+0.000912	-0.001126
		aug-cc-pVQZ	0.647950	+0.001226	-0.000379

TABLE A.3: CASPT2 dipole moments of sample molecules in atomic units as obtained by three different approaches. For details see table A.2.

Molecule (State)	CAS	Basis	unrelaxed	relaxed($\mathbf{c}_0$)	relaxed($\mathbf{c}_0$,$\mathbf{C}$)
LiH ($^1\Sigma^+$)	(2,2)	aug-cc-pVDZ	2.235325	+0.007283	+0.057282
		aug-cc-pVTZ	2.227364	+0.010441	+0.059738
		aug-cc-pVQZ	2.227598	+0.010284	+0.057084
BH ($^1\Sigma^+$)	(2,2)	aug-cc-pVDZ	0.667964	+0.001757	-0.061097
		aug-cc-pVTZ	0.629091	-0.001918	-0.102706
		aug-cc-pVQZ	0.633155	+0.001226	-0.083703
CH_2 ($^1A_1$)	(2,2)	aug-cc-pVDZ	0.655401	+0.000918	-0.010789
		aug-cc-pVTZ	0.652656	+0.001860	-0.005146
		aug-cc-pVQZ	0.651463	+0.002274	-0.000852
HF ($^1\Sigma^+$)	(2,2)	aug-cc-pVDZ	0.707022	+0.011403	+0.010227
		aug-cc-pVTZ	0.705337	+0.020003	+0.013257
		aug-cc-pVQZ	0.704373	+0.024493	+0.016414
LiF ($^1\Sigma^+$)	(2,2)	aug-cc-pVDZ	2.551462	-0.000482	-0.036802
		aug-cc-pVTZ	2.527325	+0.002738	-0.032774
		aug-cc-pVQZ	2.525646	+0.003971	-0.033200
CN ($^2\Sigma^+$)	(5,6)	aug-cc-pVDZ	0.751369	+0.027361	-0.031594
		aug-cc-pVTZ	0.750598	+0.034512	-0.034839
		aug-cc-pVQZ	0.751038	+0.037707	-0.034524
BO ($^2\Sigma^+$)	(5,6)	aug-cc-pVDZ	0.895704	+0.006877	+0.006797
		aug-cc-pVTZ	0.902834	+0.024951	+0.008525
		aug-cc-pVQZ	0.902955	+0.033039	+0.012196
CH_2 ($^1A_1$)	(6,6)	aug-cc-pVDZ	0.625251	+0.002806	+0.011845
		aug-cc-pVTZ	0.624133	+0.016409	+0.015734
		aug-cc-pVQZ	0.623338	+0.023556	+0.019468

TABLE A.4: Dipole Moments calculated in atomic units for BH using different basis sets. The results except that for FCI are presented as deviations from FCI (method - FCI). ic-MRCCSD calculations are done using (2,4) CAS. Dipole moments for methods other than ic-MRCCSD are obtained from [122]

					ic-MRCCSD	
Basis	FCI	CCSD	CCSD(T)	CCSDT	with $B_{\lambda c}$	without $B_{\lambda c}$
all electrons						
aug-cc-pCVDZ	0.52757	0.00895	0.00172	0.00056	0.00147	0.00162
valence only						
aug-cc-pVDZ	0.52782	0.00740	0.00157	0.00044	0.00148	0.00165
aug-cc-pVTZ	0.54328	0.00960	0.00172	0.00065	0.00135	0.00142
aug-cc-pVQZ	0.54554	0.01006	0.00170	0.00072	0.00122	0.00128
d-aug-cc-pVDZ	0.52730	0.00743	0.00158	0.00044	0.00144	0.00164
d-aug-cc-pVTZ	0.54283	0.00959	0.00172	0.00064	0.00134	0.00141
d-aug-cc-pVQZ	0.54556	0.01006	0.00169	0.00071	0.00121	0.00127
aug-cc-pCVDZ	0.52754	0.00761	0.00170	0.00055	0.00163	0.00177
aug-cc-pCVTZ	0.54260	0.00966	0.00177	0.00071	0.00134	0.00141
aug-cc-pCVQZ	0.54552	0.01008	0.00170	0.00073	0.00123	0.00128

TABLE A.5: Quadrupole Moments (Θ_{zz}) calculated in atomic units for BH using different basis sets. The results except that for FCI are presented as deviations from FCI (method - FCI). ic-MRCCSD calculations are done using (2,4) CAS. Dipole moments for methods other than ic-MRCCSD are obtained from [122]

					ic-MRCCSD	
Basis	FCI	CCSD	CCSD(T)	CCSDT	with $B_{\lambda c}$	without $B_{\lambda c}$
all electrons						
aug-cc-pCVDZ	-2.40215	-0.02231	-0.00550	-0.00238	0.00151	0.00087
valence only						
aug-cc-pVDZ	-2.40371	-0.01974	-0.00574	-0.00263	0.00093	0.00029
aug-cc-pVTZ	-2.32924	-0.02796	-0.00656	-0.00277	0.00128	0.00084
aug-cc-pVQZ	-2.31944	-0.02940	-0.00605	-0.00273	0.00138	0.00096
d-aug-cc-pVDZ	-2.40293	-0.01936	-0.00565	-0.00261	0.00111	0.00040
d-aug-cc-pVTZ	-2.33127	-0.0279	-0.00651	-0.00274	0.00141	0.00097
d-aug-cc-pVQZ	-2.32127	-0.0294	-0.00603	-0.00273	0.00139	0.00097
aug-cc-pCVDZ	-2.40456	-0.01953	-0.0055	-0.00247	0.00137	0.00079
aug-cc-pCVTZ	-2.32595	-0.02795	-0.00636	-0.00266	0.00157	0.00114
aug-cc-pCVQZ	-2.3184	-0.02951	-0.00599	-0.00272	0.00142	0.00101

TABLE A.6: Electric field gradients (q_{zz}) at the Boron nucleus for BH calculated in atomic units using different basis set The results except that for FCI are presented as deviations from FCI (method - FCI). ic-MRCCSD calculations are done using (2,4) CAS. Dipole moments for methods other than ic-MRCCSD are obtained from [122]

					ic-MRCCSD	
Basis	FCI	CCSD	CCSD(T)	CCSDT	with $B_{\lambda c}$	without $B_{\lambda c}$
all electrons						
aug-cc-pCVDZ	0.63342	-0.02231	-0.00550	-0.00238	-0.00081	-0.00108
valence only						
aug-cc-pVDZ	0.61237	-0.00500	-0.00124	-0.00019	-0.00093	-0.00117
aug-cc-pVTZ	0.68153	-0.00608	-0.00127	-0.00021	-0.00090	-0.00117
aug-cc-pVQZ	0.69337	-0.00654	-0.00170	-0.00076	-0.00080	-0.00108
d-aug-cc-pVDZ	0.61332	-0.005	-0.00124	-0.00019	-0.00087	-0.00117
d-aug-cc-pVTZ	0.68165	-0.00609	-0.00127	-0.00022	-0.00090	-0.00117
d-aug-cc-pVQZ	0.69334	-0.00655	-0.0017	-0.00077	-0.00080	-0.00108
aug-cc-pCVDZ	0.63215	-0.00494	-0.00122	-0.00016	-0.00092	-0.00116
aug-cc-pCVTZ	0.64067	-0.00967	-0.00552	-0.00457	-0.00082	-0.00109
aug-cc-pCVQZ	0.66141	-0.00891	-0.00443	-0.00352	-0.00078	-0.00106

TABLE A.7: Energies of the ground state of LiF for different methods using a state averaged CASSCF orbital with CAS of (2e,2o). The energies of Full CI are presented in Hartree where that of all the other methods are presented as difference to FCI energy in microHartree. Energies for the methods other than ic-MRCCSD are obtained form [124].

R in a.u.	Full CI	SRMRCC	MRexpT	ic-MRCCSD
2.95	-107.114140	516	871	1140
3.05	-107.115217	540	946	1225
3.15	-107.114826	564	1019	1316
4.5	-107.063713	784	1816	1777
5.5	-107.024631	719	2120	1866
6.5	-106.994753	640	2235	1841
7.5	-106.972336	614	2243	1804
8.5	-106.955207	617	2217	1771
9.5	-106.941815	621	2221	1770
10	-106.936192	614	2264	1803
10.5	-106.931167	587	2365	1891
11	-106.926697	501	2578	2101
11.25	-106.924684	394	2749	2282
11.5	-106.922864	176	2934	2487
12	-106.920307	2444	2645	2660
12.5	-106.919524	2040	2244	2455
13.7	-106.919261	1950	2021	2109

TABLE A.8: Energies of the excited state of LiF for different methods using a state averaged CASSCF orbital with CAS of (2e,2o). The energies of Full CI are presented in Hartree where that of all the other methods are presented as difference to FCI energy in microHartree. Energies for the methods other than ic-MRCCSD are obtained form [124].

R in a.u.	Full CI	SRMRCC	MRexpT	ic-MRCCSD
2.95	-106.866595	1948	1979	2051
3.05	-106.872691	1968	2006	2071
3.15	-106.877566	1992	2035	2095
4.5	-106.900086	2239	2321	2326
5.5	-106.906181	2272	2365	2323
6.5	-106.911066	2244	2351	2267
7.5	-106.914503	2191	2315	2214
8.5	-106.916581	2148	2284	2177
9.5	-106.917701	2135	2279	2152
10	-106.918019	2150	2294	2143
10.5	-106.918211	2198	2333	2134
11	-106.918269	2345	2424	2122
11.25	-106.918220	-851	2506	2108
11.5	-106.918067	-563	2622	2088
12	-106.916925	325	2685	2466
12.5	-106.914307	674	2121	1616
13.7	-106.907444	759	1215	1366

TABLE A.9: Dipole moments of the ground state of LiF for different methods using a state averaged CASSCF orbital with CAS of (2e,2o). The dipole moments of Full CI are presented in a.u. where that of all the other methods are presented as difference to FCI energy in 10^{-3} a.u. Dipole moments for the methods other than ic-MRCCSD are obtained form [124].

R in a.u.	Full CI	SRMRCC	MRexpT	ic-MRCCSD	
				with $B_\lambda c$	without $B_\lambda c$
2.95	2.631	-14	-9	1	0
3.05	2.718	-15	-8	0	-1
3.15	2.804	-16	-8	0	-1
4.5	3.995	-30	-5	6	2
5.5	4.956	-37	0	15	5
6.5	5.96	-42	2	31	11
7.5	6.978	-48	0	55	20
8.5	7.988	-60	-4	96	36
9.5	8.954	-90	-13	198	77
10	9.39	-131	-25	318	127
10.5	9.739	-233	-59	579	234
11	9.833	-577	-205	1185	462
11.25	9.601	-1058	-474	1587	584
11.5	8.852	-1989	-1236	1520	529
12	3.99	-2474	-2073	-890	515
12.5	0.79	-406	-380	-2151	-250
13.7	0.059	-15	-16	-50	-3

TABLE A.10: Dipole moments of the ground state of LiF for different methods using a state averaged CASSCF orbital with CAS of (2e,2o). The dipole moments of Full CI are presented in a.u. where that of all the other methods are presented as difference to FCI energy in 10^{-3} a.u. Dipole moments for the methods other than ic-MRCCSD are obtained form [124].

R in a.u.	Full CI	SRMRCC	MRexpT	ic-MRCCSD	
				with $B_\lambda c$	without $B_\lambda c$
2.95	-1.445	-8	-9	-6	-7
3.05	-1.437	-8	-9	-7	-7
3.15	-1.427	-8	-10	-7	-8
4.5	-1.134	0	-1	-11	-14
5.5	-0.737	30	29	-3	-10
6.5	-0.323	59	58	8	-6
7.5	-0.016	74	73	16	-8
8.5	0.181	93	87	23	-15
9.5	0.341	143	126	31	-34
10	0.448	212	179	35	-57
10.5	0.632	385	302	39	-105
11	1.065	960	663	24	-248
11.25	1.558	1082	1086	-4	-428
11.5	2.567	2086	1747	-26	-782
12	7.946	2034	1301	-2404	-1368
12.5	11.66	308	97	-785	-307
13.7	13.61	-3	-10	-25	0

TABLE A.11: The values of energy, dipole moment (μ), quadrupole moment(Θ), Electric Field Gradient (q), and isotropic ($A^{K,c}$) and anisotropic ($A^{K,d}$) HFCC obtained for BeH using FCI and ic-MRCCSD methods. ic-MRCCSD has been applied for five different CAS. Results of ic-MRCCSD is given as percentage of error with respect to the FCI results. All these calculations are done using aug-cc-pCVDZ basis and with the Be-H bond-distance being 1.356 Å.

Properties	FCI	ic-MRCCSD				
		(1e,1o)	(3e,3o)	(3e,5o)	(5e,4o)	(5e,6o)
energy	-15.2261015	0.000790	0.000236	0.000163	0.000239	0.000160
μ_z	1.3740248	0.000382	0.000223	0.000378	0.000224	0.000400
Θ_{zz}	8.8616263	0.034369	0.009497	0.015305	0.009607	0.014973
q(Be)	-0.3267027	-0.002329	-0.000275	-0.000537	-0.000269	-0.000516
q(H)	-0.3435008	-0.000221	0.000071	0.000056	0.000074	0.000055
$A^{K,c}$(Be)	2.4843289	0.021964	-0.000727	0.001628	-0.001674	0.000062
$A^{K,c}$(H)	0.3388078	-0.021348	-0.001534	-0.004280	-0.001253	-0.003927
$A^{K,d}$(Be)	0.1165236	0.000161	-0.000107	-0.000236	-0.000105	-0.000222
$A^{K,d}$(H)	0.0204148	0.000170	-0.000013	-0.000034	-0.000016	-0.000037

TABLE A.12: The values of energy, dipole moment (μ), quadrupole moment(Θ), Electric Field Gradient (q), and isotropic ($A^{K,c}$) and anisotropic ($A^{K,d}$) HFCC obtained for BeH using FCI and uncontracted MRCISD methods. MRCISD method is applied for five different CAS. FCI results are presented in a.u. while results of MRCISD are given as errors with respect to the FCI also in a.u.. All these calculations are done using aug-cc-pCVDZ basis with the Be-H bond-distance being 1.356 Å. All electrons are correlated for these calculations.

Properties	FCI	MRCISD				
		(1e,1o)	(3e,3o)	(3e,5o)	(5e,4o)	(5e,6o)
energy	-15.226102	0.001910	0.001065	0.000599	0.001066	0.000598
μ_z	1.374025	-0.001978	-0.004426	-0.004554	-0.004392	-0.004546
Θ_{zz}	8.861626	0.098436	0.046779	0.034674	0.046973	0.034772
q(Be)	-0.326703	-0.005533	-0.001948	-0.001523	-0.001946	-0.001520
q(H)	-0.343501	-0.000515	-0.000077	0.000127	-0.000077	0.000125
$A^{K,c}$(Be)	2.484329	0.047889	-0.004515	0.000116	-0.004528	0.000027
$A^{K,c}$(H)	0.338808	-0.049428	-0.008808	-0.007498	-0.008916	-0.007570
$A^{K,d}$(Be)	0.116524	-0.000136	-0.000188	-0.000127	-0.000201	-0.000138
$A^{K,d}$(H)	0.020415	0.000334	-0.000151	-0.000102	-0.000157	-0.000108

TABLE A.13: Isotropic ($A^{K,c}$) and anisotropic ($A^{K,d}$) hyperfine coupling constants (in MHz) for the ^{2}BO Molecule obtained using EPR-III basis sets.

	^{11}B		^{17}O	
Methods	$A^{K,c}$	$A^{K,d}$	$A^{K,c}$	$A^{K,d}$
CASCI(9e,8o)	966.29	56.23	-23.72	-24.55
CASCI(9e,16o)	920.81	50.58	-12.08	-33.90
DMRG-CASCI(9e,28o)	903.81	49.97	-2.43	-37.69
DMRG-CASCI(13e,30o)	904.59	50.04	-2.94	-37.66
CASSCF(9e,8o)	916.85	53.44	-19.02	-39.60
DMRG-CASSCF(9e,28o)	912.09	48.44	-5.67	-42.14
DMRG-CASSCF(13e,30o)	1018.33	48.87	-11.95	-41.70
B3LYP	1074.79	55.6	-11.66	-42.83
TPSS	990.76	54.07	-5.70	-50.39
BP	989.79	53.68	-7.73	-46.64
CCSD	1041.15	49.75	-11.96	-43.36
ic-MRCCSD(1e,1o)	1027.87	53.95	-15.46	-36.55
ic-MRCCSD(5e,6o)	1018.42	50.42	-14.93	-41.25
expt-gas phase	1027	54	n/a	
expt-Ne matrix	1033	50	-19	-24

TABLE A.14: Isotrpoic ($A^{K,c}$) and anisotropic ($A^{K,d}$) hyperfine coupling constants (in MHz) for the $^2CO^+$ Molecule obtained using EPR-III basis sets.

	^{13}C		^{17}O	
Methods	$A^{K,c}$	$A^{K,d}$	$A^{K,c}$	$A^{K,d}$
CASCI(9e,8o)	1469.96	96.88	7.87	58.28
CASCI(9e,16o)	1450.21	95.68	1.84	60.49
DMRG-CASCI(9e,28o)	1410.98	95.08	19.88	67.83
DMRG-CASCI(13e,30o)	1409.23	95.17	20.01	67.82
CASSCF(9e,8o)	1431.59	92.25	25.37	76.00
DMRG-CASSCF(9e,28o)	1396.59	88.28	26.56	77.46
DMRG-CASSCF(13e,30o)	1492.96	89.18	32.6	77.31
B3LYP	1548.21	100.16	39.73	88.04
TPSS	1444.78	98.52	39.73	94.21
BP	1439.34	100.43	37.39	88.88
CCSD	1557.75	87.26	32.87	85.57
ic-MRCCSD(1e,1o)	1515.57	100.76	26.52	-70.39
ic-MRCCSD(5e,6o)	1498.84	93.02	28.31	-74.81
expt - gas phase	1506	92	n/a	
expt - Ne matrix	1573	98	19	-66

TABLE A.15: Isotrpoic ($A^{K,c}$) and anisotropic ($A^{K,d}$) hyperfine coupling constants (in MHz) for the ^{2}CN Molecule obtained using EPR-III basis sets.

	^{13}C		^{14}N	
Methods	$A^{K,c}$	$A^{K,d}$	$A^{K,c}$	$A^{K,d}$
CASCI(9e,8o)	936.03	124.51	8.78	17.55
CASCI(9e,16o)	767.11	107.85	3.7	27.27
DMRG-CASCI(9e,28o)	700.91	108.69	9.04	31.02
DMRG-CASCI(13e,30o)	685.66	108.74	8.18	31.04
CASSCF(9e,8o)	629.4	102.12	-19.72	35.81
DMRG-CASSCF(9e,28o)	596.48	104.66	-3.42	38.44
DMRG-CASSCF(13e,30o)	561.95	105.82	-20.14	38.55
CASPT2(9e,8o), unrelaxed	692.9	106.0	-15.2	35.0
CASPT2(9e,8o), relaxed	540.3	108.8	-17.9	39.6
B3LYP	572.62	119.86	-18.9	43.31
TPSS	504.83	118.68	-16.35	44.25
BP	494.08	118.94	-13.65	43.16
CCSD	655.27	105.94	-20.03	39.68
CCSD	655.4	106	-20	39.7
CCSD(T)	556.1	113.5	-18.3	38.3
ic-MRCCSD(1e,1o)	599.97	114.04	-17.98	36.31
ic-MRCCSD(5e,6o)	574.10	110.15	-20.16	37.76
expt-Ar matrix	588	90	-13	30

TABLE A.16: Isotrpoic ($A^{K,c}$) and anisotropic ($A^{K,d}$) hyperfine coupling constants (in MHz) for the ^{2}AlO Molecule obtained using EPR-III basis sets.

	^{27}Al		^{17}O	
Methods	$A^{K,c}$	$A^{K,d}$	$A^{K,c}$	$A^{K,d}$
CASCI(9e,8o)	830.31	95.89	9.56	-72.81
CASCI(9e,16o)	765.57	96.64	3.81	-77.54
DMRG-CASCI(9e,21o)	727.98	94.63	-0.71	-85.13
DMRG-CASCI(15e,28o)	670.79	92.73	-2.07	-91.28
DMRG-CASCI(21e,31o)	682.79	92.79	1.57	-90.95
DMRG-CASCI(15e,33o)	702.8	92.83	-3.16	-90.51
DMRG-CASCI(21e,36o)	708.32	92.99	1.61	-90.28
CASSCF(9e,8o)	830.07	95.26	-1.27	-74.6
DMRG-CASSCF(15e,28o)	629.25	106.27	-42.28	-98.4
DMRG-CASSCF(21e,31o)	887.02	105.97	-28.35	-92.94
DMRG-CASSCF(15e,33o)	573.08	109.62	-57.34	111.09
DMRG-CASSCF(21e,36o)	712.65	108.31	-35.04	-104.4
CASPT2(9e,8o), unrelaxed	998.8	106.6	-0.5	68.8
CASPT2(9e,8o), relaxed	788.3	111.6	13.4	105.2
B3LYP	512.21	119.93	8.17	-132.43
TPSS	656.79	112.21	9.52	-119.83
BP	653.71	113.72	14.21	-119.2
CCSD	482.02	114.26	18.14	-127.71
CCSD	482.4	114.3	18.1	-127.7
CCSD(T)	565.3	112.4	19.3	-117.8
ic-MRCCSD(1e,1o)	783.35	114.23	8.20	-97.42
ic-MRCCSD(7e,6o)	672.67	120.97	10.19	-115.94
ic-MRCCSD(7e,7o)	1141.92	127.89	24.85	-76.45
expt - gas phase	738	112		n/a
expt - Ne matrix	766	104	2	-100

B | Data for the second order properties

TABLE B.1: Cartisian coordinates (in Bohr) of the constituent atoms of both p-benzyne and 2,6-pyridyne which are used to calculate different components of polarizability in Sec. 6.3. The same geometry of p-benzyne is also used to calculate excitation energies for several lower lying states.

atom	X	Y	Z
		p-Benzyne	
C	0.00000000	2.53834032	0.00000000
C	0.00000000	-2.53834032	0.00000000
C	2.27766547	1.34784760	0.00000000
C	-2.27766547	1.34784760	0.00000000
C	2.27766547	-1.34784760	0.00000000
C	-2.27766547	-1.34784760	0.00000000
H	4.07134265	2.31692057	0.00000000
H	-4.07134265	2.31692057	0.00000000
H	4.07134265	-2.31692057	0.00000000
H	-4.07134265	-2.31692057	0.00000000
		2,6-Pyridyne	
C	0.0000000000	2.2017045100	-1.2807434100
C	0.0000000000	-2.2017045100	-1.2807434100
C	0.0000000000	1.9177987700	1.2996968800
C	0.0000000000	-1.9177987700	1.2996968800
C	0.0000000000	0.0000000000	-2.7160640300
N	0.0000000000	0.0000000000	2.9393332100
H	0.0000000000	4.0682364900	-2.0947711200
H	0.0000000000	-4.0682364900	-2.0947711200
H	0.0000000000	0.0000000000	-4.7622249800

TABLE B.2: Primary data for the Fig. 6.1a. α_{ZZ} in a.u. of CH_2 for different frequencies(ω) is presented for two different variants of ic-MRCCSD-LR formulation. Description of the variants can be found in Tab. 6.1.

	ic-MRCCSD-LR			ic-MRCCSD-LR	
ω	IIA	IIB	ω	IIA	IIB
0	13.9544	13.9536	0.1723	-427.0383	61.2640
0.02	13.9892	13.9886	0.1724	-617.0246	69.4701
0.04	14.0955	14.0957	0.1725	-953.3864438	81.40033567
0.06	14.2802	14.2821	0.1726	-1633.652813	100.3372059
0.08	14.5563	14.5619	0.1727	-3345.485403	135.0247915
0.1	14.9474	14.9614	0.1728	-9996.921744	219.121478
0.12	15.4979	15.5351	0.17302	-32182.45008	-339.4683968
0.14	16.3048	16.4313	0.17305	-17045.3454	-241.9074716
0.16	17.4895	18.5321	0.1732	-3092.688165	-92.31182522
0.165	17.2161	20.1462	0.1735	-681.5342682	-33.69501506
0.17	3.8909	26.4768	0.174	-191.4161249	-9.737806894
0.171	-20.9322	31.5040	0.175	-45.2872542	3.322684761
0.172	-178.5940	47.1105	0.18	9.017260525	13.38257368
0.1721	-232.2163	50.7068	0.19	15.60156719	16.43197509
0.1722	-309.6344	55.2732	0.2	17.52735606	17.89322098

TABLE B.3: Primary data for the Fig. 6.1b. α_{XX} in a.u. of CH_2 for different frequencies(ω) is presented for two different variants of ic-MRCCSD-LR formulation. Description of the variants can be obtained from Tab. 6.1.

	ic-MRCCSD-LR			ic-MRCCSD-LR	
ω	IIA	IIB	ω	IIA	IIB
0	10.0451	10.0250	0.06246	-433.4673	188.8398
0.02	10.3111	10.3020	0.06248	-488.5536	197.8692
0.03	10.7333	10.7483	0.0625	-553.0958	207.8492
0.04	11.5964	11.6867	0.06252	-629.3134	218.9382
0.05	13.7472	14.2072	0.06255	-772.1298	238.0924
0.055	16.4710	17.9217	0.06258	-962.1833	261.0781
0.058	19.7065	23.8264	0.0626	-1125.8033	279.1388
0.06	22.1470	34.6107	0.0627	-2978.5402	429.6611
0.061	18.6264	48.6131	0.0628	-16349.2321	956.7220
0.0615	6.8924	63.2264	0.0631	-2636.7388	-336.3304
0.062	-45.7603	94.4486	0.0632	-1318.6101	-228.6594
0.0621	-73.3935	105.4970	0.0634	-552.2418	-137.5417
0.0622	-116.1401	119.7952	0.0635	-406.4126	-114.0259
0.0623	-186.0544	139.0245	0.064	-150.0541	-59.4336
0.0624	-309.5038	166.2668	0.065	-53.3594	-27.5024
0.06242	-345.1522	173.1368	0.066	-28.2382	-16.0413
0.06244	-386.1166	180.6313	0.07	-4.9347	-2.3975

TABLE B.4: Primary data for the Fig. 6.1c. α_{ZZ} in a.u. of BH for different frequencies(ω) is presented for two different variants of ic-MRCCSD-LR formulation. Description of the variants can be obtained from Tab. 6.1.

	ic-MRCCSD-LR			ic-MRCCSD-LR	
ω	IIA	IIB	ω	IIA	IIB
0	52.3718	52.3769	0.21	-125.5256	-115.1026
0.02	52.8846	52.8897	0.22	-72.8098	-64.4424
0.04	54.4923	54.4975	0.23	-40.1463	-31.2577
0.06	57.4291	57.4349	0.24	-10.7045	2.0578
0.08	62.1914	62.1996	0.25	42.7496	78.6150
0.1	69.7964	69.8138	0.252	67.4728	124.1223
0.12	82.5192	82.5705	0.254	106.3344	225.8724
0.14	106.5152	106.7172	0.255	123.8902	348.4313
0.16	166.0666	167.3038	0.256	2.5383	694.6208
0.17	247.8339	252.3910	0.257	-77144.6381	8930.8541
0.175	339.2877	350.5792	0.2574	-8633.6282	-2533.1327
0.18	559.0026	602.1281	0.2575	-5332.6687	-1924.9429
0.182	764.9251	863.5473	0.2576	-3701.1653	-1554.0680
0.184	1204.6327	1565.7650	0.2577	-2765.1430	-1304.2690
0.185	1563.5484	2685.5531	0.2578	-2172.8467	-1124.5655
0.186	-6125.6011	9861.8956	0.258	-1484.2222	-883.2629
0.187	-11445.9384	-5733.3291	0.259	-526.5884	-433.2267
0.188	-3083.1013	-2196.3245	0.26	-313.1093	-291.6278
0.189	-1702.5227	-1348.6370	0.262	-174.5704	-180.3266
0.19	-1160.8764	-967.8542	0.265	-107.1666	-117.2799
0.195	-428.3488	-386.8474	0.27	-65.5924	-74.7188
0.2	-251.5149	-231.1584	0.28	-31.9060	-39.2783

TABLE B.5: Primary data for the Fig. 6.2a. α_{ZZ} in a.u. of CH_2 for different frequencies(ω) is presented for two different variants of ic-MRCCSD-LR formulation. Description of the variants can be obtained from Tab. 6.1.

	ic-MRCCSD-LR			ic-MRCCSD-LR	
ω	IB	IIB	ω	IB	IIB
0	13.9531	13.9536	0.1724	70.8793	69.4701
0.02	13.9880	13.9886	0.1725	83.5389	81.4003
0.04	14.0952	14.0957	0.1726	103.9448	100.3372
0.06	14.2815	14.2821	0.1727	142.3141	135.0248
0.08	14.5613	14.5619	0.1728	240.6577	219.1215
0.1	14.9608	14.9614	0.1729	981.8351	719.6413
0.12	15.5345	15.5351	0.173	-337.8066	-459.0608
0.14	16.4305	16.4313	0.17302	-271.3824	-339.4684
0.16	18.5320	18.5321	0.17305	-205.9101	-241.9075
0.165	20.1488	20.1462	0.1732	-85.8231	-92.3118
0.17	26.5153	26.4768	0.1735	-32.2678	-33.6950
0.171	31.6011	31.5040	0.174	-9.3255	-9.7378
0.172	47.5611	47.1105	0.175	3.4393	3.3227
0.1721	51.2757	50.7068	0.18	13.3956	13.3826
0.1722	56.0121	55.2732	0.19	16.4352	16.4320
0.1723	62.2596	61.2640	0.2	17.8949	17.8932

TABLE B.6: Primary data for the Fig. 6.2b. α_{XX} in a.u. of CH_2 for different frequencies(ω) is presented for two different variants of ic-MRCCSD-LR formulation. Description of the variants can be obtained from Tab. 6.1.

	ic-MRCCSD-LR			ic-MRCCSD-LR	
ω	IB	IIB	ω	IB	IIB
0	10.0145	10.0250	0.06242	211.7983	173.1368
0.02	10.2922	10.3020	0.06244	222.9179	180.6313
0.03	10.7402	10.7483	0.06246	235.2837	188.8398
0.04	11.6839	11.6867	0.06248	249.1122	197.8692
0.05	14.2311	14.2072	0.0625	264.6723	207.8492
0.055	18.0184	17.9217	0.06252	282.3011	218.9382
0.058	24.1201	23.8264	0.06255	313.5945	238.0924
0.06	35.5226	34.6107	0.06258	352.5588	261.0781
0.061	50.8267	48.6131	0.0626	384.2559	279.1388
0.0615	67.3999	63.2264	0.0627	685.6074	429.6611
0.062	104.8706	94.4486	0.0628	2272.2924	956.7220
0.0621	118.8036	105.4970	0.063	-57.2972	-623.3798
0.0622	137.3584	119.7952	0.0631	-166.3359	-336.3304
0.0623	163.2438	139.0245	0.0632	-147.9040	-228.6594
0.0624	201.7486	166.2668	0.0634	-106.7427	-137.5417

TABLE B.7: Primary data for the Fig. 6.2c. α_{ZZ} in a.u. of BH for different frequencies(ω) is presented for two different variants of ic-MRCCSD-LR formulation. Description of the variants can be obtained from Tab. 6.1.

	ic-MRCCSD-LR			ic-MRCCSD-LR	
Frequency	IB	IIB	Frequency	LR-IB	IIB
0	52.4774	52.3769	0.195	-377.6576	-386.8474
0.02	52.9923	52.8897	0.2	-227.5920	-231.1584
0.04	54.6068	54.4975	0.21	-113.9896	-115.1026
0.06	57.5572	57.4349	0.22	-63.9277	-64.4424
0.08	62.3448	62.1996	0.23	-30.9750	-31.2577
0.1	70.0002	69.8138	0.24	2.2204	2.0578
0.12	82.8394	82.5705	0.25	78.6815	78.6150
0.14	107.1888	106.7172	0.252	124.1700	124.1223
0.16	168.5595	167.3038	0.254	225.9388	225.8724
0.17	255.4223	252.3910	0.255	348.6232	348.4313
0.175	356.6443	350.5792	0.256	695.7608	694.6208
0.18	620.7913	602.1281	0.257	9211.8944	8930.8541
0.182	902.6622	863.5473	0.2573	-3659.4675	-3713.6966
0.184	1696.9635	1565.7650	0.2574	-2506.9919	-2533.1327
0.185	3075.6074	2685.5531	0.2575	-1909.3124	-1924.9429
0.186	15180.8786	9861.8956	0.2576	-1543.5251	-1554.0680
0.1865	14761.9168	-27863.5203	0.2577	-1296.5885	-1304.2690
0.1866	-2108.5234	-15749.2511	0.2578	-1118.6632	-1124.5655
0.1867	-4342.8961	-10970.8366	0.258	-879.3786	-883.2629
0.1868	-4510.5526	-8413.5114	0.259	-431.9742	-433.2267
0.1869	-4252.5502	-6820.7073	0.26	-290.8989	-291.6278
0.187	-3916.5932	-5733.3291	0.262	-179.9072	-180.3266
0.188	-1926.5659	-2196.3245	0.265	-116.9955	-117.2799
0.189	-1245.6937	-1348.6370	0.27	-74.5063	-74.7188
0.19	-914.1725	-967.8542	0.28	-39.0978	-39.2783

TABLE B.8: Primary data for Fig. 6.5a. XX component of polarizability (α_{XX}) in a.u. for the ground state of *p*-Benzyne is calculated for a range of frequencies(ω) using CCSD, Mk-MRCCSD and ic-MRCCSSD. The aug-cc-pCVTZ basis set is used for all the calculations and an active space of (2e,2o) is used for multireference calculations.

CCSD				Mk-MRCCSD				ic-MRCCSD			
ω	α_{XX}	ω	α_{XX}	ω	α_{XX}	ω	α_{XX}	ω	α_{XX}	ω	α_{XX}
0	79.661	0.198	55.667	0	79.552	0.176	103.797	0	79.062	0.194	138.540
0.02	79.589	0.2	83.194	0.02	79.752	0.18	106.041	0.02	79.263	0.195	166.995
0.04	80.463	0.204	99.058	0.04	80.369	0.186	110.462	0.04	79.877	0.197	43.385
0.06	81.503	0.21	109.017	0.06	81.408	0.189	113.645	0.06	80.934	0.198	78.667
0.08	83.039	0.22	121.103	0.08	82.952	0.192	118.475	0.08	82.492	0.199	90.257
0.1	85.167	0.226	129.09	0.09	83.938	0.194	123.619	0.1	84.648	0.2	96.262
0.12	88.052	0.232	138.972	0.1	85.087	0.196	129.854	0.12	87.558	0.205	108.389
0.14	91.995	0.236	147.373	0.11	86.422	0.197	136.857	0.14	91.495	0.21	114.617
0.16	97.675	0.24	158.176	0.12	87.968	0.1975	140.318	0.16	97.011	0.22	125.796
0.17	101.745	0.242	164.931	0.13	89.765			0.18	105.945	0.23	139.762
0.18	107.83	0.244	172.991	0.14	91.864			0.19	116.763	0.24	160.961
0.185	112.938	0.246	182.853	0.149	94.073			0.191	119.275	0.245	177.176
0.19	123.523	0.248	195.31	0.158	96.673			0.192	122.787	0.25	201.122
0.193	143.66			0.167	99.813			0.193	128.266		

TABLE B.9: Primary data for Fig. 6.5b. YY component of polarizability (α_{YY}) in a.u. for the ground state of *p*-Benzyne is calculated for a range of frequencies(ω) using CCSD, Mk-MRCCSD and ic-MRCCSSD. The aug-cc-pCVDZ basis set is used for all the calculations and an active space of (2e,2o) is used for multireference calculations.

CCSD				Mk-MRCCSD				ic-MRCCSD			
ω	α_{YY}	ω	α_{YY}	ω	α_{YY}	ω	α_{YY}	ω	α_{YY}	ω	α_{YY}
0	85.359	0.175	95.375	0	73.113	0.178	91.573	0	78.413	0.15	1803.270
0.02	85.667	0.18	100.654	0.02	73.203	0.179	98.196	0.02	78.711	0.151	-369.783
0.04	86.62	0.185	105.612	0.04	73.455	0.18	101.601	0.04	79.638	0.152	-111.566
0.06	88.322	0.19	110.639	0.06	73.791	0.183	106.423	0.06	81.303	0.153	-38.368
0.08	91.011	0.197	118.414	0.08	73.981	0.186	108.954	0.08	83.957	0.155	16.708
0.1	95.242	0.204	128.104	0.09	73.825	0.189	110.903	0.1	88.208	0.16	57.189
0.11	98.367	0.209	137.46	0.1	73.225	0.192	112.698	0.12	96.055	0.17	79.955
0.12	102.795	0.22	192.363	0.105	72.604	0.196	115.121	0.13	103.952	0.18	91.112
0.125	105.886	0.222	237.869	0.11	71.605	0.2	117.738	0.135	110.961	0.2	111.035
0.13	110.056			0.115	69.98	0.203	119.901	0.14	123.852	0.21	124.725
0.135	116.24			0.12	67.236	0.206	122.28	0.142	133.025	0.22	146.448
0.14	127.056			0.125	62.241	0.209	124.929	0.144	147.794		
0.147	181.812			0.13	51.704	0.212	127.902	0.145	159.284		
0.155	14.706			0.133	38.121	0.215	131.28	0.146	176.107		
0.16	64.808			0.136	6.157	0.218	135.166	0.147	203.236		
0.165	80.453			0.139	-152.519	0.22	138.111	0.148	254.645		
0.17	89.124			0.177	71.865			0.149	390.410		

TABLE B.10: Primary data for Fig. 6.5c. ZZ component of polarizability (α_{ZZ}) in a.u. for the ground state of *p*-Benzyne is calculated for a range of frequencies(ω) using the CCSD, Mk-MRCCSD and ic-MRCCSSD methods. The aug-cc-pCVDZ basis set is used for all the calculations and an active space of (2e,2o) is used for multireference calculations.

CCSD				Mk-MRCCSD				ic-MRCCSD			
ω	α_{ZZ}	ω	α_{ZZ}	ω	α_{ZZ}	ω	α_{ZZ}	ω	α_{ZZ}	ω	α_{ZZ}
0	42.631	0.228	56.1	0	42.498	0.183	46.076	0	42.493	0.175	47.615
0.02	42.701	0.236	59.156	0.02	42.567	0.186	48.002	0.02	42.568	0.18	48.461
0.04	42.912	0.242	61.858	0.04	42.779	0.192	49.864	0.04	42.795	0.185	49.259
0.06	43.272	0.248	65.29	0.06	43.141	0.197	50.98	0.06	43.188	0.19	50.055
0.08	43.797	0.252	68.279	0.08	43.67	0.203	52.253	0.08	43.772	0.195	50.877
0.1	44.511	0.258	74.814	0.1	44.393	0.209	53.628	0.1	44.600	0.2	51.748
0.12	45.45	0.262	82.062	0.11	44.841	0.215	55.288	0.12	45.810	0.21	53.718
0.14	46.681	0.265	91.179	0.12	45.358	0.22	57.202	0.13	46.700	0.22	56.166
0.16	48.324	0.268	108.888	0.13	45.958	0.223	58.992	0.135	47.303	0.23	59.463
0.18	50.689	0.27	135.987	0.14	46.665	0.225	60.984	0.14	48.134	0.24	64.544
0.19	52.49			0.149	47.429	0.227	65.266	0.142	48.584		
0.195	53.821			0.158	48.4	0.228	70.893	0.144	49.156		
0.2	56.014			0.164	49.286	0.229	93.903	0.145	49.511		
0.204	60.264			0.17	50.747	0.231	41.493	0.146	49.932		
0.206	67.046			0.173	52.245	0.232	48.65	0.148	51.089		
0.207	77.63			0.176	56.749	0.234	53.635	0.15	53.111		
0.208	200			0.1765	58.787	0.238	57.57	0.152	57.897		
0.2088	-10			0.177	62.243	0.243	60.794	0.154	88.702		
0.21	33.817			0.1775	69.478	0.248	64.078	0.156	24.291		
0.213	47.21			0.178	94.663	0.253	68.175	0.158	38.452		
0.216	50.582			0.1787	-15.951	0.258	74.134	0.16	42.030		
0.22	52.926			0.179	19.382	0.262	81.87	0.165	45.199		
0.224	54.605			0.18	38.346	0.266	96.913	0.17	46.621		

TABLE B.11: Primary data for Fig. 6.5d. XX component of polarizability (α_{XX}) in a.u. for the ground state of 2,6-pyridyne is calculated for a range of frequencies(ω) using CCSD, Mk-MRCCSD and ic-MRCCSSD. The aug-cc-pCVDZ basis set is used for all the calculations and an active space of (2e,2o) is used for multireference calculations.

CCSD				Mk-MRCCSD				ic-MRCCSD			
ω	α_{XX}	ω	α_{XX}	ω	α_{XX}	ω	α_{XX}	ω	α_{XX}	ω	α_{XX}
0	39.358	0.155	34.413	0	39.121	0.148	50.026	0	39.031	0.146	-53.199
0.02	39.448	0.16	36.656	0.02	39.201	0.15	56.693	0.02	39.116	0.148	12.603
0.04	39.731	0.17	39.146	0.04	39.447	0.153	107.925	0.04	39.382	0.15	24.121
0.06	40.255	0.18	40.792	0.06	39.889	0.157	14.889	0.06	39.868	0.155	32.773
0.08	41.151	0.19	42.196	0.08	40.595	0.16	28.084	0.08	40.673	0.16	35.893
0.1	42.891	0.2	43.573	0.09	41.095	0.162	31.481	0.1	42.125	0.18	40.686
0.105	43.659	0.21	45.05	0.1	41.753	0.165	34.39	0.11	43.493	0.2	43.619
0.11	44.765	0.22	46.753	0.11	42.677	0.17	37.049	0.12	46.710	0.22	46.975
0.115	46.619	0.228	48.403	0.118	43.789	0.18	39.844	0.122	48.232	0.24	52.548
0.12	51.055	0.234	49.931	0.122	44.597	0.19	41.662	0.124	50.957	0.25	59.423
0.122	55.979	0.24	51.909	0.126	45.747	0.2	43.233	0.125	53.468		
0.124	74.376	0.248	56.461	0.13	47.65	0.206	44.167	0.126	58.170		
0.126	-18.138	0.252	62.716	0.133	50.461	0.212	45.14	0.13	30.047		
0.127	20.434			0.135	54.619	0.218	46.185	0.132	38.861		
0.13	37.628			0.136	59.08	0.224	47.342	0.135	43.997		
0.135	46.131			0.137	68.754	0.23	48.666	0.137	46.901		
0.14	65.189			0.14	28.005	0.236	50.249	0.14	53.353		
0.142	137.934			0.142	37.901	0.242	52.293	0.142	63.221		
0.144	-19.854			0.144	42.502	0.246	54.211	0.144	105.221		
0.15	29.7			0.145	44.267	0.25	57.81	0.145	496.072		

TABLE B.12: Primary data for Fig. 6.5e. YY component of polarizability (α_{YY}) in a.u. for the ground state of 2,6-pyridyne is calculated for a range of frequencies(ω) using CCSD, Mk-MRCCSD and ic-MRCCSSD. The aug-cc-pCVDZ basis set is used for all the calculations and an active space of (2e,2o) is used for multireference calculations.

CCSD				Mk-MRCCSD				ic-MRCCSD			
ω	α_{YY}	ω	α_{YY}	ω	α_{YY}	ω	α_{YY}	ω	α_{YY}	ω	α_{YY}
0	77.578	0.17	98.466	0	72.529	0.168	84.018	0	74.557	0.15	76.474
0.02	77.88	0.176	109.864	0.02	72.761	0.17	88.271	0.02	74.851	0.16	86.106
0.04	78.834	0.18	124.386	0.04	73.492	0.172	98.183	0.04	75.777	0.17	98.584
0.06	80.619	0.184	161.028	0.06	74.861	0.173	111.328	0.06	77.501	0.175	110.183
0.08	83.725	0.195	32.438	0.08	77.267	0.1735	125.494	0.08	80.470	0.18	137.896
0.09	86.188	0.2	59.94	0.09	79.228	0.18	14.129	0.1	86.241	0.181	149.685
0.1	89.918	0.203	68.109	0.1	82.348	0.1815	55.408	0.11	92.305	0.182	167.253
0.105	92.699	0.205	72.253	0.11	88.714	0.182	71.548	0.115	97.896	0.183	196.491
0.11	96.702	0.207	75.782	0.115	96.027	0.184	72.688	0.12	108.747	0.184	255.431
0.115	103.235	0.21	80.358	0.118	105.046	0.187	73.031	0.123	122.968	0.185	438.708
0.12	116.723	0.215	87.049	0.12	116.784	0.19	71.45	0.125	143.215	0.186	-5622.723
0.122	127.707	0.22	93.688	0.122	143.446	0.193	65.182	0.126	162.561	0.187	-231.186
0.124	148.468	0.224	100.042	0.134	54.745	0.195	52.009	0.127	199.085	0.188	-77.383
0.126	203.971	0.228	110.189	0.135	57.151	0.196	28.49	0.128	294.748	0.189	-23.865
0.13	-84.626	0.232	159.865	0.138	62.436	0.198	127.201	0.129	1228.201	0.19	3.499
0.135	44.175	0.234	-1.52	0.141	65.928	0.199	108.724	0.13	-255.483	0.195	51.255
0.14	63.678	0.236	76.561	0.145	69.227	0.2	101.586	0.131	-64.467	0.2	66.888
0.142	67.823	0.238	90.746	0.15	72.292	0.201	118.54	0.132	-11.079	0.21	82.780
0.144	71.103	0.24	98.138	0.153	73.862	0.202	150.926	0.133	14.141	0.22	95.533
0.15	78.302	0.244	108.365	0.157	75.859			0.135	38.652	0.23	120.137
0.155	83.001	0.248	118.023	0.16	77.418			0.14	61.106	0.25	127.542
0.16	87.482	0.252	131.149	0.165	80.707			0.145	70.483		

TABLE B.13: Primary data for Fig. 6.5f. ZZ component of polarizability (α_{ZZ}) in a.u. for the ground state of 2,6-pyridyne is calculated for a range of frequencies(ω) using CCSD, Mk-MRCCSD and ic-MRCCSSD. The aug-cc-pCVDZ basis set is used for all the calculations and an active space of (2e,2o) is used for multireference calculations.

CCSD				Mk-MRCCSD				ic-MRCCSD			
ω	α_{ZZ}	ω	α_{ZZ}	ω	α_{ZZ}	ω	α_{ZZ}	ω	α_{ZZ}	ω	α_{ZZ}
0	70.998	0.207	-11.593	0	70.839	0.2	33.766	0	70.267	0.1818	115.772
0.02	71.171	0.21	80.223	0.02	71.009	0.201	52.043	0.02	70.440	0.182	135.925
0.04	71.701	0.215	96.739	0.04	71.53	0.202	69.831	0.04	70.967	0.183	80.062
0.06	72.613	0.22	104.164	0.06	72.427	0.204	75.502	0.06	71.875	0.184	87.897
0.08	73.956	0.224	109.118	0.08	73.744	0.207	83.46	0.08	73.211	0.185	90.425
0.1	75.81	0.228	114.147	0.09	74.583	0.209	92.766	0.1	75.058	0.19	95.478
0.12	78.306	0.232	119.94	0.1	75.559	0.211	103.943	0.12	77.547	0.195	99.529
0.13	79.857			0.11	76.687	0.213	115.474	0.14	80.907	0.2	105.267
0.14	81.663			0.12	77.989	0.216	136.89	0.16	85.621	0.205	120.562
0.15	83.782			0.135	80.331			0.17	88.929	0.206	129.885
0.16	86.304			0.15	83.261			0.175	91.217	0.207	151.503
0.17	89.379			0.16	85.646			0.176	91.809	0.208	272.048
0.18	93.31			0.17	88.501			0.177	92.496	0.209	-24.856
0.19	98.964			0.18	92.049			0.178	93.338	0.21	56.127
0.195	103.443			0.19	97.321			0.179	94.471	0.211	74.701
0.2	112.005			0.192	100.133			0.18	96.271	0.212	83.255
0.203	126.578			0.194	108.404			0.181	100.340	0.215	94.598
0.205	171.843			0.195	125.277			0.1812	102.004	0.22	103.217

TABLE B.14: Primary data for Figure 6.4. These data represent the $\alpha_{||}$ of BH calculated using TZP basis set. An active space of (2e,2o) are used for the multireference calculations where all electrons are correlated for all the calculations. The value in the bracket for the ic-MRCCSD result at static limit is the polarizability obtained without using any approximation, i.e. the variant IA of the formulations.

Frequency	FCI	CCSD	Mk-MRCCSD	ic-MRCCSD
0	52.568	55.633	52.362	52.377 (52.496)
0.02	53.081	56.184	52.686	52.890
0.04	54.691	57.912	54.023	54.497
0.06	57.631	61.067	56.552	57.435
0.08	62.401	66.184	60.657	62.200
0.1	70.022	74.35	67.089	69.814
0.11	75.562	80.237	71.625	75.312
0.12	82.794	87.994	77.43	82.570
0.13	92.729	98.553	85.024	92.485
0.14	107.01	113.63	97.379	106.717
0.15	129.175	136.75	114.883	128.746
0.16	168.192	176.513	152.008	167.304

C | Data for the excitation energies

TABLE C.1: Energy of the 1^1A_1 state of CH_2 for different H–C–H angles, using the cc-pVDZ basis set and a C–H bond length fixed at 2.11 a_0. The FCI energies are given in E_h, the remaining data is given as error with respect to FCI in mE_h. In the linear response calculations, the initial state is 1^3B_1.

Angle / deg.	FCI[1]	CAS(2,2)			CAS(6,6)			
		Mk-MRCCSD[1]	ic-MRCCSD	ic-MRCCSD-LR	ic-MRCCSD		ic-MRCCSD-LR	
					$\eta = 10^{-5}$	$\eta = 10^{-4}$	$\eta = 10^{-5}$	$\eta = 10^{-4}$
70	−38.998453	2.835	2.552	2.604	0.463	0.491	0.338	0.187
80	−39.013324	2.611	2.385	2.430	0.438	0.497	0.290	0.173
90	−39.021995	2.415	2.269	2.304	0.409	0.481	0.220	0.156
95	−39.024215	2.326	2.232	2.258	0.393	0.466	0.165	0.146
97	−39.024732	2.291	2.220	2.242	0.388	0.462	0.149	0.143
103	−39.025076	2.189	2.198	2.204	0.390	0.455	0.084	0.140
105	−39.024806	2.155	2.193	2.194	0.391	0.454	0.075	0.142
110	−39.023346	2.069	2.191	2.173	0.396	0.456	0.056	0.153
120	−39.017435	1.882	2.213	2.146	0.404	0.471	0.055	0.196
130	−39.008459	1.674	2.269	2.139	0.399	0.500	0.118	0.225
140	−38.997904	1.548	2.341	2.156	0.385	0.537	0.210	0.273
150	−38.987759	1.980	2.295	2.204	0.437	0.576	0.323	0.351
160	−38.980214	2.015	2.266	2.275	0.535	0.597	0.456	0.434
170	−38.976333	2.050	2.244	2.327	0.570	0.827	0.554	0.555
NPE (mE_h)		1.287	0.361	0.465	0.184	0.373	0.499	0.415

[1] Ref. [85], calculations performed by F. A. Evangelista.

TABLE C.2: Energy of the 1^3B_1 state of CH_2 for different H–C–H angles, using the cc-pVDZ basis set and a C–H bond length fixed at 2.11 a_0. The FCI energies are given in E_h, the remaining data is given as error with respect to FCI in mE_h. In the linear response calculations, the initial state is 1^1A_1.

Angle / deg.	FCI[1]	CAS(2,2)			CAS(6,6)			
		Mk-MRCCSD[1]	ic-MRCCSD	ic-MRCCSD-LR	ic-MRCCSD		ic-MRCCSD-LR	
		$M_s = 1$	$M_s = 0$		$\eta = 10^{-5}$	$\eta = 10^{-4}$	$\eta = 10^{-5}$	$\eta = 10^{-4}$
70	−38.963528	2.879	2.841	3.262	0.498	0.499	0.673	0.620
80	−38.990182	2.692	2.644	2.995	0.483	0.491	0.694	0.607
90	−39.010627	2.550	2.497	2.814	0.474	0.490	0.690	0.605
95	−39.018765	2.497	2.443	2.755	0.472	0.489	0.666	0.607
97	−39.021656	2.479	2.426	2.737	0.471	0.488	0.652	0.609
103	−39.029136	2.434	2.384	2.700	0.468	0.486	0.574	0.662
105	−39.031246	2.423	2.373	2.692	0.467	0.486	0.543	0.667
110	−39.035724	2.400	2.354	2.684	0.464	0.484	0.483	0.676
120	−39.041504	2.378	2.342	2.705	0.461	0.483	0.370	0.677
130	−39.043576	2.381	2.362	2.764	0.461	0.481	0.410	0.667
140	−39.042695	2.406	2.412	2.898	0.471	0.482	0.443	0.665
150	−39.039812	2.449	2.489	3.168	0.478	0.491	0.476	0.607
160	−39.036138	2.503	2.587	3.216	0.496	0.500	0.379	0.537
170	−39.033074	2.554	2.679	3.304	0.497	0.559	0.080	0.891
NPE (mE_h)		0.501	0.499	0.620	0.037	0.078	0.614	0.354

[1] Ref. [85], calculations performed by F. A. Evangelista.

D | Publications

Publications Resulting from this Work

[**P1**] *Excited states with internally contracted multireference coupled-cluster linear response theory*
P. K. Samanta, D. Mukherjee, M. Hanauer and A. Köhn, J. Chem. Phys. **140**, 134108 (2014).

[**P2**] *Study of first order properties using internally contracted multireference coupled cluster theory*
P. K. Samanta and A. Köhn, *manuscript under preparation.*

[**P3**] *Static and Dynamic Second-Order Properties using Internally Contracted multireference Coupled-Cluster Linear Response*
P. K. Samanta and A. Köhn, *manuscript under preparation.*

Further Publications

- *Unitary group adapted state specific multireference perturbation theory: Formulation and pilot applications*
  A. Sen, S. Sen, P. K. Samanta and D. Mukherjee, J. Comp. Chem. **36**, 670 (2015).
- *Quantum tunneling during interstellar surface-catalyzed formation of water: the reaction $H + H_2O_2 = H_2O + OH$*
  T. Lamberts, P. K. Samanta, A. Köhn and J. Kästner, Phys. Chem. Chem. Phys. **18**, 33021, 2016.

Bibliography

[1] A. Szabo and N. S. Ostlund. *Modern Quantum Chemistry: Introduction to Advanced Electronic Structure Theory*. Dover Publications, Mineola, 1989.

[2] I. Shavitt and R. J. Bartlett. *Many-Body Methods in Chemistry and Physics: MBPT and Coupled-Cluster Theory*. Cambridge University Press, New York, 2009.

[3] J. Čížek, J. Chem. Phys. **45**, 4256 (1966).

[4] T. D. Crawford and H. F. Schaefer III. *An Introduction to Coupled Cluster Theory for Computational Chemists*, in *Reviews in Computational Chemistry*, edited by K. B. Lipkowitz and D. B. Boyd, volume 14, pp. 33–136. Wiley, New York, 2000.

[5] R. J. Bartlett and M. Musiał, Rev. Mod. Phys. **79**, 291 (2007).

[6] B. O. Roos, Adv. Chem. Phys. **69**, 399 (1987).

[7] B. O. Roos, K. Andersson, M. P. Fülscher, P.-Å. Malmqvist, L. Serrano-Andrés, K. Pierloot and M. Merchán, Adv. Chem. Phys. **93**, 219 (1996).

[8] H.-J. Werner, Adv. Chem. Phys. **69**, 1 (1987).

[9] P. G. Szalay, T. Müller, G. Gidofalvi, H. Lischka and R. Shepard, Chem. Rev. **112**, 108 (2012).

[10] D. I. Lyakh, M. Musiał, V. F. Lotrich and R. J. Bartlett, Chem. Rev. **112**, 182 (2012).

[11] A. Köhn, M. Hanauer, L. A. Mück, T.-C. Jagau and J. Gauss, WIREs Comput. Mol. Sci. **3**, 176 (2013).

[12] D. Mukherjee, R. K. Moitra and A. Mukhopadhyay, Mol. Phys. **33**, 955 (1977).

[13] M. A. Haque and D. Mukherjee, J. Chem. Phys. **80**, 5058 (1984).

[14] B. Jeziorski and H. J. Monkhorst, Phys. Rev. A. **24**, 1668 (1981).

[15] A. Banerjee and J. Simons, Int. J. Quantum Chem. **19**, 207 (1981).

[16] U. S. Mahapatra, B. Datta, B. Bandyopadhyay and D. Mukherjee, Adv. Quantum Chem. **30**, 163 (1998).

[17] F. A. Evangelista and J. Gauss, J. Chem. Phys. **134**, 114102 (2011).

[18] M. Hanauer and A. Köhn, J. Chem. Phys. **134**, 204111 (2011).

[19] U. S. Mahapatra, B. Datta and D. Mukherjee, J. Chem. Phys. **110**, 6171 (1999).

[20] M. Hanrath, J. Chem. Phys. **123**, 084102 (2005).

[21] A. Banerjee and J. Simons, J. Chem. Phys. **76**, 4548 (1982).

[22] A. Banerjee and J. Simons, Chem. Phys. **87**, 215 (1984).

[23] D. Mukherjee, Chem. Phys. Lett. **274**, 561 (1997).

[24] D. Mukherjee. *A Coupled Cluster Approach to the Electron Correlation Problem Using a Correlated Reference State*, in *Recent Progress in Many-Body Theories*, edited by E. Schachinger, H. Mitter and H. Sormann, volume 4, pp. 127–133. Plenum Press, New York, 1995.

[25] M. Hanauer and A. Köhn, J. Chem. Phys. **136**, 204107 (2012).

[26] W. Liu, M. Hanauer and A. Köhn, Chem. Phys. Lett. **565**, 122 (2013).

[27] J. A. Pople, J. W. McIver Jr and N. S. Ostlund, J. Chem. Phys. **49**, 2965 (1968).

[28] R. J. Bartlett and G. D. Purvis, Phys. Rev. A. **20**, 1313 (1979).

[29] G. D. Purvis and R. J. Bartlett, Phys. Rev. A. **23**, 1594 (1981).

[30] G. H. F. Diercksen, B. O. Roos and A. J. Sadlej, Chem. Phys. **59**, 29 (1981).

[31] P. Pulay, Mol. Phys. **17**, 197 (1969).

[32] H. J. Monkhorst, Int. J. Quantum Chem. **S11**, 421 (1977).

[33] E. Dalgaard and H. Monkhorst, Phys. Rev. A. **28** (1983).

[34] L. Adamowicz, W. Laidig and R. J. Bartlett, Int. J. Quantum Chem. **254**, 245 (1984).

[35] E. A. Salter, G. W. Trucks and R. J. Bartlett, J. Chem. Phys. **90**, 1752 (1989).

[36] A. C. Scheiner, G. E. Scuseria, J. E. Rice, T. J. Lee and H. F. Schaefer, J. Chem. Phys. **87**, 5361 (1987).

[37] T. J. Lee and A. P. Rendell, J. Chem. Phys. **94**, 6229 (1991).

[38] J. Gauss and J. F. Stanton, Phys. Chem. Chem. Phys. **2**, 2047 (2000).

[39] J. Gauss and J. F. Stanton, J. Chem. Phys. **116**, 1773 (2002).

[40] M. Kállay, J. Gauss and P. G. Szalay, J. Chem. Phys. **119**, 2991 (2003).

[41] G. Fitzgerald, R. Harrison, W. D. Laidig and R. J. Bartlett, J. Chem. Phys. **82**, 4379 (1985).

[42] J. Gauss and D. Cremer, Chem. Phys. Lett. **138**, 131 (1987).

[43] J. Gauss and D. Cremer, Chem. Phys. Lett. **153**, 303 (1988).

[44] G. W. Trucks, J. D. Watts, E. A. Salter and R. J. Bartlett, Chem. Phys. Lett. **153**, 490 (1988).

[45] G. W. Trucks, E. A. Salter, C. Sosa and R. J. Bartlett, Chem. Phys. Lett. **147**, 359 (1988).

[46] R. Krishnan, H. B. Schlegel and J. a. Pople, J. Chem. Phys. **72**, 4654 (1980).

[47] B. R. Brooks, W. D. Laidig, P. Saxe, J. D. Goddard, Y. Yamaguchi and H. F. Schaefer, J. Chem. Phys. **72**, 4652 (1980).

[48] J. Gauss and D. Cremer, Chem. Phys. Lett. **150**, 280 (1988).

[49] J. Gauss and D. Cremer, Chem. Phys. Lett. **163**, 549 (1989).

[50] H. Koch, H. Jensen, P. Jørgensen, T. Helgaker, G. E. Scuseria and H. F. Schaefer, J. Chem. Phys. **92**, 4924 (1990).

[51] R. Kobayashi, H. Koch and P. Jørgensen, J. Chem. Phys. **101**, 4956 (1994).

[52] H. Koch and P. Jørgensen, J. Chem. Phys. **93**, 3333 (1990).

[53] O. Christiansen, P. Jørgensen and C. Hättig, Int. J. Quantum Chem. **68**, 1 (1998).

[54] E. A. Salter, H. Sekino and R. J. Bartlett, J. Chem. Phys. **87**, 502 (1987).

[55] J. Noga and M. Urban, Theo. Chim. Acta. **73**, 291 (1988).

[56] M. Medved, M. Urban and J. Noga, Theor Chem Acc. **98**, 75 (1997).

[57] T. Korona and B. Jeziorski, J. Chem. Phys. **125** (2006).

[58] G. H. Diercksen, B. O. Roos and A. J. Sadlej, Chem. Phys. **59**, 29 (1981).

[59] P. G. Szalay, Int. J. Quantum Chem. **55**, 151 (1995).

[60] J. Pittner and J. Šmydke, J. Chem. Phys. **127** (2007).

[61] E. Prochnow, F. A. Evangelista, H. F. Schaefer III, W. D. Allen and J. Gauss, J. Chem. Phys. **131**, 064109 (2009).

[62] T.-C. Jagau, E. Prochnow, F. A. Evangelista and J. Gauss, J. Chem. Phys. **132**, 144110 (2010).

[63] S. Chattopadhyay, U. S. Mahapatra and D. Mukherjee, J. Chem. Phys. **111**, 3820 (1999).

[64] T.-C. Jagau and J. Gauss, J. Chem. Phys. **137**, 044115 (2012).

[65] T.-C. Jagau and J. Gauss, J. Chem. Phys. **137**, 044116 (2012).

[66] D. Mukherjee and P. K. Mukherjee, Chem. Phys. **39**, 325 (1979).

[67] E. Dalgaard and H. J. Monkhorst, Phys. Rev. A. **28**, 1217 (1983).

[68] H. Sekino and R. J. Bartlett, Int. J. Quantum Chem. **26 S18**, 255 (1984).

[69] J. F. Stanton and R. J. Bartlett, J. Chem. Phys. **98**, 7029 (1993).

[70] R. J. Bartlett, WIREs Comput. Mol. Sci. **2**, 126 (2012).

[71] K. Kowalski and P. Piecuch, J. Chem. Phys. **113**, 8490 (2000).

[72] K. Kowalski and P. Piecuch, J. Chem. Phys. **115**, 643 (2001).

[73] P. Piecuch, J. Gour and M. Włoch, Int. J. Quantum Chem. **109**, 3268 (2009).

[74] S. Chattopadhyay, U. Mahapatra and D. Mukherjee, J. Chem. Phys. **112**, 7939 (2000).

[75] M. Musiał, A. Perera and R. J. Bartlett, J. Chem. Phys. **134**, 114108 (2011).

[76] P. Szalay, T. Müller, G. Gidofalvi, H. Lischka and R. Shepard, Chem. Rev. **112**, 108 (2011).

[77] S. R. Langhoff and E. R. Davidson, Int. J. Quantum Chem. **8**, 61 (1974).

[78] J. A. Pople, R. Seeger and R. Krishnan, Int. J. Quantum Chem. **11**, 149 (1977).

[79] X. Li and J. Paldus, J. Chem. Phys. **119**, 5320 (2003).

[80] B. Jeziorski, Mol. Phys. **108**, 3043 (2010).

[81] I. Hubač and P. Neogrády, Phys. Rev. A. **50**, 4558 (1994).

[82] J. Mášik and I. Hubač, Adv. Quantum Chem. **31**, 75 (1998).

[83] F. A. Evangelista, W. D. Allen and H. F. Schaefer III, J. Chem. Phys. **125**, 154113 (2006).

[84] S. Das, D. Mukherjee and M. Kállay, J. Chem. Phys. **132**, 074103 (2010).

[85] R. Maitra, D. Sinha and D. Mukherjee, J. Chem. Phys. **137**, 024105 (2012).

[86] M. Hanrath. *A Possibility For a Multi-Reference Coupled-Cluster: The MRexpT Ansatz*, in *Recent Progress in Coupled Cluster Methods*, edited by J. Leszczynski, P. Čársky, J. Paldus and J. Pittner, pp. 175–190. Springer, London, 2010.

[87] W. Kutzelnigg and D. Mukherjee, J. Chem. Phys. **107**, 432 (1997).

[88] W. Kutzelnigg, K. R. Shamasundar and D. Mukherjee, Mol. Phys. **108**, 433 (2010).

[89] T. Helgaker, P. Jørgensen and J. Olsen. *Molecular Electronic-Structure Theory*. John Wiley & Sons Ltd., Chichester, 2000.

[90] J. Gauss. *Molecular Properties*, in *Modern Methods and Algorithms of Quantum Chemistry*, edited by J. Grotendorst, pp. 509–560. John von Neumann Institute for Computing, Jülich, 2000.

[91] T. Helgaker, S. Coriani, P. Jørgensen, K. Kristensen, J. Olsen and K. Ruud, Chem. Rev. **112**, 543 (2012).

[92] M. Hanauer. *Internally contracted multireference coupled-cluster methods*. PhD thesis, Johannes Gutenberg University, Mainz, Germany, 2013. Available at http://ubm.opus.hbz-nrw.de/volltexte/2013/3423.

[93] M. R. Hoffmann and J. Simons, J. Chem. Phys. **88**, 993 (1988).

[94] Z. Chen and M. R. Hoffmann, J. Chem. Phys. **137**, 014108 (2012).

[95] H.-J. Werner and P. J. Knowles, J. Chem. Phys. **89**, 5803 (1988).

[96] L. Kong, K. R. Shamasundar, O. Demel and M. Nooijen, J. Chem. Phys. **130**, 114101 (2009).

[97] K. Andersson, P.-Å. Malmqvist, B. O. Roos, A. J. Sadlej and K. Wolinski, J. Phys. Chem. **94**, 5483 (1990).

[98] R. Fink and V. Staemmler, Theor. Chim. Acta. **87**, 129 (1993).

[99] P.-O. Löwdin, Adv. Quantum Chem. **5**, 185 (1970).

[100] D. Sinha, R. Maitra and D. Mukherjee, Comput. Theor. Chem. **1003**, 62 (2013).

[101] M. Hanauer and A. Köhn. Personal Communication.

[102] W. Kutzelnigg, Theor. Chim. Acta. **83**, 263 (1992).

[103] T. Helgaker and J. Almlöf, Int. J. Quantum Chem. **26**, 275 (1984).

[104] N. C. Handy and H. F. Schaefer III, J. Chem. Phys. **81**, 5031 (1984).

[105] T. Helgaker and P. Jørgensen, Adv. Quantum Chem. **19**, 183 (1988).

[106] T. Helgaker and P. Jørgensen, Theor. Chim. Acta. **75**, 111 (1989).

[107] Y. Osamura, Y. Yamaguchi and H. F. Schafer III, J. Chem. Phys. **77**, 383 (1982).

[108] J. Simons and P. Jørgensen, J. Chem. Phys. **79**, 334 (1983).

[109] P. Pulay, J. Chem. Phys. **78**, 5043 (1983).

[110] Y. Yamaguchi, Y. Osamura, J. D. Goddard and H. F. Schaffer III. *A new dimension to quantum chemistry: Anylutic derivative methods in ab initio molecular electronic structure theory.* Oxford University Press, New York, 1994.

[111] P. J. Knowles and H.-J. Werner, Chem. Phys. Lett. **145**, 514 (1988).

[112] K. R. Shamasundar, G. Knizia and H.-J. Werner, J. Chem. Phys. **135**, 054101 (2011).

[113] H.-J. Werner, Mol. Phys. **89**, 645 (1996).

[114] P. Celani and H.-J. Werner, J. Chem. Phys. **112**, 5546 (2000).

[115] P. Celani and H.-J. Werner, J. Chem. Phys. **119**, 5044 (2003).

[116] F. Aiga, K. Sasagane and R. Itoh, Int. J. Quantum Chem. **51**, 87 (1994).

[117] T. B. Pedersen, H. Koch and C. Hättig, J. Chem. Phys. **110**, 8318 (1999).

[118] M. Hanauer and A. Köhn, J. Chem. Phys. **137**, 131103 (2012).

[119] Y. A. Aoto and A. Köhn, J. Chem. Phys. **144**, 074103 (2016).

[120] H.-J. Werner, P. J. Knowles, G. Knizia, F. R. Manby, M. Schütz et al. Molpro, version 2015.1, a package of *ab initio* programs, see http://www.molpro.net.

[121] H.-J. Werner, P. Knowles, G. Knizia, F. Manby and M. Schütz, WIREs Comput. Mol. Sci. **2**, 242 (2012).

[122] A. Halkier, H. Larsen, J. Olsen, P. Jørgensen and J. Gauss, J. Chem. Phys. **110**, 734 (1999).

[123] K. P. Huber and G. H. Herzberg. *Molecular Spectra and Molecular Structure. Constant of Diatomic Molecules*. Van Nostrand-Reinhold, New York, 1979.

[124] M. Hanrath, Mol. Phys. **106**, 1949 (2008).

[125] C. W. Bauschlicher Jr. and S. R. Langhoff, J. Chem. Phys. **89**, 4246 (1988).

[126] L. Adamowicz and R. J. Bartlett, Chem. Phys. Lett. **129**, 159 (1986).

[127] G. E. Scuseria, T. P. Hamilton and H. F. Schaefer III, J. Chem. Phys. **92**, 568 (1990).

[128] H. Nakano, J. Nakatani and K. Hirao, J. Chem. Phys. **114**, 1133 (2001).

[129] J. Finley, P.-Å. Malmqvist, B. Roos and L. Serrano-Andrés, Chem. Phys. Lett. **288**, 299 (1998).

[130] N. Oliphant and L. Adamowicz, J. Chem. Phys. **94**, 1229 (1991).

[131] P. Piecuch, N. Oliphant and L. Adamowicz, J. Chem. Phys. **99**, 1875 (1993).

[132] M. Hanrath, Chem. Phys. Lett. **420**, 426 (2006).

[133] T. N. Lan, Y. Kurashige and T. Yanai, J. Chem. Theory Comput. **10**, 1953 (2014).

[134] T. Shiozaki and T. Yanai, J. Chem. Theory Comput. **12**, 4347 (2016).

[135] G. H. Herzberg. *Molecular Spectra and Molecular Structure: spectra of Diatomic Molecules*. Van Nostrand-Reinhold, New York, 1950.

[136] G. K.-L. Chan and M. Head-Gordon, J. Chem. Phys. **116**, 4462 (2002).

[137] G. K.-L. Chan and M. Head-Gordon, J. Chem. Phys. **118**, 8551 (2003).

[138] G. K.-L. Chan, J. J. Dorando, D. Ghosh, J. Hachmann, E. Neuscamman and T. Yanai, Quantum Syst. Chem. Phys. pp. 49–65 (2008).

[139] D. Zgid and M. Nooijen, J. Chem. Phys. **130**, 144116 (2008).

[140] D. Ghosh, J. Hachmann, T. Yanai and G. K.-L. Chan, J. Chem. Phys. **130**, 144117 (2009).

[141] K. Boguslawski, K. H. Marti, Ö. Legeza and M. Reiher, J. Chem. Theory Comput. **8**, 1970 (2012).

[142] A. Schäfer, H. Horn and R. Ahlrichs, J. Chem. Phys. **97**, 2571 (1992).

[143] H. Koch, O. Christiansen, P. Jørgensen and J. Olsen, Chem. Phys. Lett. **244**, 75 (1995).

[144] T. H. Dunning Jr., J. Chem. Phys. **90**, 1007 (1989).

[145] H. Koch, O. Christiansen, P. Jørgensen, A. M. Sanchez de Merás and T. Helgaker, J. Chem. Phys. **106**, 1808 (1997).

[146] K. Hald, P. Jørgensen, J. Olsen and M. Jaszunski, J. Chem. Phys. **115**, 671 (2001).

[147] H. H. Wenk, M. Winkler and W. Sander, Angew. Chem. Int. Ed. **42**, 502 (2003).

[148] X. Li and J. Paldus, J. Chem. Phys. **129**, 174101 (2008).

[149] X. Li and J. Paldus, J. Chem. Phys. **132**, 114103 (2010).

[150] F. A. Evangelista, W. D. Allen and H. F. Schaefer III, J. Chem. Phys. **127**, 024102 (2007).

[151] L. V. Slipchenko and A. I. Krylov, J. Chem. Phys. **117**, 4694 (2002).

[152] P. U. Manohar and A. I. Krylov, J. Chem. Phys. **129**, 194105 (2008).

[153] V. Vanovschi, A. I. Krylov and P. G. Wenthold, Theor. Chem. Acc. **120**, 45 (2008).

[154] R. Lindh, A. Bernhardsson and M. Schütz, J. Phys. Chem. A. **103**, 9913 (1999).

[155] C. J. Cramer, J. J. Nash and R. R. Squires, Chem. Phys. Lett. **277**, 311 (1997).

[156] S. P. de Visser, M. Filatov and S. Shaik, Phys. Chem. Chem. Phys. **2**, 5046 (2000).

[157] H. Li, S.-Y. Yu, M.-B. Huang and Z.-X. Wang, Chem. Phys. Lett. **450**, 12 (2007).

[158] T.-C. Jagau. Personal Communication.

[159] CFOUR, a quantum chemical program package written by J. F. Stanton, J. Gauss, M. E. Harding, P. G. Szalay with contributions from A. A. Auer, R. J. Bartlett, U. Benedikt, C. Berger, D. E. Bernholdt, Y. J. Bomble, L. Cheng, O. Christiansen, M. Heckert, O. Heun, C. Huber, T.-C. Jagau, D. Jonsson, J. Jusélius, K. Klein, W. J. Lauderdale, D. A. Matthews, T. Metzroth, L. A. Mück, D. P. O'Neill, D. R. Price, E. Prochnow, C. Puzzarini, K. Ruud, F. Schiffmann, W. Schwalbach, S. Stopkowicz, A. Tajti, J. Vázquez, F. Wang, J. D. Watts and the integral packages

MOLECULE (J. Almlöf and P. R. Taylor), PROPS (P. R. Taylor), ABACUS (T. Helgaker, H. J. Aa. Jensen, P. Jørgensen, and J. Olsen), and ECP routines by A. V. Mitin and C. van Wüllen. For the current version, see http://www.cfour.de.

[160] S. Nishihara, S. Yamanaka, T. Saito, Y. Kitagawa, T. Kawakami, M. Okumura and K. Yamaguchi, Int. J. Quantum Chem. **110**, 3015 (2010).

[161] D. Sinha, R. Maitra and D. Mukherjee, J. Chem. Phys. **137**, 094104 (2012).

[162] J. M. Junquera-Hernández, J. Sánchez-Marín, G. L. Bendazzoli and S. Evangelisti, J. Chem. Phys. **120**, 8405 (2004).

[163] R. J. Harrison and N. C. Handy, Chem. Phys. Lett. **123**, 321 (1986).

[164] T. J. Lee, A. P. Rendell and P. R. Taylor, J. Chem. Phys. **92**, 489 (1990).

[165] K. Kowalski, S. Hirata, M. Wloch, P. Piecuch and T. L. Windus, J Chem. Phys. **123**, 074319 (2005).

[166] J. M. Junquera-Hernández, J. Sánchez-Marín, G. L. Bendazzoli and S. Evangelisti, J. Chem. Phys. **121**, 7103 (2004).

[167] R. L. Christensen, M. M. Enriquez, N. L. Wagner, A. Y. Peacock-Villada, C. Scriban, R. R. Schrock, T. Polívka, H. A. Frank and R. R. Birge, J. Phys. Chem. A. **117**, 1449 (2013).

[168] R. Send, D. Sundholm, M. P. Johansson and F. Pawłowski, J. Chem. Theory Comput. **5**, 2401 (2009).

[169] D. Zhang and C. Liu, J. Chem. Phys. **135**, 134117 (2011).

[170] L. Serrano-Andrés, R. Lindh, B. O. Roos and M. Merchán, J. Phys. Chem. **97**, 9360 (1993).

[171] D. Casanova, J. Chem. Phys. **137**, 084105 (2012).

[172] C. Angeli and M. Pastore, J. Chem. Phys. **134**, 184302 (2011).

[173] M. A. Watson and G. K.-L. Chan, J. Chem. Theory Comput. **8**, 4013 (2012).

[174] M. Schmidt and P. Tavan, J. Chem. Phys. **136**, 124309 (2012).

[175] C. Daday, S. Smart, G. H. Booth, A. Alavi and C. Filippi, J. Chem. Theory Comput. **8**, 4441 (2012).

[176] M. Schreiber, M. R. Silva-Junior, S. P. A. Sauer and W. Thiel, J. Chem. Phys. **128**, 134110 (2008).

[177] M. R. Silva-Junior, M. Schreiber, S. P. A. Sauer and W. Thiel, J. Chem. Phys. **129**, 104103 (2008).

[178] M. R. Silva-Junior, M. Schreiber, S. P. A. Sauer and W. Thiel, J. Chem. Phys. **133**, 174318 (2010).

[179] O. Demel, D. Datta and M. Nooijen, J. Chem. Phys. **138**, 134108 (2013).